Space-time Spectral Collocation Methods for the Magnetohydrodynamics Equations.

by

W.L.C.Piyasundara

A thesis submitted to the Faculty of Graduate Studies of
The University of Manitoba
in partial fulfilment of the requirements of the degree of

MASTER OF SCIENCE

Department of Mathematics
University of Manitoba
Winnipeg

Abstract

Spectral methods are used to solve partial differential equations numerically. When the solution is analytic, the rate of convergence of the numerical solution is exponential; that is, the error decays exponentially. In time-dependent PDEs, low order finite difference schemes and spectral schemes are traditionally being used for the time and spatial derivatives, respectively. However, applying spectral schemes in both space and time has been thought of recently. These methods have spectral convergence in both spatial and temporal domains. In this thesis, both Chebyshev and Legendre spectral collocation methods are implemented for the Navier–Stokes and Magnetohydrodynamics equations. Numerical solutions for both equations converge exponentially when the solutions are analytic. Moreover, Navier-Stokes and Magnetohydrodynamic equations are implemented for high Reynolds numbers using nonlinear preconditioning methods, ASPIN and RASPEN, which are defined using spectral domain decomposition.

Acknowledgements

I take this opportunity to express my gratitude to the people who have been instrumental in the successful completion of this project. I would like to extend my appreciation especially to the following. First and foremost, my heartfelt gratitude and sincere thanks go to my supervisor Prof. Shaun Lui, Dept. of Mathematics, University of Manitoba, who helped me through this project consistently and, I highly appreciate his constant guidance, motivation, enthusiasm, immense knowledge and dedication to help me to understand this project profoundly. I am also very thankful to him for giving me much of his precious time carefully supervising and guiding me throughout my study. Without his guidance and help, this research would not be possible. I will be forever grateful for his patience and expertise throughout my studies. I also wish to thank the Department of Mathematics for the financial support they provided throughout my years of study.

I further extend my appreciation to my parents for their endless support even after I moved across the world to pursue my studies. Last but not least, my appreciation goes to my beloved husband for his understanding and constant support throughout my time of study.

Contents

List of Figures

List of Tables

1

Introduction

1.1 Motivation

The study and modeling of fluids have paved the way for engineering miracles that are inseparable from the human way of life. Ranging from airplanes to hydropower generation to sports cars, fluid dynamics play an imperative role in the daily life of human beings. While fluid flows are highly complex and unpredictable, a set of partial differential equations have been derived to model them, namely, the Navier-Stokes equations. Although the Navier-Stokes equations are widely used in fluid flow modeling, fundamental questions such as the existence, uniqueness, and regularity of a solution in three dimensions are open. Consequently, they are studied widely by many researchers.

Magnetohydrodynamics (or MHD) is also a study in the realm of fluid dynamics that has gained increased traction in the recent past. MHD is the study of interactions between conductive fluids moving in magnetic fields. At the very core of MHD are two prominent sets of equations, the Navier-Stokes and Maxwell's equations. The study of magnetism in conducting fluids did not attract attention among physicists

until the 20th century. Realization of the fact that plasma and magnetic fields are frequently present throughout the universe made studying MHD seem much more enticing thereafter. As a result of this, the concepts of MHD have been developed, and they have helped us understand a variety of natural phenomena such as plasmas in the earth and solar astrophysics.

The significance of the two-dimensional Navier-Stokes and MHD equations has encouraged the study of them in different formulations, namely, the stream function formulation. While finite difference methods have been frequently implemented to solve those equations numerically, not many studies are present for implementing space-time spectral methods to solve them. Therefore, in this study, space-time Chebyshev and Legendre collocation methods for stream function formulation of the above nonlinear PDEs are proposed and analyzed. In addition to the above two PDEs, we also study stream function formulation of Stokes equation (which is a simplified version of the Navier-Stokes equations) through space-time spectral methods thereof. The Stokes equations are a system of linear PDEs that model fluid with very small Reynolds numbers.

Further, using space-time collocation methods to solve the above two nonlinear PDEs become increasingly difficult as the Reynolds numbers increase. Due to the strong nonlinearities of Navier-Stokes and MHD equations, we implement them for high Reynolds numbers using two nonlinear preconditioning methods, ASPIN and RASPEN, that were theorized in the 21st century. They are improved preconditioners for Newton's method that utilize spectral domain decomposition to solve the two PDEs.

1.2 Outline of Thesis

In this thesis, space-time spectral collocation methods for the Navier-Stokes equations and MHD equations are discussed. The thesis consists of six chapters.

Chapter 1 summarizes the concepts that are required to understand this thesis properly. In Chapter 2, we introduce the notations used in this thesis and discuss the space-time Chebyshev spectral collocation method for the 1D heat equation. In Chapter 3, space-time spectral collocation method for the Stokes problem and Navier-Stokes equations are introduced. In Chapter 4, some fundamentals concepts of MHD are explained. A space-time spectral collocation method for the MHD equations is established. In Chapter 5, overlapping and non-overlapping spectral domain decomposition methods are discussed for linear and nonlinear PDEs. In Chapter 6, numerical experiments done in MATLAB are shown to demonstrate the accuracy and efficiency of space-time spectral methods for Stokes, Navier-Stokes and MHD equations.

2

Space-Time Spectral Collocation Method

2.1 Introduction

Spectral methods are among the most important and dominant methods that are used to solve ODEs and PDEs relating to various physical phenomena. They apply global smooth functions to approximate solutions of ODEs and PDEs. The main advantage is that, for elliptic differential equations which have an analytic solution, the rate of convergence of the numerical solution is an exponential function of the number of basis functions that are used. While Legendre or Chebyshev polynomials (which are eigenfunctions of singular Sturm-Liouville problems) could be used as basis functions for non-periodic boundary conditions, it is more practical to use trigonometric functions where boundary conditions are periodic. In spectral collocation, an interpolating polynomial is used to approximate a given ODE or PDE at a set of interior collocation points, called Gauss-Lobatto points.

The typical approach when solving time-dependent PDEs is to use a low order scheme such as a finite difference method for the time derivative and a spectral scheme for

the spatial derivative. However, when a low order and high order scheme are implemented together, the error of time discretization is substantially higher than the error of spatial discretization. Two of the very early studies on space-time spectral methods are [37] and [36]. These works explain how to apply space-time spectral methods for PDEs with periodic boundary conditions. Other references include [35], [23], [42], [43] and the references therein. These works use Gauss-Lobatto quadrature and Gaussian quadrature based collocations for space and time, respectively.
Space-time spectral methods employ spectral discretization in both space and time. See [38], [24], [27] and [28]. When the solution is analytic, exponential decay of the numerical error can be observed as number of spectral modes increase. One major drawback of space-time spectral methods is that time stepping cannot be implemented. PDEs have to be solved for all times simultaneously.

Instead, the equations have to be solved for all times simultaneously. Consequently, solving PDEs with three spatial dimensions become increasingly difficult and this is particularly true for PDEs that are non-linear. However, in contrast to traditional methods, fewer unknowns are required to obtain equal tolerance as low order schemes. This is due to the exponential convergence of the solution.
There have been many works that attempted to overcome the inability of time stepping. See [11], [18], [22] and references therein for such attempts thereof. See [16] to obtain an overview of four different time parallel methods. Moreover, references [4], [5], [20] and [21] are some excellent works that review theory and practice of spectral methods.

2.2 Basic notation and preliminaries

Let us briefly summarize the matrix notations that frequently appear in space-time spectral methods. The $n \times n$ identity matrix is denoted by I_n. Consider a square matrix M of size $n \times n$. Another matrix $[M]$ of size $(n-1) \times (n-1)$ is obtained by removing the last row and column of M. Similarly, $[[M]]$ of size $(n-2) \times (n-2)$ is obtained by removing the first and last rows and columns of M. The transpose and complex conjugate transpose of M is denoted by M^T and M^* respectively. Also, let $\overline{a}$ denote the complex conjugate for any complex number a and, $\Re(a)$ and $\Im(a)$ denotes real and imaginary parts of the complex number a thereof. Two vector/matrix norms, namely, the 2-norm and the ∞-norm, are denoted by $|\cdot|$ and $|\cdot|_\infty$ respectively. Let $diag(v)$ denote a diagonal matrix whose diagonal entries comprise of elements from vector v. Let $\mathbb{M}$ denote $\mathbb{R}$ or $\mathbb{C}$.

Definition 2.1. The Kronecker (tensor) product of the matrix $A \in \mathbb{M}^{p\times q}$ with the matrix $B \in \mathbb{M}^{r\times s}$ is defined as

$$A \otimes B = \begin{bmatrix} a_{11}B & \cdots & a_{1q}B \\ \vdots & \vdots & \vdots \\ a_{p1}B & \cdots & a_{pq}B \end{bmatrix} \in \mathbb{M}^{pr\times qs}.$$

Two theorems that will be instrumental for this study are given below.

Theorem 2.2. Let $A \in \mathbb{M}^{m\times m}$ and $B \in \mathbb{M}^{n\times n}$. Furthermore, let $\lambda \in \Lambda(A)$ with corresponding eigenvector x, and $\mu \in \Lambda(B)$ with corresponding eigenvector y. Then $\lambda\mu$ is an eigenvalue of $A \otimes B$ with corresponding eigenvector $x \otimes y$. Any eigenvalue of $A \otimes B$ arises as such a product of eigenvalues of A and B.

It follows directly that if $A \in \mathbb{M}^{m\times m}$ and $B \in \mathbb{M}^{n\times n}$ are positive (semi) definite matrices, then $A \otimes B$ is also positive (semi) definite.

Theorem 2.3. Let $A \in \mathbb{M}^{m\times m}$ and $B \in \mathbb{M}^{n\times n}$. Furthermore, let $\lambda \in \Lambda(A)$ with corresponding eigenvector x, and $\mu \in \Lambda(B)$ with corresponding eigenvector y. Then $\lambda + \mu$ is an eigenvalue of $(I_n \otimes A) + (B \otimes I_m)$ with corresponding eigenvector $y \otimes x$. Any eigenvalue of $(I_n \otimes A) + (B \otimes I_m)$ arises as such a sum of eigenvalues of A and B.

Definition 2.4. For any matrix $A \in \mathbb{M}^{m\times n}$ define

$$vec(A) = (a_{11}, \cdots, a_{m1}, a_{12}, \cdots, a_{m2}, \cdots, a_{1n}, \cdots, a_{mn})^T.$$

That is, columns of matrix A are ordered one below the other to construct a vector of length mn. The Kronecker product can be utilized to transform a linear matrix equation to an equation which is a combination of matrices and vectors. For example,

$$AX + YB = C \quad \Leftrightarrow \quad (I \otimes A)vec(X) + (B^T \otimes I)vec(Y) = vec(C).$$

Further, $(X \otimes Y)z = vec(YZX^T)$ for matrices $X \in \mathbb{M}^{n\times n}$, $Y \in \mathbb{M}^{m\times m}$ and $z \in \mathbb{M}^{mn}$. Here $vec(Z) = z$, is the vector representation of Z.

Let N be some positive integer and P_N denote the space of polynomials of degree at most N in x for a fixed t and degree at most N in t for a fixed x. Let T_N denote the Nth degree Chebyshev polynomial and x_j be the zeros of the polynomial $(1 - x^2)T_N'(x)$. We shall take $x_0 = 1$, $x_N = -1$ and $x_1, \ldots, x_{N-1}$ as the descending zeros of the function thereof. The set $x_0, \ldots, x_N$ is defined as Chebyshev Gauss-Lobatto nodes in space. Similarly, the Chebyshev Gauss-Lobatto nodes along the t

axis are denoted by $\{t_k\}$. Let

$$x_h = \begin{bmatrix} x_1 \\ \vdots \\ x_{N-1} \end{bmatrix} \qquad t_h = \begin{bmatrix} t_0 \\ \vdots \\ t_{N-1} \end{bmatrix}$$

Note that x_h excludes both boundary points x_0 and x_N, while t_h excludes only the initial point $t_N = -1$. For $0 \leq j \leq N$, let ℓ_j be the Lagrange polynomial interpolant in x_j and degree N so that $\ell_j(x_k) = \delta_{jk}$. It will be worth remembering that D, the Chebyshev pseudospectral derivative matrix is defined as,

$$D_{jk} = \frac{d\ell_k(x_j)}{dx}, \quad 0 \leq j, k \leq N.$$

Further, let d_h denote the first N entries of the last column of D. That is, $d_h = D(0 : N-1, N)$. For any continuous u in x, the Chebyshev interpolation operator is defined as,

$$\mathcal{L}_N u = \sum_{j=0}^{N} u(x_j)\ell_j. \tag{2.1}$$

Let us also briefly remember a property of the Chebyshev quadrature. Consider any polynomial of degree less than or equal to $2N-1$. We may write,

$$\int_{-1}^{1} v(x)w(x)dx = \sum_{k=0}^{N} v(x_k)\rho_k, \qquad w(x) = \frac{1}{\sqrt{1-x^2}},$$

where ρ_k is the set of weights pertaining to Chebyshev Gauss-Lobatto quadrature. The $(N+1) \times (N+1)$ diagonal matrix W_h has $\{\rho_k\}$ as its diagonal entries. A continuous function v on $\Omega := (-1, 1)^2$ will have the weighted L^2-norm of

$$\|v\| := \left(\int_\Omega |v(x,t)|^2 w(x)w(t)dxdt \right)^{1/2}.$$

The discrete norm corresponding to v is,

$$\|v\|_N := \left(\sum_{j,k=0}^{N} \rho_j \rho_k |v(x_j, t_k)|^2 \right)^{1/2}.$$

For all such polynomials v of degree at most N, it is observed that discrete and weighted L^2-norms are equivalent:

$$\|v\| \leq \|v\|_N \leq 2\|v\|. \tag{2.2}$$

If v is a single variable function, the L^2-norm is also denoted by

$$\|v\| := \left(\int_{-1}^{1} |v(x)|^2 w(x) dx \right)^{1/2}.$$

2.3 Space-time collocation method

Let us discuss a space-time spectral collocation to one of the simplest PDEs, the one-dimensional heat equation. The spatial and temporal domains are taken as $(-1, 1)$. While $(-1, 1)$ may seem unorthodox for a temporal domain, there is no loss of generalization and it is evident that a simple transformation would suffice to accomplish this. Now consider the 1D heat equation

$$u_t = u_{xx} + f(x, t) \ \ on \ \ (-1, 1)^2, \tag{2.3}$$

with boundary conditions $u(\pm 1, t) = 0$ and initial condition $u(x, -1) = u_0(x)$. We will calculate a numerical solution $u \in P_N$ at $t = 1$.

The spectral equations are

$$(I_{N+1} \otimes D)u_h = (D^2 \otimes I_{N+1})u_h + f_h,$$

where u_h and f_h are the vectors of u and f, respectively, evaluated at the collocation points. We obtain two vectors $\hat{u}_h$ and $\hat{f}_h$ by removing the corresponding boundary and initial points from u_h and f_h, respectively. The linear equation can now be written as

$$A_h\hat{u}_h = \hat{f}_h - (u_{0h} \otimes d_h), \quad A_h = (I_{N-1} \otimes [D]) - ([[D^2]] \otimes I_N). \tag{2.4}$$

Let U_h and F_h be $N \times (N-1)$ matrices and, $vec(U_h) = \hat{u}_h$ and $vec(F_h) = \hat{f}_h - (u_{0h} \otimes d_h)$. Then we can see that equation (2.5) is equivalent to the Sylvester equation $[D]U_h - U_h[[D^2]]^T = F_h$ which can be solved by the algorithm of Bartels and Stewart in $O(N^3)$ operations. Observe that all unknowns over all times must be solved simultaneously.

Next, the spectral condition number estimate and spectral convergence of the heat equation will be briefly discussed. The spectral condition number is defined by,

$$\kappa(M) = \frac{max_{\lambda \in \Lambda(M)}|\lambda|}{min_{\lambda \in \Lambda(M)}|\lambda|},$$

where $\Lambda(M)$ is the spectrum of matrix M.
A few important lemmas (see [28]) relating to the condition number are mentioned below.

Lemma 2.5. Let $N \geq 1$. Then the real part of every eigenvalue of $[D]$ is larger than some positive constant independent of N.

Lemma 2.6. Let $N \geq 1$ and λ be an eigenvalue of $[D]$. Then $|\lambda| \leq cN^2$.

The next lemma is well known; see [41].

Lemma 2.7. Let $N \geq 2$. Then the eigenvalue of $-[[D^2]]$ are real, bounded below by c and above by CN^4, where c and C are positive and independent of N.

The following theorem gives an estimation of spectral condition number of the discrete spectral differentiation operator A_h. The proof relies on the above Lemmas.

Theorem 2.8. [27] Let $N \geq 2$. Let A_h be the Chebyshev spectral collocation matrix defined by (2.4) and λ be an eigenvalue of A_h. Then

$$c \leq |\lambda| \leq CN^4.$$

Consequently,

$$\kappa(A_h) \leq CN^4.$$

Further, below theorem shows the spectral convergence of the heat equation.

Theorem 2.9. [27] For any integer $N \geq 2$, let u be the solution of the heat equation (2.3). Assume that $u(x,t)$ is separately analytic in each variable. Define the error vector E_h as the difference of u evaluated at the collocation points and $\hat{u}_h$. Then

$$\left|W^{1/2}E_h\right|_2 \leq cN^{3.5}e^{-CN}.$$

Spectral convergence and condition number estimates for other linear PDEs are shown in [27], [28].

3

Navier-Stokes Equations

Fluid flows occurring in reality can be modeled by the Navier-Stokes equations and therefore are of major importance. There are seven millennium problems listed by the Clay Mathematics Institute and, determining the existence, uniqueness and regularity of solutions of the Navier-Stokes equations is one of them. Since an analytical solution to the Navier-Stokes equation is rarely available, it is evident that obtaining a numerical solution would be the next best option for solving the PDE. Disparate numerical solvers for the Navier-Stokes have been introduced over the years. Finite difference, finite elements, finite volume methods and discontinuous Galerkin methods are such popular solvers. Navier-Stokes equations are being used to model a number of engineering concepts that are indispensable to human life and therefore, the numerical solution must be both accurate and efficient when computed. The numerical simulation of these equations is used in weather forecast, aircraft design, water supply and drainage, among other domains. The Navier-Stokes equations are so versatile that they can be used to model many a fluid flow with subtle adaptations. For instance, in aircraft design, the fluid away from the aircraft body (which is actually air in this case) is considered to be compressible in contrast to a tidal wave model where the fluid (which is water) is considered incompressible. In this

chapter, we undertake the numerical investigation of the space-time spectral methods for the steady and unsteady Stokes and Navier-Stokes equations. MATLAB codes are developed and used to simulation both these equations. The incompressible two-dimensional fluid flow in a square container where the top lid is moving, better known as the lid-driven cavity, is tested as a benchmark problem. The Navier-Stokes equations are nonlinear. We first discuss a linear version.

3.1 Stokes Problem

The Stokes equations are a simplified version of the Navier-Stokes equations. The Stokes equations are a system of linear PDEs that model fluid with very small Reynolds numbers, i.e., $Re \ll 1$. In this scenario where a minuscule length of fluid flow is considered, or the fluid velocities are very small, or the fluid is greatly viscous, is known as Stokes flow. The name takes after Sir George Gabriel Stokes. The equations which model Stokes flow are referred to as the Stokes equations. In this study, we consider the Stokes equations in both steady and unsteady states along with Dirichlet boundary conditions.

Let Ω be a bounded domain in $\mathbf{R}^2$ with a Lipschitz boundary. The velocity field, denoted by u, is a vector quantity. We consider $u \in V := (H_0^1(\Omega))^2 = H_0^1(\Omega) \times H_0^1(\Omega)$. The pressure, denoted by p, is a scalar quantity. We consider $p \in L_0^2(\Omega)$, where

$$L_0^2(\Omega) := \left\{ q \in L^2(\Omega) | \int_\Omega q = 0 \right\}.$$

The norm of p is given as,

$$\|p\|_0 = \left[\int_\Omega |p|^2 \right]^{1/2}, \tag{3.1}$$

and the inner product on the space $L_0^2(\Omega)$ is defined to be the same as that for $L^2(\Omega)$, which is given by

$$(u, v)_0 := \int_\Omega uv, \quad \forall u, v \in L^2(\Omega).$$

The following two bilinear forms are defined for $u, v \in V$ and $q \in L_0^2(\Omega)$,

$$a(u, v) : = \int_\Omega \nabla u \cdot \nabla v = \sum_{i=1}^{2} \int_\Omega \nabla u_i \cdot \nabla v_i \tag{3.2}$$

$$b(q, v) : = - \int_\Omega q(\nabla \cdot v). \tag{3.3}$$

The bilinear form $a(u, v)$, for all $u = (u_1, u_2), v = (v_1, v_2) \in V$, is an inner product on the space V. The norm on the space V is denoted by $\|\cdot\|$ and it is defined for all $u = (u_1, u_2) \in V$ as,

$$\|u\| := \sqrt{a(u, u)} = \left[\int_\Omega |\nabla u_1|^2 + |\nabla u_2|^2 \right]^{1/2}. \tag{3.4}$$

Definition 3.1 (Inverse Laplacian)**.** The inverse Laplacian is denoted by $\Delta^{-1} : (H^{-1}(\Omega))^2 \to V$. Let $u \in (H^{-1}(\Omega))^2$, we say $\Delta^{-1}u = v \in V$ if

$$\begin{aligned} \Delta v &= u \quad in \ \ \Omega, \\ v &= 0 \quad on \ \ \partial\Omega. \end{aligned}$$

Here, Δ is the vector laplacian as $v \in V$ is a vector having two components. Now, we define $V^{'}$ as the dual of the space V, thus, $V^{'} := (H^{-1}(\Omega))^2$. The norm on $V^{'}$ is denoted as $\|\cdot\|^{'}$. For any $f \in V^{'}$, the norm is defined as

$$\|f\|^{'} := \sup_{\substack{v \in V \\ v \neq 0}} \frac{\langle f, v \rangle_{V^{'}, V}}{\|v\|}, \tag{3.5}$$

or equivalently

$$\|f\|'^2 = \int_\Omega \nabla((-\Delta)^{-1}f) \cdot \nabla((-\Delta)^{-1}f). \tag{3.6}$$

Definition 3.2 (Stokes problem)**.** On a bounded domain Ω with a Lipschitz boundary and for $(u, p) \in V \times L_0^2(\Omega), f \in V'$ the Stokes problem is given as,

$$-\Delta u + \nabla p = f \quad in \quad \Omega, \tag{3.7}$$

$$\nabla \cdot u = 0 \quad in \quad \Omega, \tag{3.8}$$

$$u = 0 \quad on \quad \partial\Omega. \tag{3.9}$$

The weak formulation of the Stokes problem for all $v \in V$ and $q \in L_0^2(\Omega)$ is

$$a(u, v) + b(p, v) = f(v),$$
$$b(q, u) = 0.$$

We now convert equations (3.7)-(3.9) into stream function form. Here, we treat u and f as a vectors with two components: $u = [u_1, u_2]^T$ and $f = [f_1, f_2]^T$. Now we define a stream function ψ such that $u_1 = \frac{\partial \psi}{\partial y}, u_2 = -\frac{\partial \psi}{\partial x}$.
When considering a sufficiently smooth scalar function f, one may write

$$\nabla \times \nabla f = \nabla \times [f_x, f_y, f_z] = [f_{zy} - f_{yz}, f_{xz} - f_{zx}, f_{yx} - f_{xy}] = \underline{0}.$$

This speaks to the fact that the curl annihilates the gradient. Thus, a model absent of the pressure term can be obtained by taking the curl of (3.7).

$$\nabla \times (-\Delta u + \nabla p) = \nabla \times f.$$

The other advantage of the stream function formulation is that the number of un-

knowns reduces to one from three (u_1, u_2, p). This is a fourth-order PDE and so more difficult to solve than second order ones. Now, our new model is

$$\Delta^2 \psi = f_{2x} - f_{1y} \quad in \quad \Omega, \tag{3.10}$$

$$\psi = \frac{\partial \psi}{\partial \nu} = 0 \quad on \quad \partial\Omega. \tag{3.11}$$

Here $f_{2x} = \frac{\partial f_2}{\partial x}$ and $f_{1y} = \frac{\partial f_1}{\partial y}$. Similarly to the above calculation, it can be shown that a stream function model can be obtained for the unsteady Stokes equation as well.

$$u_t - \Delta u + \nabla p = f \quad in \quad \Omega,$$

$$\nabla \cdot u = 0 \quad in \quad \Omega,$$

$$u = 0 \quad on \quad \partial\Omega,$$

$$u(x, y, -1) = u_0(x, y) \quad in \quad \Omega.$$

(We take the initial time at $t = -1$).

Now, by taking the curl and using $u = \frac{\partial \psi}{\partial y}\underline{i} - \frac{\partial \psi}{\partial x}\underline{j}$, we have

$$-\Delta \psi_t + \Delta^2 \psi = f_{2x} - f_{1y} \quad in \quad \Omega, \tag{3.12}$$

$$\psi = \frac{\partial \psi}{\partial \nu} = 0 \quad on \quad \partial\Omega, \tag{3.13}$$

$$\psi(x, y, -1) = \psi_0(x, y) \quad in \quad \Omega. \tag{3.14}$$

3.2 Space-time spectral methods for Stokes problem

In this section, we discuss a space-time spectral method for the stream function form of the unsteady Stokes equations (3.12). Here, we will consider the simplest case where the spatial and temporal domains are both $(-1, 1)$.

Consider the stream function formulation for the 1D unsteady Stokes equation

$$(\psi_t)_{xx} = \psi_{xxxx} + f,$$

with initial condition $\psi(x, -1) = \psi_0(x)$ and homogeneous Dirichlet boundary conditions. Based on concepts discussed in the previous section, a space-time spectral collocation scheme for the 1D unsteady Stokes equation can be written as

$$(D^2 \otimes D)\psi_h = (D^4 \otimes I_{N+1})\psi_h + f_h,$$

where ψ_h and f_h are the vectors of ψ and f respectively, evaluated at the collocation points. A spectral approximation of the second derivative can be derived by considering the corresponding boundary conditions.

Let $\psi = \psi(x)$ be a polynomial so that $\psi(\pm 1) = \psi^{'}(\pm 1) = 0$. Let Z vanish at ± 1 so that $\psi(x) = (1-x^2)Z(x)$. That is, ψ automatically satisfies the boundary conditions if Z vanishes at the boundary. By differentiating ψ twice, we obtain the following.

$$\psi^{''}(x) = (1 - x^2)Z^{''}(x) - 4xZ^{'}(x) - 2Z(x). \tag{3.15}$$

Let M be a $(N-1) \times (N-1)$ diagonal matrix with diagonal entries $1 - x_j^2$. Also, take X to be a diagonal matrix of the same size but with diagonal entries x_j. Here $1 \leq j \leq N-1$. Therefore, the spectral approximation of the second derivative

(denoted by B_2) satisfying the four boundary conditions can be written as,

$$B_2 := (M[[D^2]] - 4X[[D]] - 2I)M^{-1}. \tag{3.16}$$

Similarly, the spectral approximation of the fourth derivative can be defined as:

$$\psi''''(x) = (1 - x^2)Z''''(x) - 8xZ'''(x) - 12Z''(x). \tag{3.17}$$

Then, the spectral approximation of the fourth derivative satisfying the four boundary conditions is

$$B_4 := (M[[D^4]] - 8X[[D^3]] - 12[[D^2]])M^{-1}. \tag{3.18}$$

The resulting spectral equation for the Stokes equation is

$$(B_2 \otimes [D])\hat{\psi}_h - (B_4 \otimes I_N)\hat{\psi}_h = \hat{f}_h - (\psi_{0h} \otimes d_h),$$

where ψ_{0h} is ψ_0 evaluated at the (interior spatial) collocation points. The two vectors $\hat{\psi}_h$ and $\hat{f}_h$ are obtained by removing the corresponding boundary and initial points from ψ_h and f_h, respectively. The linear equation now can be written as

$$A_h\hat{\psi}_h = \hat{f}_h - (\psi_{0h} \otimes d_h),$$

where

$$A_h = (B_2 \otimes [D]) - (B_4 \otimes I_N). \tag{3.19}$$

Now, consider the stream function formulation for the 2D unsteady Stokes equation

$$(\psi_t)_{xx} + (\psi_t)_{yy} = \psi_{xxxx} + \psi_{yyyy} + 2\psi_{xxyy} + f,$$

with initial condition $\psi(x, y, -1) = \psi_0(x, y)$ and homogeneous Dirichlet boundary conditions. The space-time spectral scheme is

$$\Big\{D \otimes \Big((D^2 \otimes I_{N+1}) + (I_{N+1} \otimes D^2)\Big)\Big\}\,\psi_h = \Big\{I_{N+1} \otimes \Big((D^4 \otimes I_{N+1}) + (I_{N+1} \otimes D^4) + 2(D^2 \otimes D^2)\Big)\Big\}\psi_h + f_h,$$

where ψ_h and f_h are the vectors of ψ and f, respectively, evaluated at the collocation points. Let B_2 be the spectral second derivative (3.16) and B_4 be the spectral fourth derivative (3.18) defined for the 1D Stokes problem. Finally, we may write

$$\Big\{[D] \otimes \Big((B_2 \otimes I_{N-1}) + (I_{N-1} \otimes B_2)\Big) - I_{N-1} \otimes \Big((B_4 \otimes I_{N-1}) + (I_{N-1} \otimes B_4) + 2(B_2 \otimes B_2)\Big)\Big\}\hat{\psi}_h = \hat{f}_h - (d_h \otimes \psi_{0h}),$$

where ψ_{0h} is ψ_0 evaluated at the interior collocation points. Here, the known boundary and initial values have been removed. Thus, the linear equation to be solved becomes

$$A_h \hat{\psi}_h = \hat{f}_h - (d_h \otimes \psi_{0h}),$$

where

$$A_h = [D] \otimes \Big((B_2 \otimes I_{N-1}) + (I_{N-1} \otimes B_2)\Big) - I_{N-1} \otimes \Big((B_4 \otimes I_{N-1}) + (I_{N-1} \otimes B_4) + 2(B_2 \otimes B_2)\Big), \tag{3.20}$$

is the space-time Stokes operator. Further, eigenvalues of B_4 are found to be real numerically. Although the result can be obtained numerically, it is yet to be theoretically proven. By using this result and Lemmas 2.5, 2.6 and 2.7, it may be possible to prove a condition number estimate of A_h. It is still an open problem at this point. However, we have numerically shown a condition number estimate of the space-time Stokes operator $\kappa(A_h) \leq CN^8$.

Moreover, Bartels-Stewart or Hessenberg-Schur algorithm can be used to solve the linear system arising from the space-time spectral scheme for the Stokes equations in two space dimensions. Bartels–Stewart algorithm is a popular and efficient method used to solve the matrix equation $AX + XB = C$; $A \in \mathbf{R}^{m\times m}$ and $B \in \mathbf{R}^{n\times n}$. The algorithm transforms the equation into a triangular system by applying Schur decomposition:

$$R = U^T AU, \qquad S = V^T B^T V. \tag{3.21}$$

The matrices R and S are upper quasi-triangular matrices with diagonal blocks of size 1×1 or 2×2 and U, V are orthogonal. Forward or backward substitution can now be used to solve the simplified system.

$$RY + YS^T = F \qquad (F = U^T CV, \quad Y = U^T XV).$$

Assuming $S_{k,k-1}$ is zero, then it follows that

$$(R + S_{kk}I)y_k = f_k - \sum_{j=k+1}^{n} S_{kj}y_j,$$

where y_k is the kth column of Y. Now the solution can be found using $X = UYV^T$.

Time taken by a computer to run an algorithm is known as the time complexity, which is the total number of elementary operations performed by the algorithm. Therefore, the time complexity of the Bartels-Stewart algorithm can be summarized as follows. Firstly, we shall assume that $10m^3$ and $10n^3$ operations are required for the Schur decompositions mentioned in (3.21).

- Reduce A and B^T to upper triangular matrices by orthogonal matrices
  $R = U^T AU$ $10m^3$.

$S = V^T B^T V$ $\qquad 10n^3.$

- Update the right hand side

  $F = U^T C V$ $\qquad m^2 n + mn^2.$

- Back substitute for Y

  $RY + YS^T = F$ $\qquad \frac{1}{2}m^2 n + \frac{1}{2}mn^2.$

- Obtain solution

  $X = UYV^T$ $\qquad m^2 n + mn^2.$

Therefore, the overall time complexity for the Bartels-Stewart algorithm is given by

$$10m^3 + 10n^3 + 2.5(m^2 n + mn^2).$$

Consider the system (3.20). Take $A_1 = (B_2 \otimes I_{N-1}) + (I_{N-1} \otimes B_2)$ and $A_2 = -\Big((B_4 \otimes I_{N-1}) + (I_{N-1} \otimes B_4) + 2(B_2 \otimes B_2)\Big)$. Now we have

$$\Big(I_{N-1} \otimes A_2 A_1^{-1} + [D] \otimes I_{N-1}\Big)\hat{\psi}_h = (I_N \otimes A_1^{-1})(\hat{f}_h - (d_h \otimes \psi_{0h})).$$

Then the system is equivalent to the Sylvester equation $A_2 A_1^{-1}\hat{\psi}_h + \hat{\psi}_h[D]^T = F_h$, where $vec(F_h) = (I_N \otimes A_1^{-1})(\hat{f}_h - (d_h \otimes \psi_{0h}))$. Thus, the time complexity of solving the above system using Bartels-Stewart algorithm is $O(10N^6)$, where $N = n$ and $m = O(N^2)$. By taking advantage of the structure of the system, it is possible to improve the complexity of the method.

As mentioned previously, the Hessenberg-Schur algorithm can also be used to solve the matrix equation $AX + XB = C$. Decompositions for the Hessenberg-Schur algorithm are defined as,

$$H = U^T A U \qquad\qquad S = V^T B^T V. \tag{3.22}$$

Here, the first Schur decomposition of Bartels-Stewart is replaced by $H = U^T AU$, where H is an upper-Hessenberg matrix. This leads to a system that has the form $HY + YS^T = F$, which can be solved in a similar manner to the Bartels-Stewart algorithm. Therefore, the time complexity of the Hessenberg-Schur algorithm can be summarized as below.

- Reduce A to upper Hessenberg and B^T to upper triangular matrices

  $H = U^T AU$ $\quad\quad$ $\frac{5}{3}m^3$.

  $S = V^T B^T V$ $\quad\quad$ $10n^3$.

- Update the right hand side

  $F = U^T CV$ $\quad\quad$ $m^2 n + mn^2$.

- Back substitute for Y

  $HY + YS^T = F$ $\quad\quad$ $3m^2 n + \frac{1}{2}mn^2$.

- Obtain solution

  $X = UYV^T$ $\quad\quad$ $m^2 n + mn^2$.

Thus, overall time complexity for the Hessenberg-Schur algorithm is given by

$$\frac{5}{3}m^3 + 10n^3 + 5m^2 n + \frac{5}{2}mn^2.$$

Hence, we can conclude that the Hessenberg-Schur algorithm is considerably faster than the Bartels-Stewart algorithm since $H = U^T AU$ can be found using Householder reflections at a cost of $\frac{5}{3}m^3$. Thus, the time complexity of solving the Stokes equation using the Hessenberg-Schur algorithm is $O(\frac{5}{3}N^6)$, where $m = O(N^2)$. Again this complexity can be lowered by taking into account of the structure of the system.

We derive some properties of the eigenvalues of B_2. Firstly, we consider the Chebyshev case.

We begin with a couple of important lemmas which will be needed to estimate the condition number.

Lemma 3.3. [4] Let $v \in H^1_{0,w}(-1,1)$. Then

$$\int_{-1}^{1} v^2 w^5 \leq \frac{2}{3}\|v^{'}\|^2.$$

Lemma 3.4. For all $u, v \in H^1_{0,w}(-1,1)$ (see Lemma 5.31 in [26]),

$$\int_{-1}^{1} u^{'}(vw)^{'}dx \leq 2\|u^{'}\|\|v^{'}\|, \quad \int_{-1}^{1} u^{'}(uw)^{'}dx \geq \frac{1}{4}\|u^{'}\|^2.$$

Lemma 3.5 (Trace Inequality)**.** For all $v \in P_N$, $|v(\pm 1)|^2 \leq \frac{2N}{\pi}\|v\|^2$, where $\|v\|^2 = \int_{-1}^{1} v^2 w$.

Proof. Using inequality (2.2) and the fact that $\rho_0 = \rho_N = \frac{\pi}{2N}$, we obtain
$\rho_0 v^2(+1) + \rho_N v^2(-1) = \frac{\pi}{2N}(v^2(+1) + v^2(-1)) \leq \sum_{i=0}^{N} v^2(x_j)\rho_j \leq 2\int_{-1}^{1} v^2 w$.
Therefore, $|v(\pm 1)|^2 \leq \frac{2N}{\pi}\|v\|^2$. □

Proposition 3.6. Let $N \geq 2$. Let B_2 be the Chebyshev spectral collocation matrix defined by (3.16) and λ be an eigenvalue of $-B_2$. Then

$$c \leq |\lambda| \leq CN^4,$$

where c and C are positive and independent of N.

Proof. Let u_h be an eigenvector of $-B_2$ corresponding to λ. Let $v \in P_N$ so that $v(\pm 1) = 0$ and $v(x_h) = M^{-1}u_h$, where M is diagonal with entries of the form $1 - x_j^2$. Define $u(x) = (1 - x^2)v(x) \in P_{N+2}$. Note that $u(x_h) = Mv(x_h) = u_h$. Now

$$\lambda u(x_h) = \lambda u_h = -B_2 u_h = -(M[[D^2]] - 4X[[D]] - 2I_{N-1})M^{-1}v(x_h) = -u^{''}(x_h)$$

by (3.15). Note that $u(\pm 1) = 0 = u^{'}(\pm 1)$. Therefore,

$$\lambda \sum_{j=1}^{N-1} \frac{|u(x_j)|^2}{(1-x_j^2)} \rho_j = -\sum_{j=1}^{N-1} u^{''}(x_j) \frac{\overline{u(x_j)}}{(1-x_j^2)} \rho_j.$$

Since $u^{''}(x) = -2v(x) - 4xv^{'}(x) + (1-x^2)v^{''}(x)$,

$$\begin{aligned}
\lambda \sum_{j=1}^{N-1} |v(x_j)|^2 \rho_j &= \sum_{j=1}^{N-1} \left(2v(x_j) + 4x_j v^{'}(x_j) - (1-x_j^2)v^{''}(x_j)\right) \frac{\overline{v(x_j)}}{(1-x_j^2)} \rho_j \\
&= 2\sum_{j=1}^{N-1} \frac{v(x_j)\overline{v(x_j)}}{(1-x_j^2)} \rho_j + 4\sum_{j=1}^{N-1} \frac{x_j v^{'}(x_j)\overline{v(x_j)}}{(1-x_j^2)} \rho_j - \sum_{j=1}^{N-1} v^{''}(x_j)\overline{v(x_j)} \rho_j.
\end{aligned}$$

$$\begin{aligned}
\lambda \sum_{j=0}^{N} |v(x_j)|^2 \rho_j &= 2\sum_{j=0}^{N} \frac{v(x_j)\overline{v(x_j)}}{(1-x_j^2)} \rho_j + 4\sum_{j=0}^{N} \frac{x_j v^{'}(x_j)\overline{v(x_j)}}{(1-x_j^2)} \rho_j - \sum_{j=0}^{N} v^{''}(x_j)\overline{v(x_j)} \rho_j \\
&\quad - 2\left(\frac{v(x_0)\overline{v(x_0)}}{(1-x_0^2)} \rho_0 + \frac{v(x_N)\overline{v(x_N)}}{(1-x_N^2)} \rho_N\right) \\
&\quad - 4\left(\frac{x_0 v^{'}(x_0)\overline{v(x_0)}}{(1-x_0^2)} \rho_0 + \frac{x_N v^{'}(x_N)\overline{v(x_N)}}{(1-x_N^2)} \rho_N\right).
\end{aligned}$$

We know that $x_0 = 1, x_N = -1$ and $\rho_0 = \rho_N = \frac{\pi}{2N}$.

Therefore, in the first and third sum on the right hand side of the last equality, terms $j = 0$ and $j = N$ are zero. Also, in the second sum of the last equality, terms $j = 0$ and $j = N$ are taken by considering their limits as the denominator is zero. Therefore,

$$\begin{aligned}
\lambda \sum_{j=0}^{N} |v(x_j)|^2 \rho_j &= 2\sum_{j=0}^{N} \frac{v(x_j)\overline{v(x_j)}}{(1-x_j^2)} \rho_j + 4\sum_{j=0}^{N} \frac{x_j v^{'}(x_j)\overline{v(x_j)}}{(1-x_j^2)} \rho_j - \sum_{j=0}^{N} v^{''}(x_j)\overline{v(x_j)} \rho_j \\
&\quad - \frac{\pi}{N}\left(|v^{'}(-1)|^2 - |v^{'}(1)|^2\right).
\end{aligned}$$

Next we move to boundary term estimation. Let $v(x) = (1-x^2)\xi(x)$ with $\xi \in P_{N-2}$. It follows that $v^{'}(1) = -2\xi(1)$ and $v^{'}(-1) = 2\xi(-1)$.

By Lemma 3.3 and Lemma 3.5,

$$|v^{'}(\pm 1)|^2 = 4|\xi(\pm 1)|^2 \leq c(N-2)\|\xi\|^2 = c(N-2)\int_{-1}^{1} \frac{|v|^2 w}{(1-x^2)^2} \leq CN\|v^{'}\|^2.$$

Further, by the inverse estimate, we know that $\|v^{'}\| \leq cN^2\|v\|$. Thus

$$\frac{\pi}{2N}|v^{'}(\pm 1)|^2 \leq CN^4\|v\|^2.$$

Finally, the magnitude of the eigenvalue can be estimated as follows, using the fact that quadrature is exact for polynomials of degree at most $2N-1$ and Lemmas 3.3 and 3.4,

$$\begin{aligned}
|\lambda|\sum_{j=0}^{N}|v(x_j)|^2\rho_j &\leq 2\left|\int_{-1}^{1}\frac{v\overline{v}w}{1-x^2}\right| + 4\left|\int_{-1}^{1}\frac{xv^{'}\overline{v}w}{1-x^2}\right| + \left|\int_{-1}^{1} v^{''}\overline{v}w\right| + CN^4\|v\|^2 \\
&\leq 2\|v\|\left(\int_{-1}^{1}\frac{|v|^2 w}{(1-x^2)^2}\right)^{1/2} + 4\|v^{'}\|\left(\int_{-1}^{1}\frac{|v|^2 w}{(1-x^2)^2}\right)^{1/2} + \left|\int_{-1}^{1} v^{'}(\overline{v}w)^{'}\right| + CN^4\|v\|^2 \\
&\leq C\|v\|\ \|v^{'}\| + CN^2\|v\|\ \|v^{'}\| + 2\|v^{'}\|\ \|\overline{v}^{'}\| + CN^4\|v\|^2 \leq CN^4\|v\|^2.
\end{aligned}$$

Since discrete and weighted L^2-norms are equivalent, $|\lambda| \leq CN^4$.
Now we can estimate the lower bound of $|\lambda|$ as follows. Let $u \in P_N \cap H_0^2(-1,1)$ so that, $u_h = u(x_h)$ is an eigenvector of $-B_2$ with corresponding eigenvalue λ.

$$-u^{''}(x) = \lambda u(x) + \frac{\lambda}{N}(A_0 x^0 T_N^{'}(x) + A_1 x^1 T_N^{'}(x)). \tag{3.23}$$

for some $A_0, A_1 \in \mathbb{C}$. Note that $u^{''} \in P_{N-2}$ and the last term on the right-hand side forces the degree of the polynomial on the right-hand side to be at most $N-2$. Evaluate (3.23) at the collocation points $x_j, 0 \leq j \leq N$ to get

$$-u^{''}(x_j) = \lambda u(x_j) + \frac{\lambda}{N}(A_0 x_j^0 T_N^{'}(x_j) + A_1 x_j^1 T_N^{'}(x_j)). \tag{3.24}$$

Multiply both sides of (3.24) by $\overline{u(x_j)}\rho_j$ and take the sum over $0 \leq j \leq N$ to get

$$-\sum_{j=0}^{N} u^{''}(x_j)\overline{u(x_j)}\rho_j = \lambda \sum_{j=0}^{N} u(x_j)\overline{u(x_j)}\rho_j + \frac{\lambda}{N}\sum_{j=0}^{N}(A_0 x_j^0 T_N^{'}(x_j) + A_1 x_j^1 T_N^{'}(x_j))\overline{u(x_j)}\rho_j. \tag{3.25}$$

Then multiply the complex conjugate of (3.24) by $u(x_j)\rho_j$ and then sum over $0 \leq j \leq N$ to get

$$-\sum_{j=0}^{N} \overline{u^{''}(x_j)}u(x_j)\rho_j = \overline{\lambda}\sum_{j=0}^{N} \overline{u(x_j)}u(x_j)\rho_j + \frac{\overline{\lambda}}{N}\sum_{j=0}^{N}(A_0 x_j^0 T_N^{'}(x_j) + A_1 x_j^1 T_N^{'}(x_j))u(x_j)\rho_j. \tag{3.26}$$

It can be observed that, for any $0 \leq j \leq N$, both $T_N^{'}(x_j)u(x_j)$ and its complex conjugate vanish. By (3.25) and (3.26) we get

$$\begin{aligned} -\sum_{j=0}^{N}\left(u^{''}(x_j)\overline{u(x_j)} + \overline{u^{''}(x_j)}u(x_j)\right)\rho_j &= 2Re\lambda\sum_{j=0}^{N}|u(x_j)|^2\rho_j \\ -Re\left(\sum_{j=0}^{N} u^{''}(x_j)\overline{u(x_j)}\rho_j\right) &= Re\lambda, \end{aligned} \tag{3.27}$$

where $1 = \sum_{j=0}^{N}|u(x_j)|^2\rho_j$ is assumed to be the discrete norm of the eigenvector u_h. Again, recalling that discrete and weighted L^2-norms are equivalent, we may write

$$\sum_{j=0}^{N}|u(x_j)|^2\rho_j \leq C_2\|u\|^2. \tag{3.28}$$

Define

$$f(x) = Re(u^{''}(x)\overline{u(x)}).$$

Let $f(x) = \sum_{k=0}^{2N-2} b_k T_k(x) \in P_{2N-2}$. Thus

$$\begin{aligned}\int_{-1}^{1} f(x)w(x)dx &= \sum_{j=0}^{N} f(x_j)\rho_j \\ &= Re\left(\sum_{j=0}^{N} u^{''}(x_j)\overline{u(x_j)}\rho_j\right).\end{aligned}$$

Therefore, by (3.27)

$$\begin{aligned}-Re\left(\int_{-1}^{1} u^{''}(x)\overline{u(x)}w(x)dx\right) &= Re\left(\int_{-1}^{1} u^{'}(x)(\overline{u(x)}w(x))^{'}dx\right) \\ &\geq \frac{1}{4}\int_{-1}^{1} |u^{'}(x)|^2 w(x)dx \quad (By \quad Lemma \quad 3.4) \\ &\geq C_4 \int_{-1}^{1} |u(x)|^2 w(x)dx \quad (weighted \quad Poincaré \quad inequality) \\ &= C_4\|u\|^2. \qquad (3.29)\end{aligned}$$

By (3.27), (3.28) and (3.29) we get,

$$Re\lambda \geq \frac{C_4}{C_2} := c.$$

Thus, now we have

$$c \leq |\lambda| \leq CN^4.$$

□

Therefore, above properties implies that $-B_2$ has nonzero eigenvalues. Hence, B_2 is invertible. Further, numerically every eigenvlaue λ of $-B_2$ found to be real and positive. Secondly, we consider the Legendre case.

Proposition 3.7. Let $N \geq 2$. Let B_2 be the Legendre spectral collocation matrix and λ be an eigenvalue of $B_h = -B_2$. The eigenvalues of B_h are real and positive, bounded above by CN^4 and bounded away from zero.

Proof. By Lemma (2.7), we know that eigenvalues of $A_h = -[[D]]^2$ are real, bounded below by c and above by CN^4, where c and C are positive and independent of N. We also know that (see [26]) A_h is non-symmetric and A_h can be symmetrized through left-multiplication by a diagonal matrix ($[W]$) with diagonal entries weights. $[W]A_h = S_h$ is symmetric. Define inner product $\langle x, y\rangle = x^T[W]y$. Then it is easy to see that A_h is self-adjoint in this inner product. By the variational characterization of λ_{min}, the smallest eigenvalue of A_h,

$$\lambda_{min} = \inf_{v\in\mathbb{R}^{N-1}} \frac{\langle v, A_h v\rangle}{\langle v, v\rangle} = \inf_{v\in\mathbb{R}^{N-1}} \frac{v^T S_h v}{v^T[W]v} \geq c.$$

Given $v \in \mathbb{R}^{N-1}$. Suppose u is a polynomial of degree N which vanishes at the boundary and $u(x_h) = v$, where x_h denotes all interior collocation points. Let $P_{N,0}$ be all polynomials of degree N such that $u(\pm 1) = 0$. Therefore,

$$\lambda_{min} = \inf_{u\in P_{N,0}} \frac{u(x_h)^T S_h u(x_h)}{u(x_h)^T W u(x_h)} \leq \inf_{\substack{u\in P_{N,0} \\ u'(\pm 1)=0}} \frac{u(x_h)^T S_h u(x_h)}{u(x_h)^T W u(x_h)}.$$

Thus, we can say that the characterization of the minimum eigenvalue of B_h and A_h are the same with the one exception of B_h having an additional constraint $u'(\pm 1) = 0$. That is, the constraint set of B_h is a superset of the constraint set of A_h. Hence we can conclude that eigenvalues of B_h are real and the minimum eigenvalue of B_h is always greater than or equal to the minimum eigenvalue of A_h. In particular, the smallest eigenvalue of B_h is positive and bounded away from zero and B_h is invertible. Also the maximum eigenvalue of B_h is no greater than that of A_h. □

3.3 Navier-Stokes Equations

The Navier–Stokes Equations attracted the limelight with the 1822 paper of C.L.M.H. Navier (Ann. Chim. Phys. 19, 234–245), where he derived equations for homogeneous and incompressible fluids by considering the exerted forces on a fluid particle. The continuum derivation of the Navier-Stokes equations is due to J.C. Saint-Venant (1843) and G.G. Stokes (Trans. Cambridge Philos. Soc. 1845, 8, 287–319). The Navier-Stokes equations are the widely accepted basis for studying fluid dynamics, irrespective of the complexity and the unpredictability of the fluid flow. These equations are at the heart of many branches of engineering and science such as aerodynamics, atmospheric physics, geology and geophysics, oceanography, civil and hydro-engineering, and biology and medicine. The Navier-Stokes equations for an incompressible, homogeneous Newtonian fluid over a bounded domain with a Lipshitz boundary are described by a set of two equations. These involve very basic physics concepts of momentum and mass conservation where equations (3.30) and (3.31) describe the former and latter, respectively;

$$\rho\Big(u_t + (u \cdot \nabla)u\Big) = -\nabla p + \mu\Delta u + f \quad in \quad \Omega, \tag{3.30}$$

$$\nabla \cdot u = 0 \quad in \quad \Omega, \tag{3.31}$$

$$u = 0 \quad on \quad \partial\Omega, \tag{3.32}$$

$$u(x, y, -1) = u_0(x, y) \quad in \quad \Omega. \tag{3.33}$$

In the equations above, u represents the velocity vector, p is the pressure, and both are functions of space and time. In practical applications, μ and ρ are assumed to be positive constants, which represent the viscosity and density of the fluid, respectively. These equations are formulated by considering fluid as a continuum. They are used to model weather, airflow around a wing and the study of the flow of blood in a body, etc. Although they are very significant, fundamental issues such as the

existence, uniqueness and regularity of a solution in three dimensions are still open. Consequently, they are studied widely by many researchers.

Now let us consider the non-dimensionalization of the Navier-Stokes equations. As the name suggests, we derive a dimensionless version of the Navier-Stokes equations. Characteristic length L, characteristic velocity U, fluid density ρ and viscosity $\nu = \frac{\mu}{\rho}$ are used to construct dimensionless quantities. Using these references, we define

$$\overline{u} = u/U, \quad \overline{p} = p/\rho U^2, \quad \overline{x} = x/L, \quad \overline{t} = tU/L, \quad and \quad \overline{f} = Lf/U^2,$$

where a bar above each symbol denotes the non-dimensional character corresponding to each of the quantities. Then the momentum equation (3.30) can now be written as,

$$u_t + (u \cdot \nabla)u + \nabla p - \frac{1}{Re}\Delta u = f. \tag{3.34}$$

Here, we have adopted the dimensional symbols to conveniently denote corresponding non-dimensional variables.

The non-dimensional quantity $\frac{LU}{\nu}$ is known as the Reynolds number and is denoted by the symbol Re. This non-dimensional number plays a pivotal role in fluid dynamics. The magnitude of Re is an indication to how significant inertial forces are compared to viscous forces. For $Re \ll 1$, it is possible to neglect the non-linearity (inertial effects) and the Navier-Stokes equations reduce to the Stokes equations. Fluid flow can be identified under two categories. At low Re, the flow is considered to be laminar, which means sheetlike flow. In this case, fluid particles flow in an orderly, predictable manner. However, as Re increases, the flow tends to be more complex. In many flows of interest, Re is substantially large. For example, river flows and tidal waves have Reynolds numbers as high as $Re \approx 10^7$. When $Re \gg 1$, the flow

typically becomes turbulent.

Similarly to the Stokes problem, it can be shown that a stream function model can be obtained for the Navier-Stokes equations as well in the 2D case. By taking the curl and using $u = \frac{\partial \psi}{\partial y}\underline{i} - \frac{\partial \psi}{\partial x}\underline{j}$, we can obtain the stream function form;

$$-\Delta\psi_t + \frac{1}{Re}\Delta^2\psi - \psi_y\psi_{xxx} + \psi_x\psi_{yyy} + \psi_x\psi_{yxx} - \psi_y\psi_{xyy} = f_{2x} - f_{1y} \quad in \quad \Omega, \quad (3.35)$$

$$\psi = \frac{\partial \psi}{\partial \nu} = 0 \quad on \quad \partial\Omega, \quad (3.36)$$

$$\psi(x, y, -1) = \psi_0(x, y) \quad in \quad \Omega. \quad (3.37)$$

3.4 Space-time spectral methods for Navier-Stokes Equations

In this section, we discuss space-time spectral method for the stream function form of the Navier-stokes equation. First consider the steady Navier-Stokes equation:

$$\frac{1}{Re}\Delta^2\psi - \psi_y\psi_{xxx} + \psi_x\psi_{yyy} + \psi_x\psi_{yxx} - \psi_y\psi_{xyy} = f,$$

with homogeneous Dirichlet boundary conditions. A spectral scheme is

$$\begin{aligned}
&\frac{1}{Re}\Big((D^4 \otimes I_{N+1}) + (I_{N+1} \otimes D^4) + 2(D^2 \otimes D^2)\Big)\psi_h \\
&- diag\Big((I_{N+1} \otimes D)\psi_h\Big)(D^3 \otimes I_{N+1})\psi_h + diag\Big((D \otimes I_{N+1})\psi_h\Big)(I_{N+1} \otimes D^3)\psi_h \\
&+ diag\Big((D \otimes I_{N+1})\psi_h\Big)(D^2 \otimes D)\psi_h - diag\Big((I_{N+1} \otimes D)\psi_h\Big)(D \otimes D^2)\psi_h = f_h,
\end{aligned}$$

where ψ_h and f_h are the vectors of ψ and f, respectively, evaluated at the collocation points. Let B_2 be the spectral second derivative (3.16) and B_4 be the spectral fourth derivative (3.18) defined for the 1D Stokes problem.

Similarly, we can derive a spectral approximation for the third derivative with zero Dirichlet boundary conditions. Let Z be a polynomial vanishing at the boundary and $\psi(x) = (1-x^2)Z(x)$. Then

$$\psi^{'''}(x) = (1-x^2)Z^{'''}(x) - 6xZ^{''}(x) - 6Z^{'}(x). \tag{3.38}$$

Then, the spectral approximation of the third derivative satisfying the four boundary conditions is

$$B_3 := (M[[D^3]] - 6X[[D^2]] - 6[[D]])M^{-1}. \tag{3.39}$$

The final scheme can be written as

$$\begin{aligned}
&\frac{1}{Re}\Big((B_4 \otimes I_{N-1}) + (I_{N-1} \otimes B_4) + 2(B_2 \otimes B_2)\Big)\hat{\psi}_h \\
&- diag\Big((I_{N-1} \otimes [[D]])\hat{\psi}_h\Big)(B_3 \otimes I_{N-1})\hat{\psi}_h + diag\Big(([[D]] \otimes I_{N-1})\hat{\psi}_h\Big)(I_{N-1} \otimes B_3)\hat{\psi}_h \\
&+ diag\Big(([[D]] \otimes I_{N-1})\hat{\psi}_h\Big)(B_2 \otimes [[D]])\hat{\psi}_h - diag\Big((I_{N-1} \otimes [[D]])\hat{\psi}_h\Big)([[D]] \otimes B_2)\hat{\psi}_h \\
&= \hat{f}_h,
\end{aligned}$$

where known boundary values have been removed. This nonlinear system can be solved using an iterative algorithm, where each iteration requires the solution of a linear equation as suggested below. Below $k \geq 0$ is the iteration number:

$$\begin{aligned}
&\frac{1}{Re}\Big((B_4 \otimes I_{N-1}) + (I_{N-1} \otimes B_4) + 2(B_2 \otimes B_2)\Big)\hat{\psi}_h^{k+1} \\
&- diag\Big((I_{N-1} \otimes [[D]])\hat{\psi}_h^{k}\Big)(B_3 \otimes I_{N-1})\hat{\psi}_h^{k+1} + diag\Big(([[D]] \otimes I_{N-1})\hat{\psi}_h^{k}\Big)(I_{N-1} \otimes B_3)\hat{\psi}_h^{k+1} \\
&+ diag\Big(([[D]] \otimes I_{N-1})\hat{\psi}_h^{k}\Big)(B_2 \otimes [[D]])\hat{\psi}_h^{k+1} - diag\Big((I_{N-1} \otimes [[D]])\hat{\psi}_h^{k}\Big)([[D]] \otimes B_2)\hat{\psi}_h^{k+1} \\
&= \hat{f}_h.
\end{aligned} \tag{3.40}$$

Now, consider the stream function form of the unsteady Navier-Stokes equation:

$$-\Delta\psi_t + \frac{1}{Re}\Delta^2\psi - \psi_y\psi_{xxx} + \psi_x\psi_{yyy} + \psi_x\psi_{yxx} - \psi_y\psi_{xyy} = f,$$

with initial condition $\psi(x, y, -1) = \psi_0(x, y)$ and homogeneous Dirichlet boundary conditions. A spectral scheme based on the space-time collocation method is

$$\begin{aligned}
&-\Big\{D \otimes \Big((D^2 \otimes I_{N+1}) + (I_{N+1} \otimes D^2)\Big)\Big\}\psi_h + \frac{1}{Re}\Big\{I_{N+1} \otimes \Big((D^4 \otimes I_{N+1}) + (I_{N+1} \otimes D^4)\\
&+ 2(D^2 \otimes D^2)\Big)\Big\}\psi_h - diag\Big(I_{N+1} \otimes (I_{N+1} \otimes D)\psi_h\Big)(I_{N+1} \otimes (D^3 \otimes I_{N+1}))\psi_h\\
&+ diag\Big(I_{N+1} \otimes (D \otimes I_{N+1})\psi_h\Big)(I_{N+1} \otimes (I_{N+1} \otimes D^3))\psi_h\\
&+ diag\Big(I_{N+1} \otimes (D \otimes I_{N+1})\psi_h\Big)(I_{N+1} \otimes (D^2 \otimes D))\psi_h\\
&- diag\Big(I_{N+1} \otimes (I_{N+1} \otimes D)\psi_h\Big)(I_{N+1} \otimes (D \otimes D^2))\psi_h = f_h,
\end{aligned}$$

where ψ_h and f_h are the vectors of ψ and f, respectively, evaluated at the collocation points. Let B_2 be the spectral second derivative (3.16), B_3 be the spectral third derivative (3.35) and B_4 be the spectral fourth derivative (3.18) defined above.

Finally we may write

$$\begin{aligned}
&-\Big\{[D] \otimes \Big((B_2 \otimes I_{N-1}) + (I_{N-1} \otimes B_2)\Big)\Big\}\hat{\psi}_h + \frac{1}{Re}\Big\{I_N \otimes \Big((B_4 \otimes I_{N-1}) + (I_{N-1} \otimes B_4)\\
&+ 2(B_2 \otimes B_2)\Big)\Big\}\hat{\psi}_h - diag\Big(I_N \otimes (I_{N-1} \otimes [[D]])\hat{\psi}_h\Big)(I_N \otimes (B_3 \otimes I_{N-1}))\hat{\psi}_h\\
&+ diag\Big(I_N \otimes ([[D]] \otimes I_{N-1})\hat{\psi}_h\Big)(I_N \otimes (I_{N-1} \otimes B_3))\hat{\psi}_h\\
&+ diag\Big(I_N \otimes ([[D]] \otimes I_{N-1})\hat{\psi}_h\Big)(I_N \otimes (B_2 \otimes [[D]]))\hat{\psi}_h\\
&- diag\Big(I_N \otimes (I_{N-1} \otimes [[D]])\hat{\psi}_h\Big)(I_N \otimes ([[D]] \otimes B_2))\hat{\psi}_h = \hat{f}_h - (d_h \otimes \psi_{0h}).
\end{aligned}$$

Here, the known boundary and initial values have been removed. This nonlinear system can be linearized by replacing one variable by an old iterate in nonlinear

terms. Then a simple fixed point iteration ($k \geq 0$) can be used to solve it.

$$A_k \psi_h^{k+1} = \widetilde{f}_h,$$

where $\widetilde{f}_h = \hat{f}_h - (d_h \otimes \psi_{0h})$ and

$$\begin{aligned} A_k = &-[D] \otimes \Big((B_2 \otimes I_{N-1}) + (I_{N-1} \otimes B_2)\Big) + \frac{1}{Re} I_N \otimes \Big((B_4 \otimes I_{N-1}) + (I_{N-1} \otimes B_4) \\ &+ 2(B_2 \otimes B_2)\Big) - diag\Big(I_N \otimes (I_{N-1} \otimes [[D]])\hat{\psi}_h^k\Big)(I_N \otimes (B_3 \otimes I_{N-1})) \\ &+ diag\Big(I_N \otimes ([[D]] \otimes I_{N-1})\hat{\psi}_h^k\Big)(I_N \otimes (I_{N-1} \otimes B_3)) \\ &+ diag\Big(I_N \otimes ([[D]] \otimes I_{N-1})\hat{\psi}_h^k\Big)(I_N \otimes (B_2 \otimes [[D]])) \\ &- diag\Big(I_N \otimes (I_{N-1} \otimes [[D]])\hat{\psi}_h^k\Big)(I_N \otimes ([[D]] \otimes B_2)). \end{aligned}$$

This iterative formula can be solved using a relaxation method. The concept behind relaxation is to use a relaxation parameter γ in order to reduce the number of iterations required. The iteration process for the model problem $u = F(u)$ is

$$\begin{aligned} \widetilde{u}^{k+1} &= F(u^k) \\ u^{k+1} &= \gamma u^k + (1-\gamma)\widetilde{u}^{k+1}. \end{aligned}$$

For the Navier-Stokes equations, a relaxation method is

$$\psi_h^{k+1} = \gamma \psi_h^k + (1-\gamma) A_k^{-1} \widetilde{f}_h.$$

We tested our program for the $0 \leq \gamma \leq 0.5$ and observed faster convergence when γ is small. However, the improvement is not significant. Furthermore, the iteration is divergent when the Re is large. In chapter 5, we shall discuss nonlinear preconditioning techniques that are able to simulate the Navier-Stokes equations at high Reynolds numbers.

4

Magnetohydrodynamics Equations

Magnetohydrodynamics (MHD) equations describe the motion of an electrically conducting fluid. Navier-Stokes equations, the equations for fluids, were described in the last chapter. In the first section of this chapter, we discuss the Maxwell's equations, the governing equations for electromagnetism. This will be followed by an exposition of MHD. In section 4.3, we examine a space-time spectral method for MHD.

4.1 Electromagnetism

Electromagnetism primarily deals with electromagnetic forces that occur between electrically charged particles. Electromagnetism, as the name suggests, describes the coexistence of electricity and magnetism. As Michael Faraday discovered, electricity is generated when a change of magnetic flux occurs in the presence of an electrical conductor. After some time, it was found that the inverse of this is also true, i.e., the flow of electricity through a conductor creates a magnetic field around it. The right-hand rule can be used to find the direction of the magnetic field. The electromagnetic force is a highly significant, commonly occurring, fundamental force of nature. It plays, for lack of a better word, an indispensable role in the universe. Matter only exists because of the electromagnetic forces that exist at the atomic

level. These electromagnetic forces act between charged particles and are a combination of both electrical and magnetic forces. Similar to electric and magnetic forces, electromagnetic forces can be attractive or repulsive. In the 1860s, James Clerk Maxwell published a series of papers that introduced the four Maxwell's equations, which describe how electromagnetism works.

In the next section, we will give a quick introduction to Maxwell's equations.

4.1.1 Maxwell's equations

Maxwell's equations are a set of four PDEs that describe how electromagnetism behaves. The equations are named after the renowned physicist James Clerk Maxwell (1831-1878). Maxwell's equations govern how electric and magnetic fields interact. The four equations thereof consist of Gauss's Electric Field Law, Gauss's Magnetic Field Law, Faraday's Law and the Ampere Maxwell Law. Maxwell was one of the first people to realize that light is actually an electromagnetic wave. Maxwell's equations were later simplified by Oliver Heaviside and Josiah Willard Gibbs and the simplified version of Maxwell's equations is shown below.

$$\nabla \cdot E = \frac{\rho}{\epsilon_0} \quad Gauss's \;\; Electric \;\; Field \;\; Law$$

$$\nabla \cdot B = 0 \quad Gauss's \;\; Magnetic \;\; Field \;\; Law$$

$$\nabla \times B = \mu_0\Big(J + \epsilon_0 \frac{\partial E}{\partial t}\Big) \quad Ampère - Maxwell \;\; Law$$

$$\nabla \times E = -\frac{\partial B}{\partial t} \quad Maxwell - Faraday \;\; Law$$

where the vector functions E and B are usually called electric field (volt/meter) and magnetic induction (tesla), respectively.

The universal constants ϵ_0 and μ_0 are the permittivity of free space and the permeability of free space respectively. These electromagnetic fields are generated by two

sources related to the continuity equation

$$\nabla \cdot J + \frac{\partial \rho}{\partial t} = 0,$$

where

J: electric current density (ampere/meter^2),

ρ: electric charge density (coulomb/meter^3).

I will now very briefly explain what each of those equations means. Gauss's Electric Field Law defines the relation between charge and electric field. This basically states that the net outflow of an electric field through some closed surface will be proportional to the charge enclosed by the surface. The next equation, which is Gauss's Magnetic Law, defines the relationship between magnetic poles and the magnetic field. This equation simply states that the magnetic flux through any Gaussian surface is zero. Consequently, this explains that unlike electrical positive or negative electrical charges that can exist alone, magnetic mono-poles do not exist. The third equation, which is the Ampere-Maxwell Law, describes the magnetic fields produced by varying electric currents. The equation explains that magnetic fields can be generated by either electrical current or by changing an electrical field. The last equation, Maxwell-Faraday Law, states that a time-varying magnetic field induces a time-varying electric field and vice versa.

4.2 Magnetohydrodynamics

4.2.1 Brief history of MHD

The study of magnetism and fluids have been around since the 19th century. However, the study of magnetism in conducting fluids did not attract much attention until the 20th century as there was little to no incentive for engineers and scientists

to study it. Magnetohydrodynamics, popularly known by its abbreviation MHD, did attract some attention from researchers such as Michael Faraday during the 19th century, but there simply were not enough practical applications at the time for the subject. After all, electricity and electromagnetism were capturing most of the attention at the time. After Michael Faraday had introduced magnetic induced electricity, geophysicists had started to suspect that the magnetic field of the earth was created within the liquid metal core due to a dynamo-like action. At the early stages of the 19th century, an engineer named J. Hartman, who was studying MHD at the time, developed the electromagnetic pump in 1918. He also carried out numerous experiments regarding the flow of mercury through magnetic fields. Today Hartman is widely considered to be the father of liquid-metal MHD. Things however started to change and by the 1940s, physicists realized that magnetic fields and plasma were omnipresent throughout the universe. The discovery of the Alfven wave in 1942 made MHD a field of much more interest among physicists and engineering applications started developing step by step. During the 1950s, physicists who study plasma showed an interest in the stability (or lack thereof) of plasma confined by magnetic fields. Half a century later, magnetic fields are widely used to induce various movements in liquid metals in various branches of engineering and the MHD concepts are at the heart of them.

4.2.2 What is MHD?

The term Magnetohydrodynamics is derived from combining three words, magneto-hydro-dynamics. Here, "magneto" means magnetic fields, "hydro" means water or fluids and "dynamics" means movement. Hence, it is evident that magnetohydrodynamics or MHD is the study of interactions between conductive fluids moving in magnetic fields. The interaction between a magnetic field B, and a velocity field u, arises as a combined result of Faraday and Ampere laws and, Lorentz force applied

to a current-carrying body.

At the heart of MHD studies are two of the most ingenious sets of equations, Maxwell's equations and Navier-Stokes equations. In 1942, Hannes Alfven proposed an uncanny idea that a mathematical theory could be obtained by coupling Maxwell's and Navier-Stokes equations together. Though unorthodox at first, this new mathematical theory was able to successfully explain the macroscopic behavior of plasmas in a variety of laboratory experiments. MHD theory has been able to help us understand a variety of natural phenomena such as plasmas in the earth and solar astrophysics.

The MHD equations are not onefold. The coupling between the electric field, Ohms law and current density will vary according to the underlying assumptions. Therefore, different formulations of the MHD equations exist. Three very popular formulations are ideal MHD, resistive MHD and Hall MHD.

Ideal MHD assumes the fluid in question to have negligible resistivity and therefore is considered to have perfect conductance. This is the simplest form of the MHD equations. Ideal MHD equations are obtained by making Reynolds number Re and magnetic Reynolds number Re_m approach infinity. The ideal MHD equations are,

$$\partial_t u + (u \cdot \nabla)u - (B \cdot \nabla)B + \nabla p = 0, \tag{4.1}$$

$$\partial_t B + (u \cdot \nabla)B - (B \cdot \nabla)u = 0, \tag{4.2}$$

$$\nabla \cdot u = \nabla \cdot B = 0. \tag{4.3}$$

Three conservation laws are present in the ideal MHD. These laws give us a sense of the solution class we are working with. The *total energy* and *cross helicity* can be obtained by directly comparing the MHD equations with the Euler equation. For

smooth solutions of ideal MHD, the total energy

$$\varepsilon(t) = \frac{1}{2}\int_{\mathbb{T}^2} |u(x,t)|^2 + |B(x,t)|^2 dx,$$

gives the only known conserved quantity, where $\mathbb{T}^2$ is the two dimensional periodic box. The ideal MHD equations (4.1-4.3) can be re-written using Elsasser variables to obtain that $\varepsilon(t)$ is a constant function of time. Let

$$z_+ = u + B \quad and \quad z_- = u - B. \tag{4.4}$$

Therefore, the system of equations (4.1-4.3) becomes,

$$\partial_t z_\pm + (z_\mp \cdot \nabla) z_\pm + \nabla q = 0, \;\; q = p + \frac{|B|^2}{2},$$
$$div\ z_\pm = 0.$$

Assume that both z_+ and z_- are incompressible. Then by integrating over $\mathbb{T}^2$, we obtain that if $u, B \in C_t^1 C_x^1$ (and thus $z_\pm \in C_t^1 C_x^1$), then

$$\frac{d}{dt}\int_{\mathbb{T}^2} |z_+(x,t)|^2 = \frac{d}{dt}\int_{\mathbb{T}^2} |z_-(x,t)|^2 = 0. \tag{4.5}$$

Further, from (4.4) we get that

$$\varepsilon(t) = \frac{1}{4}\int_{\mathbb{T}^2} |z_+(x,t)|^2 + |z_-(x,t)|^2.$$

We can show that ε is conserved for smooth solutions by combining the above equality with (4.5).

In addition to the total energy, the MHD equations have another Elsaasser invariant,

the cross helicity

$$\mathcal{H}_{\omega,B}(t) = \int_{\mathbb{T}^2} u(x,t) \cdot B(x,t)dx = \frac{1}{4}\int_{\mathbb{T}^2} \left(|z_+(x,t)|^2 - |z_-(x,t)|^2\right) dx, \tag{4.6}$$

where $\omega = \nabla \times u$ is the vorticity.

Again, (4.5) shows that $\mathcal{H}_{\omega,B}$ is conserved for smooth solutions. Finally, conservation of the magnetic helicity is defined as

$$\mathcal{H}_{B,B}(t) = \int_{\mathbb{T}^2} A(\cdot,t) \cdot B(\cdot,t), \tag{4.7}$$

where A is a zero mean periodic vector potential field for B, such that $curl A = B$. Since B is incompressible and $\mathbb{T}^2$ is a simply connected domain, magnetic helicity ($\mathcal{H}_{B,B}(t)$) is independent of the gradient part of A. Therefore, A can be chosen so that $A = \nabla \times (-\Delta)^{-1}B$ when $div\, A = 0$. For smooth solutions (u, B) of system (4.1-4.3) we have

$$\frac{d}{dt}\mathcal{H}_{B,B} = 0. \tag{4.8}$$

Since $div\, u = 0 = div\, B$ and the Biot-Savart operator $B \longmapsto A$ is self-adjoint we can rewrite $B \cdot \nabla u - u \cdot \nabla B = \nabla \times (u \times B) = \partial_t B$. Using integration by parts,

$$\begin{aligned}
\frac{d}{dt}\mathcal{H}_{B,B} &= 2\int_{\mathbb{T}^2} (\nabla \times (-\Delta)^{-1}B) \cdot \partial_t B \\
&= 2\int_{\mathbb{T}^2} (\nabla \times (-\Delta)^{-1}B) \cdot (\nabla \times (u \times B)) \\
&= 2\int_{\mathbb{T}^2} \nabla \times (\nabla \times (-\Delta)^{-1}B) \cdot (u \times B) = 2\int_{\mathbb{T}^2} (\nabla \times A) \cdot (u \times B) \\
&= 2\int_{\mathbb{T}^2} B \cdot (u \times B) = 0.
\end{aligned}$$

Now consider the resistive MHD, which is a system of nonlinear PDEs that describes three basic concepts of mass, momentum and energy conservation coupled with Faraday's Law of Induction. In this resistive MHD model, a single velocity and pressure field is used to describe both electrons and ions. This model does not have the finite Larmor radius effect when applying to a magnetized plasma. In comparison to macroscopic length scales, the plasma particle collision length is considered to be small. This chapter develops space-time spectral methods for the resistive MHD equations. When the magnetic Reynolds number increases, the hyperbolic terms in the resistive MHD tend to overwhelm other terms. This hyperbolic portion of the resistive MHD produces three different MHD wave modes, namely, Alfven wave, Slow MHD wave and Fast MHD wave.

Lastly, let us very briefly discuss Hall MHD, which is applicable for studying plasma dynamics with length scales greater than the electron inertial length and less than the ion inertial scale length. On these scales, ions move relative to the magnetic field but electrons do not. Hall MHD is very useful to model and comprehend numerous space and laboratory plasma phenomena such as sub-Alfven plasma expansions and magnetic reconnection.

For the purpose of this study, we consider the resistive MHD equations henceforth.

4.2.3 Governing equations for MHD

The governing equations for MHD are derived by coupling electromagnetism and fluid dynamics. As we mentioned above, we will consider only resistive MHD. The resultant PDEs, so-called resistive MHD equations, are

$$u_t + (u \cdot \nabla)u + \nabla p = \frac{1}{Re}\Delta u + (\nabla \times B) \times B + f \quad in \quad \Omega, \tag{4.9}$$

$$\nabla \cdot u = 0 \quad in \quad \Omega, \tag{4.10}$$

$$B_t + \frac{1}{Re_m}\nabla \times (\nabla \times B) = \nabla \times (u \times B) + g \quad in \quad \Omega, \tag{4.11}$$

$$\nabla \cdot B = 0 \quad in \quad \Omega. \tag{4.12}$$

Here, the unknowns are fluid velocity u, fluid pressure p and magnetic field B, and f and g are given. The usual Reynolds number Re and the magnetic Reynolds number Re_m are dimensionless parameters. The magnetic Reynolds number is defined as $Re_m = \frac{\mu_0 UL}{\eta}$, where μ_0 is the free space magnetic permeability, η is the magnetic resistivity, and U and L are characteristic velocity and length scales, respectively. First boundary condition is $u = 0$. Second boundary condition is $\nu \cdot B = 0$ and $\nu \times (\nabla \times B)$ for a perfectly conducting boundary.

Similar to the Stokes problem, it can be shown that a stream function formulation can be obtained for the resistive MHD equations as well. Here, we treat u, B, f and g as a vectors with two components: $u = [u_1, u_2]^T$, $B = [\widetilde{B}_1, \widetilde{B}_2]^T$, $f = [f_1, f_2]^T$ and $g = [g_1, g_2]^T$. Then we define a fluid stream function $\psi : \mathbf{R}^2 \to \mathbf{R}$ such that $u_1 = \frac{\partial \psi}{\partial y}$, $u_2 = -\frac{\partial \psi}{\partial x}$ and magnetic stream function $\phi : \mathbf{R}^2 \to \mathbf{R}$ such that $\widetilde{B}_1 = \frac{\partial \phi}{\partial y}$, $\widetilde{B}_2 = -\frac{\partial \phi}{\partial x}$. The boundary conditions for ψ become $\psi = \frac{\partial \psi}{\partial \nu} = 0$ while those for ϕ are $\phi = \Delta\phi = 0$.

Now, by taking the curl and using stream functions ψ and ϕ we can obtain the stream function model without a pressure term for the non-dimensionalization resistive MHD. Further, the number of unknown functions reduces from five $(u_1, u_2, p, \widetilde{B}_1, \widetilde{B}_2)$

to two (ψ, ϕ). The full system is

$$-\Delta\psi_t + \frac{1}{Re}\Delta^2\psi - \psi_y\psi_{xxx} + \psi_x\psi_{yyy} + \psi_x\psi_{yxx} - \psi_y\psi_{xyy} = \phi_{yxx}\phi_x + \phi_{yyy}\phi_x$$
$$-\phi_{xxx}\phi_y - \phi_{xyy}\phi_y + f_{2x} - f_{1y} \quad in \quad \Omega, \tag{4.13}$$

$$\psi = \frac{\partial\psi}{\partial\nu} = 0 \quad on \quad \partial\Omega, \tag{4.14}$$

$$\psi(x, y, -1) = \psi_0(x, y) \quad in \quad \Omega, \tag{4.15}$$

$$-\Delta\phi_t + \frac{1}{Re_m}\Delta^2\phi = \psi_{xxy}\phi_x - \psi_x\phi_{xxy} + \psi_y\phi_{yyx} - \psi_{yyx}\phi_y + \psi_y\phi_{xxx} - \psi_x\phi_{yyy} + \psi_{yyy}\phi_x$$
$$-\psi_{xxx}\phi_y + 2\psi_{xy}\phi_{xx} - 2\psi_{xx}\phi_{xy} + 2\psi_{yy}\phi_{yx} - 2\psi_{yx}\phi_{yy} + g_{2x} - g_{1y} \quad in \quad \Omega, \tag{4.16}$$

$$\phi = \Delta\phi = 0 \quad on \quad \partial\Omega, \tag{4.17}$$

$$\phi(x, y, -1) = \phi_0(x, y) \quad in \quad \Omega. \tag{4.18}$$

4.3 Space-time spectral methods for MHD

In this section, we discuss space-time spectral method for the stream function form of the resistive MHD equation. First consider the steady case:

$$\begin{aligned}\frac{1}{Re}\Delta^2\psi - \psi_y\psi_{xxx} + \psi_x\psi_{yyy} + \psi_x\psi_{yxx} - \psi_y\psi_{xyy} &= \phi_{yxx}\phi_x + \phi_{yyy}\phi_x \\ -\phi_{xxx}\phi_y - \phi_{xyy}\phi_y + f,& \\ \frac{1}{Re_m}\Delta^2\phi = \psi_{xxy}\phi_x - \psi_x\phi_{xxy} + \psi_y\phi_{yyx} - \psi_{yyx}\phi_y + \psi_y\phi_{xxx} - \psi_x\phi_{yyy} + \psi_{yyy}\phi_x& \\ -\psi_{xxx}\phi_y + 2\psi_{xy}\phi_{xx} - 2\psi_{xx}\phi_{xy} + 2\psi_{yy}\phi_{yx} - 2\psi_{yx}\phi_{yy} + g,&\end{aligned}$$

with the set of boundary conditions (4.14) and (4.17). Since the boundary conditions for ϕ are $\phi = \Delta\phi = 0$, we introduce a new variable $\Phi = -\Delta\phi$. Therefore, above stream function formulation can be re-written as follows.

$$\begin{aligned}\frac{1}{Re}\Delta^2\psi - \psi_y\psi_{xxx} + \psi_x\psi_{yyy} + \psi_x\psi_{yxx} - \psi_y\psi_{xyy} &= \Phi_y(\Delta^{-1}\Phi)_x - \Phi_x(\Delta^{-1}\Phi)_y + f, \\ -\frac{1}{Re_m}\Delta\Phi = \psi_x\Phi_y - \psi_y\Phi_x - (\psi_{xxy} + \psi_{yyy})(\Delta^{-1}\Phi)_x + (\psi_{yyx} + \psi_{xxx})(\Delta^{-1}\Phi)_y + 2\psi_{xy}\Phi& \\ -4\psi_{xy}(\Delta^{-1}\Phi)_{xx} + 2(\psi_{xx} - \psi_{yy})(\Delta^{-1}\Phi)_{xy} + g.&\end{aligned}$$

A spectral scheme is

$$\begin{aligned}&\frac{1}{Re}\Big((D^4 \otimes I_{N+1}) + (I_{N+1} \otimes D^4) + 2(D^2 \otimes D^2)\Big)\psi_h \\ &- diag\Big((I_{N+1} \otimes D)\psi_h\Big)(D^3 \otimes I_{N+1})\psi_h + diag\Big((D \otimes I_{N+1})\psi_h\Big)(I_{N+1} \otimes D^3)\psi_h \\ &+ diag\Big((D \otimes I_{N+1})\psi_h\Big)(D^2 \otimes D)\psi_h - diag\Big((I_{N+1} \otimes D)\psi_h\Big)(D \otimes D^2)\psi_h \\ &= \Big((I_{N+1} \otimes D)\Phi_h\Big)(D \otimes I_{N+1})\Big((D^2 \otimes I_{N+1}) + (I_{N+1} \otimes D^2)\Big)^{-1}\Phi_h \\ &- \Big((D \otimes I_{N+1})\Phi_h\Big)(I_{N+1} \otimes D)\Big((D^2 \otimes I_{N+1}) + (I_{N+1} \otimes D^2)\Big)^{-1}\Phi_h + f_h,\end{aligned}$$

$$
\begin{aligned}
&-\frac{1}{Re_m}\Big((D^2\otimes I_{N+1})+(I_{N+1}\otimes D^2)\Big)\Phi_h = diag\Big((D\otimes I_{N+1})\psi_h\Big)(I_{N+1}\otimes D)\Phi_h\\
&-diag\Big((I_{N+1}\otimes D)\psi_h\Big)(D\otimes I_{N+1})\Phi_h\\
&-diag\Big((D^2\otimes D)\psi_h+(I_{N+1}\otimes D^3)\psi_h\Big)(D\otimes I_{N+1})\Big((D^2\otimes I_{N+1})+(I_{N+1}\otimes D^2)\Big)^{-1}\Phi_h\\
&+diag\Big((D\otimes D^2)\psi_h+(D^3\otimes I_{N+1})\psi_h\Big)(I_{N+1}\otimes D)\Big((D^2\otimes I_{N+1})+(I_{N+1}\otimes D^2)\Big)^{-1}\Phi_h\\
&+2diag\Big((D\otimes D)\psi_h\Big)\Phi_h-4diag\Big((D\otimes D)\psi_h\Big)(D^2\otimes I_{N+1})\Big((D^2\otimes I_{N+1})+(I_{N+1}\otimes D^2)\Big)^{-1}\Phi_h\\
&+2diag\Big((I_{N+1}\otimes D^2)\psi_h-(D^2\otimes I_{N+1})\psi_h\Big)(D\otimes D)\Big((D^2\otimes I_{N+1})+(I_{N+1}\otimes D^2)\Big)^{-1}\Phi_h+g_h,
\end{aligned}
$$

where ψ_h, Φ_h, f_h and g_h are the vectors of ψ, Φ, f, and g respectively, evaluated at the collocation points. Let B_2 be the spectral second derivative (3.16), B_3 be the spectral third derivative (3.39) and B_4 be the spectral fourth derivative (3.18). Finally we may write

$$
\begin{aligned}
&\frac{1}{Re}\Big((B_4\otimes I_{N-1})+(I_{N-1}\otimes B_4)+2(B_2\otimes B_2)\Big)\hat{\psi}_h\\
&-diag\Big((I_{N-1}\otimes[[D]])\hat{\psi}_h\Big)(B_3\otimes I_{N-1})\hat{\psi}_h+diag\Big(([[D]]\otimes I_{N-1})\hat{\psi}_h\Big)(I_{N-1}\otimes B_3)\hat{\psi}_h\\
&+diag\Big(([[D]]\otimes I_{N-1})\hat{\psi}_h\Big)(B_2\otimes[[D]])\hat{\psi}_h-diag\Big((I_{N-1}\otimes[[D]])\hat{\psi}_h\Big)([[D]]\otimes B_2)\hat{\psi}_h\\
&=\Big((I_{N-1}\otimes[[D]])\hat{\Phi}_h\Big)([[D]]\otimes I_{N-1})\Big(([[D^2]]\otimes I_{N-1})+(I_{N-1}\otimes[[D^2]])\Big)^{-1}\hat{\Phi}_h\\
&-\Big(([[D]]\otimes I_{N-1})\hat{\Phi}_h\Big)(I_{N-1}\otimes[[D]])\Big(([[D^2]]\otimes I_{N-1})+(I_{N-1}\otimes[[D^2]])\Big)^{-1}\hat{\Phi}_h+\hat{f}_h,
\end{aligned}
$$

$$
\begin{aligned}
&- \frac{1}{Re_m}\Big(([[D^2]] \otimes I_{N-1}) + (I_{N-1} \otimes [[D^2]])\Big)\hat{\Phi}_h = diag\Big(([[D]] \otimes I_{N-1})\hat{\psi}_h\Big)(I_{N-1} \otimes [[D]])\hat{\Phi}_h \\
&- diag\Big((I_{N-1} \otimes [[D]])\hat{\psi}_h\Big)([[D]] \otimes I_{N-1})\hat{\Phi}_h \\
&- diag\Big((B_2 \otimes [[D]])\hat{\psi}_h + (I_{N-1} \otimes B_3)\hat{\psi}_h\Big)([[D]] \otimes I_{N-1})\Big(([[D^2]] \otimes I_{N-1}) + (I_{N-1} \otimes [[D^2]])\Big)^{-1}\hat{\Phi}_h \\
&+ diag\Big(([[D]] \otimes B_2)\hat{\psi}_h + (B_3 \otimes I_{N-1})\hat{\psi}_h\Big)(I_{N-1} \otimes [[D]])\Big(([[D^2]] \otimes I_{N-1}) + (I_{N-1} \otimes [[D^2]])\Big)^{-1}\hat{\Phi}_h \\
&+ 2diag\Big(([[D]] \otimes [[D]])\hat{\psi}_h\Big)\hat{\Phi}_h \\
&- 4diag\Big(([[D]] \otimes [[D]])\hat{\psi}_h\Big)([[D^2]] \otimes I_{N-1})\Big(([[D^2]] \otimes I_{N-1}) + (I_{N-1} \otimes [[D^2]])\Big)^{-1}\hat{\Phi}_h \\
&+ 2diag\Big((I_{N-1} \otimes B_2)\hat{\psi}_h - (B_2 \otimes I_{N+1})\hat{\psi}_h\Big)([[D]] \otimes [[D]])\Big(([[D^2]] \otimes I_{N-1}) + (I_{N-1} \otimes [[D^2]])\Big)^{-1}\hat{\Phi}_h \\
&+ \hat{g}_h.
\end{aligned}
$$

Here, the known boundary values have been removed. This nonlinear system can be linearized by replacing one variable by an old iterate in nonlinear terms. Then a simple fixed point iteration ($k \geq 0$) can be used to solve it.

$$
\begin{aligned}
&\frac{1}{Re}\Big((B_4 \otimes I_{N-1}) + (I_{N-1} \otimes B_4) + 2(B_2 \otimes B_2)\Big)\hat{\psi}_h^{k+1} \\
&- diag\Big((I_{N-1} \otimes [[D]])\hat{\psi}_h^k\Big)(B_3 \otimes I_{N-1})\hat{\psi}_h^{k+1} + diag\Big(([[D]] \otimes I_{N-1})\hat{\psi}_h^k\Big)(I_{N-1} \otimes B_3)\hat{\psi}_h^{k+1} \\
&+ diag\Big(([[D]] \otimes I_{N-1})\hat{\psi}_h^k\Big)(B_2 \otimes [[D]])\hat{\psi}_h^{k+1} - diag\Big((I_{N-1} \otimes [[D]])\hat{\psi}_h^k\Big)([[D]] \otimes B_2)\hat{\psi}_h^{k+1} \\
&= \Big((I_{N-1} \otimes [[D]])\hat{\Phi}_h^k\Big)([[D]] \otimes I_{N-1})\Big(([[D^2]] \otimes I_{N-1}) + (I_{N-1} \otimes [[D^2]])\Big)^{-1}\hat{\Phi}_h^k \\
&- \Big(([[D]] \otimes I_{N-1})\hat{\Phi}_h^k\Big)(I_{N-1} \otimes [[D]])\Big(([[D^2]] \otimes I_{N-1}) + (I_{N-1} \otimes [[D^2]])\Big)^{-1}\hat{\Phi}_h^k + \hat{f}_h,
\end{aligned}
$$

$$
\begin{aligned}
&- \frac{1}{Re_m}\Big(([[D^2]] \otimes I_{N-1}) + (I_{N-1} \otimes [[D^2]])\Big)\hat{\Phi}_h^{k+1} = diag\Big(([[D]] \otimes I_{N-1})\hat{\psi}_h^{k+1}\Big)(I_{N-1} \otimes [[D]])\hat{\Phi}_h^{k+1} \\
&- diag\Big((I_{N-1} \otimes [[D]])\hat{\psi}_h^{k+1}\Big)([[D]] \otimes I_{N-1})\hat{\Phi}_h^{k+1} \\
&- diag\Big((B_2 \otimes [[D]])\hat{\psi}_h^{k+1}\Big)([[D]] \otimes I_{N-1})\Big(([[D^2]] \otimes I_{N-1}) + (I_{N-1} \otimes [[D^2]])\Big)^{-1}\hat{\Phi}_h^{k+1} \\
&- diag\Big((I_{N-1} \otimes B_3)\hat{\psi}_h^{k+1}\Big)([[D]] \otimes I_{N-1})\Big(([[D^2]] \otimes I_{N-1}) + (I_{N-1} \otimes [[D^2]])\Big)^{-1}\hat{\Phi}_h^{k+1} \\
&+ diag\Big(([[D]] \otimes B_2)\hat{\psi}_h^{k+1}\Big)(I_{N-1} \otimes [[D]])\Big(([[D^2]] \otimes I_{N-1}) + (I_{N-1} \otimes [[D^2]])\Big)^{-1}\hat{\Phi}_h^{k+1} \\
&+ diag\Big((B_3 \otimes I_{N-1})\hat{\psi}_h^{k+1}\Big)(I_{N-1} \otimes [[D]])\Big(([[D^2]] \otimes I_{N-1}) + (I_{N-1} \otimes [[D^2]])\Big)^{-1}\hat{\Phi}_h^{k+1} \\
&+ 2diag\Big(([[D]] \otimes [[D]])\hat{\psi}_h^{k+1}\Big)\hat{\Phi}_h^{k+1} \\
&- 4diag\Big(([[D]] \otimes [[D]])\hat{\psi}_h^{k+1}\Big)([[D^2]] \otimes I_{N-1})\Big(([[D^2]] \otimes I_{N-1}) + (I_{N-1} \otimes [[D^2]])\Big)^{-1}\hat{\Phi}_h^{k+1} \\
&+ 2diag\Big((I_{N-1} \otimes B_2)\hat{\psi}_h^{k+1}\Big)([[D]] \otimes [[D]])\Big(([[D^2]] \otimes I_{N-1}) + (I_{N-1} \otimes [[D^2]])\Big)^{-1}\hat{\Phi}_h^{k+1} \\
&- 2diag\Big((B_2 \otimes I_{N+1})\hat{\psi}_h^{k+1}\Big)([[D]] \otimes [[D]])\Big(([[D^2]] \otimes I_{N-1}) + (I_{N-1} \otimes [[D^2]])\Big)^{-1}\hat{\Phi}_h^{k+1} \\
&+ \hat{g}_h.
\end{aligned}
$$

Now, consider the stream function form for the unsteady resistive MHD equations:

$$
\begin{aligned}
-\Delta\psi_t + \frac{1}{Re}\Delta^2\psi - \psi_y\psi_{xxx} + \psi_x\psi_{yyy} + \psi_x\psi_{yxx} - \psi_y\psi_{xyy} &= \phi_{yxx}\phi_x + \phi_{yyy}\phi_x \\
-\phi_{xxx}\phi_y - \phi_{xyy}\phi_y + f, \\
-\Delta\phi_t + \frac{1}{Re_m}\Delta^2\phi = \psi_{xxy}\phi_x - \psi_x\phi_{xxy} + \psi_y\phi_{yyx} - \psi_{yyx}\phi_y + \psi_y\phi_{xxx} - \psi_x\phi_{yyy} + \psi_{yyy}\phi_x \\
-\psi_{xxx}\phi_y + 2\psi_{xy}\phi_{xx} - 2\psi_{xx}\phi_{xy} + 2\psi_{yy}\phi_{yx} - 2\psi_{yx}\phi_{yy} + g.
\end{aligned}
$$

with the set of boundary conditions (4.14) and (4.17). We can re-write the above

stream function formulations in terms of Φ as follows.

$$-\Delta\psi_t + \frac{1}{Re}\Delta^2\psi - \psi_y\psi_{xxx} + \psi_x\psi_{yyy} + \psi_x\psi_{yxx} - \psi_y\psi_{xyy} = \Phi_y(\Delta^{-1}\Phi)_x - \Phi_x(\Delta^{-1}\Phi)_y + f,$$
$$\Phi_t - \frac{1}{Re_m}\Delta\Phi = \psi_x\Phi_y - \psi_y\Phi_x - (\psi_{xxy} + \psi_{yyy})(\Delta^{-1}\Phi)_x + (\psi_{yyx} + \psi_{xxx})(\Delta^{-1}\Phi)_y + 2\psi_{xy}\Phi$$
$$-4\psi_{xy}(\Delta^{-1}\Phi)_{xx} + 2(\psi_{xx} - \psi_{yy})(\Delta^{-1}\Phi)_{xy} + g.$$

A space-time spectral scheme is

$$\begin{aligned}
&- \Big\{D \otimes \Big((D^2 \otimes I_{N+1}) + (I_{N+1} \otimes D^2)\Big)\Big\}\psi_h + \frac{1}{Re}\Big\{I_{N+1} \otimes \Big((D^4 \otimes I_{N+1}) + (I_{N+1} \otimes D^4)\\
&+ 2(D^2 \otimes D^2)\Big)\Big\}\psi_h - diag\Big(I_{N+1} \otimes (I_{N+1} \otimes D)\psi_h\Big)(I_{N+1} \otimes (D^3 \otimes I_{N+1}))\psi_h\\
&+ diag\Big(I_{N+1} \otimes (D \otimes I_{N+1})\psi_h\Big)(I_{N+1} \otimes (I_{N+1} \otimes D^3))\psi_h\\
&+ diag\Big(I_{N+1} \otimes (D \otimes I_{N+1})\psi_h\Big)(I_{N+1} \otimes (D^2 \otimes D))\psi_h\\
&- diag\Big(I_{N+1} \otimes (I_{N+1} \otimes D)\psi_h\Big)(I_{N+1} \otimes (D \otimes D^2))\psi_h\\
&= \Big(I_{N+1} \otimes (I_{N+1} \otimes D)\Phi_h\Big)\Big(I_{N+1} \otimes (D \otimes I_{N+1})\Big)\Big(I_{N+1} \otimes (D^2 \otimes I_{N+1} + I_{N+1} \otimes D^2)\Big)^{-1}\Phi_h\\
&- \Big(I_{N+1} \otimes (D \otimes I_{N+1})\Phi_h\Big)\Big(I_{N+1} \otimes (I_{N+1} \otimes D)\Big)\Big(I_{N+1} \otimes (D^2 \otimes I_{N+1} + I_{N+1} \otimes D^2)\Big)^{-1}\Phi_h + f_h,
\end{aligned}$$

$$
\begin{aligned}
&\Big\{D \otimes (I_{N+1} \otimes I_{N+1})\Big\}\Phi_h - \frac{1}{Re_m}\Big(I_{N+1} \otimes (D^2 \otimes I_{N+1} + I_{N+1} \otimes D^2)\Big)\Phi_h \\
&= diag\Big(I_{N+1} \otimes (D \otimes I_{N+1})\psi_h\Big)\Big(I_{N+1} \otimes (I_{N+1} \otimes D)\Big)\Phi_h \\
&\quad - diag\Big(I_{N+1} \otimes (I_{N+1} \otimes D)\psi_h\Big)\Big(I_{N+1} \otimes (D \otimes I_{N+1})\Big)\Phi_h \\
&\quad - diag\Big(I_{N+1} \otimes (D^2 \otimes D)\psi_h\Big)\Big(I_{N+1} \otimes (D \otimes I_{N+1})\Big)\Big(I_{N+1} \otimes (D^2 \otimes I_{N+1} + I_{N+1} \otimes D^2)\Big)^{-1}\Phi_h \\
&\quad - diag\Big(I_{N+1} \otimes (I_{N+1} \otimes D^3)\psi_h\Big)\Big(I_{N+1} \otimes (D \otimes I_{N+1})\Big)\Big(I_{N+1} \otimes (D^2 \otimes I_{N+1} + I_{N+1} \otimes D^2)\Big)^{-1}\Phi_h \\
&\quad + diag\Big(I_{N+1} \otimes (D \otimes D^2)\psi_h\Big)\Big(I_{N+1} \otimes (I_{N+1} \otimes D)\Big)\Big(I_{N+1} \otimes (D^2 \otimes I_{N+1} + I_{N+1} \otimes D^2)\Big)^{-1}\Phi_h \\
&\quad + diag\Big(I_{N+1} \otimes (D^3 \otimes I_{N+1})\psi_h\Big)\Big(I_{N+1} \otimes (I_{N+1} \otimes D)\Big)\Big(I_{N+1} \otimes (D^2 \otimes I_{N+1} + I_{N+1} \otimes D^2)\Big)^{-1}\Phi_h \\
&\quad + 2diag\Big(I_{N+1} \otimes (D \otimes D)\psi_h\Big)\Phi_h \\
&\quad - 4diag\Big(I_{N+1} \otimes (D \otimes D)\psi_h\Big)\Big(I_{N+1} \otimes (D^2 \otimes I_{N+1})\Big)\Big(I_{N+1} \otimes (D^2 \otimes I_{N+1} + I_{N+1} \otimes D^2)\Big)^{-1}\Phi_h \\
&\quad + 2diag\Big(I_{N+1} \otimes (I_{N+1} \otimes D^2)\psi_h\Big)\Big(I_{N+1} \otimes (D \otimes D)\Big)\Big(I_{N+1} \otimes (D^2 \otimes I_{N+1} + I_{N+1} \otimes D^2)\Big)^{-1}\Phi_h \\
&\quad - 2diag\Big(I_{N+1} \otimes (D^2 \otimes I_{N+1})\psi_h\Big)\Big(I_{N+1} \otimes (D \otimes D)\Big)\Big(I_{N+1} \otimes (D^2 \otimes I_{N+1} + I_{N+1} \otimes D^2)\Big)^{-1}\Phi_h \\
&\quad + g_h,
\end{aligned}
$$

where ψ_h, Φ_h, f_h and g_h are the vectors of ψ, Φ, f, and g respectively, evaluated at the collocation points. Let B_2 be the spectral second derivative (3.16), B_3 be the spectral third derivative (3.39) and B_4 be the spectral fourth derivative (3.18).

Finally we may write

$$
\begin{aligned}
&- \Big\{[D] \otimes \Big((B_2 \otimes I_{N-1}) + (I_{N-1} \otimes B_2)\Big)\Big\}\hat{\psi}_h + \frac{1}{Re}\Big\{I_N \otimes \Big((B_4 \otimes I_{N-1}) + (I_{N-1} \otimes B_4)\\
&+ 2(B_2 \otimes B_2)\Big)\Big\}\hat{\psi}_h - diag\Big(I_N \otimes (I_{N-1} \otimes [[D]])\hat{\psi}_h\Big)(I_N \otimes (B_3 \otimes I_{N-1}))\hat{\psi}_h\\
&+ diag\Big(I_N \otimes ([[D]] \otimes I_{N-1})\hat{\psi}_h\Big)(I_N \otimes (I_{N-1} \otimes B_3))\hat{\psi}_h\\
&+ diag\Big(I_N \otimes ([[D]] \otimes I_{N-1})\hat{\psi}_h\Big)(I_N \otimes (B_2 \otimes [[D]]))\hat{\psi}_h\\
&- diag\Big(I_N \otimes (I_{N-1} \otimes [[D]])\hat{\psi}_h\Big)(I_N \otimes ([[D]] \otimes B_2))\hat{\psi}_h\\
&= \Big(I_N \otimes (I_{N-1} \otimes [[D]])\hat{\Phi}_h\Big)\Big(I_N \otimes ([[D]] \otimes I_{N-1})\Big)\Big(I_N \otimes ([[D^2]] \otimes I_{N-1} + I_{N-1} \otimes [[D^2]])\Big)^{-1}\hat{\Phi}_h\\
&- \Big(I_N \otimes ([[D]] \otimes I_{N-1})\hat{\Phi}_h\Big)\Big(I_N \otimes (I_{N-1} \otimes [[D]])\Big)\Big(I_N \otimes ([[D^2]] \otimes I_{N-1} + I_{N-1} \otimes [[D^2]])\Big)^{-1}\hat{\Phi}_h\\
&+ \hat{f}_h - (d_h \otimes \psi_{0h}),
\end{aligned}
$$

$$
\begin{aligned}
&\Big\{[D] \otimes (I_{N-1} \otimes I_{N-1})\Big\}\hat{\Phi}_h - \frac{1}{Re_m}\Big(I_N \otimes ([[D^2]] \otimes I_{N-1} + I_{N-1} \otimes [[D^2]])\Big)\hat{\Phi}_h\\
&= diag\Big(I_N \otimes (D \otimes I_{N-1})\hat{\psi}_h\Big)\Big(I_N \otimes (I_{N-1} \otimes [[D]])\Big)\hat{\Phi}_h\\
&- diag\Big(I_N \otimes (I_{N-1} \otimes [[D]])\hat{\psi}_h\Big)\Big(I_N \otimes ([[D]] \otimes I_{N-1})\Big)\hat{\Phi}_h\\
&- diag\Big(I_N \otimes (B_2 \otimes [[D]])\hat{\psi}_h\Big)\Big(I_N \otimes ([[D]] \otimes I_{N-1})\Big)\Big(I_N \otimes ([[D^2]] \otimes I_{N-1} + I_{N-1} \otimes [[D^2]])\Big)^{-1}\hat{\Phi}_h\\
&- diag\Big(I_N \otimes (I_{N-1} \otimes B_3)\hat{\psi}_h\Big)\Big(I_N \otimes ([[D]] \otimes I_{N-1})\Big)\Big(I_N \otimes ([[D^2]] \otimes I_{N-1} + I_{N-1} \otimes [[D^2]])\Big)^{-1}\hat{\Phi}_h\\
&+ diag\Big(I_N \otimes ([[D]] \otimes B_2)\hat{\psi}_h\Big)\Big(I_N \otimes (I_{N-1} \otimes [[D]])\Big)\Big(I_N \otimes ([[D^2]] \otimes I_{N-1} + I_{N-1} \otimes [[D^2]])\Big)^{-1}\hat{\Phi}_h\\
&+ diag\Big(I_N \otimes (B_3 \otimes I_{N-1})\hat{\psi}_h\Big)\Big(I_N \otimes (I_{N-1} \otimes [[D]])\Big)\Big(I_N \otimes ([[D^2]] \otimes I_{N-1} + I_{N-1} \otimes [[D^2]])\Big)^{-1}\hat{\Phi}_h\\
&+ 2diag\Big(I_N \otimes ([[D]] \otimes [[D]])\hat{\psi}_h\Big)\hat{\Phi}_h - 4diag\Big(I_N \otimes ([[D]] \otimes [[D]])\hat{\psi}_h\Big)\\
&\Big(I_N \otimes ([[D^2]] \otimes I_{N-1})\Big)\Big(I_N \otimes ([[D^2]] \otimes I_{N-1} + I_{N-1} \otimes [[D^2]])\Big)^{-1}\hat{\Phi}_h\\
&+ 2diag\Big(I_N \otimes (I_{N-1} \otimes B_2)\hat{\psi}_h\Big)\Big(I_N \otimes ([[D]] \otimes [[D]])\Big)\Big(I_N \otimes ([[D^2]] \otimes I_{N-1} + I_{N-1} \otimes [[D^2]])\Big)^{-1}\hat{\Phi}_h\\
&- 2diag\Big(I_N \otimes (B_2 \otimes I_{N-1})\hat{\psi}_h\Big)\Big(I_N \otimes ([[D]] \otimes [[D]])\Big)\Big(I_N \otimes ([[D^2]] \otimes I_{N-1} + I_{N-1} \otimes [[D^2]])\Big)^{-1}\hat{\Phi}_h\\
&+ \hat{g}_h - (d_h \otimes \phi_{0h}).
\end{aligned}
$$

Here, the known boundary and initial values have been removed. This nonlinear system can be linearized as before. Then a simple fixed point iteration ($k \geq 0$) can be used to solve it.

$$
\begin{aligned}
&- \Big\{[D] \otimes \Big((B_2 \otimes I_{N-1}) + (I_{N-1} \otimes B_2)\Big)\Big\}\hat{\psi}_h^{k+1} + \frac{1}{Re}\Big\{I_N \otimes \Big((B_4 \otimes I_{N-1}) + (I_{N-1} \otimes B_4) \\
&+ 2(B_2 \otimes B_2)\Big)\Big\}\hat{\psi}_h^{k+1} - diag\Big(I_N \otimes (I_{N-1} \otimes [[D]])\hat{\psi}_h^k\Big)(I_N \otimes (B_3 \otimes I_{N-1}))\hat{\psi}_h^{k+1} \\
&+ diag\Big(I_N \otimes ([[D]] \otimes I_{N-1})\hat{\psi}_h^k\Big)(I_N \otimes (I_{N-1} \otimes B_3))\hat{\psi}_h^{k+1} \\
&+ diag\Big(I_N \otimes ([[D]] \otimes I_{N-1})\hat{\psi}_h^k\Big)(I_N \otimes (B_2 \otimes [[D]]))\hat{\psi}_h^{k+1} \\
&- diag\Big(I_N \otimes (I_{N-1} \otimes [[D]])\hat{\psi}_h^k\Big)(I_N \otimes ([[D]] \otimes B_2))\hat{\psi}_h^{k+1} \\
= &\Big(I_N \otimes (I_{N-1} \otimes [[D]])\hat{\Phi}_h^k\Big)\Big(I_N \otimes ([[D]] \otimes I_{N-1})\Big)\Big(I_N \otimes ([[D^2]] \otimes I_{N-1} + I_{N-1} \otimes [[D^2]])\Big)^{-1}\hat{\Phi}_h^k \\
&- \Big(I_N \otimes ([[D]] \otimes I_{N-1})\hat{\Phi}_h^k\Big)\Big(I_N \otimes (I_{N-1} \otimes [[D]])\Big)\Big(I_N \otimes ([[D^2]] \otimes I_{N-1} + I_{N-1} \otimes [[D^2]])\Big)^{-1}\hat{\Phi}_h^k \\
&+ \hat{f}_h - (d_h \otimes \psi_{0h}),
\end{aligned}
$$

$$
\begin{aligned}
&\Big\{[D] \otimes (I_{N-1} \otimes I_{N-1})\Big\}\hat{\Phi}_h^{k+1} - \frac{1}{Re_m}\Big(I_N \otimes ([[D^2]] \otimes I_{N-1} + I_{N-1} \otimes [[D^2]])\Big)\hat{\Phi}_h^{k+1} \\
= &\, diag\Big(I_N \otimes (D \otimes I_{N-1})\hat{\psi}_h^{k+1}\Big)\Big(I_N \otimes (I_{N-1} \otimes [[D]])\Big)\hat{\Phi}_h^{k+1} \\
&- diag\Big(I_N \otimes (I_{N-1} \otimes [[D]])\hat{\psi}_h^{k+1}\Big)\Big(I_N \otimes ([[D]] \otimes I_{N-1})\Big)\hat{\Phi}_h^{k+1} \\
&- diag\Big(I_N \otimes (B_2 \otimes [[D]])\hat{\psi}_h^{k+1}\Big)\Big(I_N \otimes ([[D]] \otimes I_{N-1})\Big) \\
&\Big(I_N \otimes ([[D^2]] \otimes I_{N-1} + I_{N-1} \otimes [[D^2]])\Big)^{-1}\hat{\Phi}_h^{k+1} \\
&- diag\Big(I_N \otimes (I_{N-1} \otimes B_3)\hat{\psi}_h^{k+1}\Big)\Big(I_N \otimes ([[D]] \otimes I_{N-1})\Big) \\
&\Big(I_N \otimes ([[D^2]] \otimes I_{N-1} + I_{N-1} \otimes [[D^2]])\Big)^{-1}\hat{\Phi}_h^{k+1} \\
&+ diag\Big(I_N \otimes ([[D]] \otimes B_2)\hat{\psi}_h^{k+1}\Big)\Big(I_N \otimes (I_{N-1} \otimes [[D]])\Big) \\
&\Big(I_N \otimes ([[D^2]] \otimes I_{N-1} + I_{N-1} \otimes [[D^2]])\Big)^{-1}\hat{\Phi}_h^{k+1} \\
&+ diag\Big(I_N \otimes (B_3 \otimes I_{N-1})\hat{\psi}_h^{k+1}\Big)\Big(I_N \otimes (I_{N-1} \otimes [[D]])\Big) \\
&\Big(I_N \otimes ([[D^2]] \otimes I_{N-1} + I_{N-1} \otimes [[D^2]])\Big)^{-1}\hat{\Phi}_h^{k+1}
\end{aligned}
$$

$$
\begin{aligned}
&+ 2diag\Big(I_N \otimes ([[D]] \otimes [[D]])\hat{\psi}_h^{k+1}\Big)\hat{\Phi}_h^{k+1} - 4diag\Big(I_N \otimes ([[D]] \otimes [[D]])\hat{\psi}_h^{k+1}\Big) \\
&\Big(I_N \otimes ([[D^2]] \otimes I_{N-1})\Big)\Big(I_N \otimes ([[D^2]] \otimes I_{N-1} + I_{N-1} \otimes [[D^2]])\Big)^{-1}\hat{\Phi}_h^{k+1} \\
&+ 2diag\Big(I_N \otimes (I_{N-1} \otimes B_2)\hat{\psi}_h^{k+1}\Big)\Big(I_N \otimes ([[D]] \otimes [[D]])\Big) \\
&\Big(I_N \otimes ([[D^2]] \otimes I_{N-1} + I_{N-1} \otimes [[D^2]])\Big)^{-1}\hat{\Phi}_h^{k+1} \\
&- 2diag\Big(I_N \otimes (B_2 \otimes I_{N-1})\hat{\psi}_h^{k+1}\Big)\Big(I_N \otimes ([[D]] \otimes [[D]])\Big) \\
&\Big(I_N \otimes ([[D^2]] \otimes I_{N-1} + I_{N-1} \otimes [[D^2]])\Big)^{-1}\hat{\Phi}_h^{k+1} \\
&+ \hat{g}_h - (d_h \otimes \phi_{0h}).
\end{aligned}
$$

Similar to how relaxation was implemented for the Navier-Stokes equations, relaxation can be implemented for MHD equations as well. However, the iteration is divergent when the Re and Re_m are large. In the next chapter, we shall discuss nonlinear preconditioning techniques that are able to simulate the MHD equations at high Re and Re_m.

5

Spectral Domain Decomposition

5.1 Introduction

Domain decomposition methods (DD for short) are widely used to solve large algebraic systems involving industrial applications. The idea of domain decomposition is to partition the domain into several subdomains and then solve the PDE in all subdomains in parallel. Here, a set of sub-problems smaller in size will replace the original problem. Iterative methods defined on Krylov spaces typically use DD methods as preconditioners. GMRES and conjugate gradient method are such examples. DD methods can be divided in to two categories based on how spatial decomposition is done. They are overlapping (Schwarz methods) and non-overlapping (Schur complement methods). Schwarz methods calculate iterates that are subdomain solutions of the PDE. The connection between adjacent subdomains is maintained using boundary conditions. Schur complement methods solve for the unknown function along the artificial interface. While there are many advantages in using DD methods, there are a couple that stand out. DD methods are able to create parallel algorithms effectively. Further, when used as preconditioners, DD methods can solve large ill-conditioned problems in an efficient and accurate way.

5.2 Linear Preconditioning

5.2.1 Overlapping Domain Decomposition

5.2.1.1 Additive Schwarz Method

Overlapping subdomains occur when a part of one subdomain intersects with another and this is the basis for overlapping domain decomposition. The "Schwarz Alternating" and "Additive Schwarz" methods are the two main methods of overlapping domain decomposition. In this section, we focus on the Additive Schwarz method for the Poisson equation and biharmonic equation (3.20).

For ease of explaining, we consider the Poisson equation $-\Delta u = f$ on Ω with $f \in L^2(\Omega)$. We seek the solution $u \in H_0^1(\Omega)$. Let the inner product on $H_0^1(\Omega)$ be

$$[w, v] = \int_\Omega \nabla w \cdot \nabla v, \quad v, w \in H_0^1(\Omega),$$

and $\|v\| = [v, v]^{1/2}$ be the associated norm. Also let $(\cdot, \cdot) := (\cdot, \cdot)_{0,\Omega}$ be the $L^2(\Omega)$ inner product. For simplicity, we consider Ω to consist of two open overlapping subdomains $\Omega_i, i = 1, 2$ where $\Omega_1 \cap \Omega_2 \neq \emptyset$. An example is shown in figure 5.1 below.

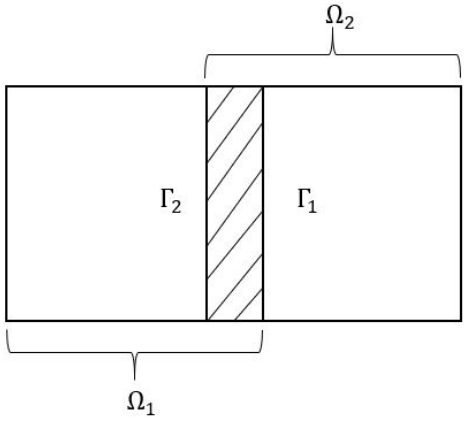

Figure 5.1: Two rectangle domains with an overlap.

Overlapping is defined as below.

$$H_0^1(\Omega) = H_0^1(\Omega_1) + H_0^1(\Omega_2).$$

Let P_i be the orthogonal projection from $H_0^1(\Omega)$ onto $H_0^1(\Omega_i), i = 1, 2$. A function in $H_0^1(\Omega_i)$ can be extended by zero to be a function in $H_0^1(\Omega)$. With an initial guess $u^{(0)} \in H_0^1(\Omega)$, parallel Schwarz method (both subdomain PDEs are solved simultaneously) constructs the following sequence:

$$u^{n+1} = u^n + \omega(u_1^{n+1} - u^n) + \omega(u_2^{n+1} - u^n), \tag{5.1}$$

where ω is a positive constant and

$$\begin{aligned} -\Delta u_1^{n+1} &= f \quad on \quad \Omega_1 \\ u_1^{n+1} &= 0 \quad on \quad \partial\Omega_1 \backslash \Gamma_1 \\ u_1^{n+1} &= u^n \quad on \quad \Gamma_1, \end{aligned}$$

and

$$\begin{aligned} -\Delta u_2^{n+1} &= f \quad on \quad \Omega_2 \\ u_2^{n+1} &= 0 \quad on \quad \partial\Omega_2 \backslash \Gamma_2 \\ u_2^{n+1} &= u^n \quad on \quad \Gamma_2. \end{aligned}$$

Further, for the parallel Schwarz sequence, the error $e^n = u^n - u$ satisfies

$$e^{n+1} = (I - \omega(P_1 + P_2))e^n, \tag{5.2}$$

and $\left\|e^{(n)}\right\| \to 0$ if $0 < \omega < 1$. Here $P_1 + P_2$ is a sum of two orthogonal projections which are self-adjoint positive semi-definite operators.

Let us now discuss an algebraic discrete version of the parallel Schawarz method. Take R_i to be the matrix which restricts all unknowns in global domain Ω to unknowns in subdomains $\Omega_i, i = 1, 2$. Since R_i is a restriction matrix, R_i^T will act as an extension matrix that will extend a vector (of unknowns) in $\Omega_i, i = 1, 2$ by zeros, to a vector in the global domain. Let the global problem in Ω be $Au = f$. Therefore, discrete differential operators for the local domains $\Omega_i, i = 1, 2$ can be written as $A_i = R_i A R_i^T$ and corresponding $f_i = R_i f$. Take u_i^n as the local iterates of the parallel Schwarz method. Define

$$\widetilde{A}_{ij} = (R_i A - A_i R_i) R_j^T, \quad 1 \leq i \neq j \leq 2.$$

It can be shown that

$$A_1 u_1^{n+1} = f_1 - \widetilde{A}_{12} u_2^n, \qquad A_2 u_2^{n+1} = f_2 - \widetilde{A}_{21} u_1^n.$$

Recall the parallel Schwarz method defined in (5.1). This can be used as a preconditioner. From the error equation (5.2), when $\omega = 1$, the iteration matrix becomes $G = I - (P_1 + P_2)$. We know that, the parallel Schwarz method defined in (5.1) can be used as a preconditioner. Let M be any non-singular operator. Then the given linear system $-\Delta u = f$ can be written as, $Mu + (-\Delta - M)u = f$ or,

$$u = (I - M^{-1}(-\Delta))u + M^{-1} f.$$

Therefore, an iterative method can be defined as

$$u^{n+1} = G u^n + M^{-1} f,$$

where $G = I - M^{-1}(-\Delta)$ is the iteration operator. Hence $M^{-1}(-\Delta) = P_1 + P_2$ is the preconditioned operator. Now the preconditoned system can be written as

$$(P_1 + P_2)u = g, \tag{5.3}$$

where $g = M^{-1}f$. When M defined above is taken as the preconditioner, the additive Schwarz methods gives an algorithm that solves the Poisson equation thereof by using GMRES. Since we use spectral methods, in general we cannot use PCG because the matrix is non-symmetric. In certain situations, such as in [2], it is possible to implement PCG for spectral methods. Similarly, one can formulate a preconditioned system for the biharmonic equation which can be solved using Additive Schwarz method.

5.2.1.2 Legendre Interpolation

The Legendre pseudospectral derivative matrix D used in spectral methods is defined using Legengre Gauss-Lobatto nodes in the domain $[-1, 1]$. When spectral methods are applied for domain decomposition problems, we need to rescale the subdomains $[-1, a]$ and $[b, 1]$ to $[-1, 1]$, where $b < a$. This scaling is required because Gauss-Lobatto nodes are not equally spaced unlike in finite difference methods where nodes are usually equally spaced. Therefore, global and local subdomain Gauss-Lobatto nodes do not coincide. Thus, interpolation is required to convert function values at the subdomain nodes to function values at the global points. This interpolation can be done using Lagrange polynomials defined on the Legendre Gauss-Lobatto nodes $\{x_0, \ldots, x_n\}$.

Define the Lagrange polynomials for $x_0, \ldots, x_n$ by

$$l_j(x) = -\frac{1}{n(n+1)L_n(x_j)} \frac{(1-x^2)L_n^{'}(x)}{x - x_j}, \quad j = 0, \ldots, n.$$

We claim that $l_j(x_k) = \delta_{kj}$. Since x_k are the roots of $(1-x^2)L_n^{'}(x)$, it is immediate that $l_j(x_k) = 0$ if $j \neq k$. Now

$$\begin{aligned} l_j(x_j) &= -\frac{1}{n(n+1)L_n(x_j)} \lim_{x \to x_j} \frac{(1-x^2)L_n^{'}(x)}{x - x_j} \\ &= \frac{1}{n(n+1)L_n(x_j)} \frac{n(n+1)L_n(x_j)}{1} = 1. \end{aligned}$$

Define

$$p(x) = \sum_{j=0}^{n} f(x_j) l_j(x),$$

where $p(x)$ is a polynomial that interpolates $f(x)$ at the nodes and is called 1D-Legendre polynomial interpolant.

Similaly, the 2D-Legendre interpolant can be described as follows. It is derived by considering 1D-Legendre interpolation for two orthogonal directions and combining them. Define the 2D Lagrange polynomial

$$l_{ij}(x,y) = l_i(x)l_j(y), \quad 0 \le i \le n, \;\; 0 \le j \le m.$$
$$l_i(x) = -\frac{1}{n(n+1)L_n(x_i)}\frac{(1-x^2)L_n^{'}(x)}{x-x_i},$$
$$l_j(y) = -\frac{1}{m(m+1)L_m(y_j)}\frac{(1-y^2)L_m^{'}(y)}{y-y_j},$$

where $\{y_0, \ldots, y_m\}$ are the Legendre Lobatto nodes. So we have

$$l_{ij}(x_r, y_s) = \begin{cases} 1, & \text{if } i = r, j = s; \\ 0, & \text{otherwise.} \end{cases}$$

It follows that

$$p(x,y) = \sum_{i=0}^{n}\sum_{j=0}^{m} f(x_i, y_j)l_{ij}(x,y),$$

is a polynomial that interpolates $f(x,y)$ at the nodes and is called 2D-Legendre polynomial interpolant. Similarly, one can define a Chebyshev polynomial interpolant.

5.2.2 Non-overlapping Domain Decomposition

5.2.2.1 Introduction

Subdomains intersecting only at their interface are known as non-overlapping subdomains and are the basis for non-overlapping domain decomposition methods. These also go by the name iterative substructuring methods [13]. We will solve the Poisson equation (with homogeneous Dirichlet boundary conditions) using this domain decomposition. For simplicity, we consider the global domain Ω to consist of two non-overlapping subdomains, that is, $\overline{\Omega} = \overline{\Omega}_1 \cup \overline{\Omega}_2$ with $\Omega_1 \cap \Omega_2 = \emptyset$ and $\Gamma = \partial\Omega_1 \cap \partial\Omega_2$. See Figure 5.2 for an example of non-overlapping subdomains.

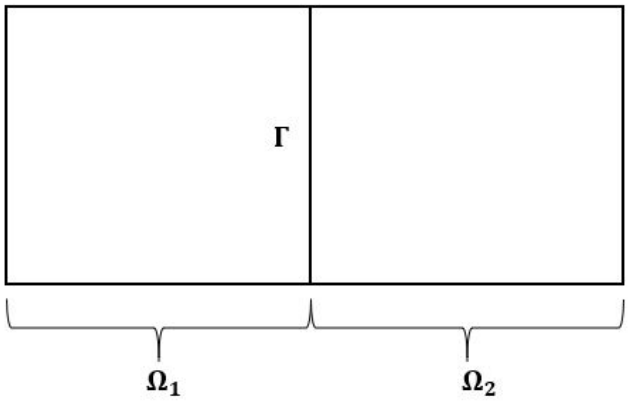

Figure 5.2: Two rectangular subdomains without overlap.

We solve the subproblems

$$\begin{aligned} -\Delta u_1 &= f \quad on \quad \Omega_1 \\ u_1 &= 0 \quad on \quad \partial\Omega_1 \backslash \Gamma \\ u_1 &= g \quad on \quad \Gamma, \end{aligned}$$

and

$$\begin{aligned} -\Delta u_2 &= f \quad on \quad \Omega_2 \\ u_2 &= 0 \quad on \quad \partial\Omega_2 \backslash \Gamma \\ u_2 &= g \quad on \quad \Gamma, \end{aligned}$$

where g is an unknown function defined on Γ to be determined by

$$\frac{\partial u_1}{\partial \nu_1} + \frac{\partial u_2}{\partial \nu_2} = 0 \quad on \quad \Gamma. \tag{5.4}$$

The equation (5.4) is called the transmission condition and ν_1 and ν_2 are outward pointing normals to the first and second subdomains, respectively.

Let us examine this transmission condition further. For $i = 1, 2$, let $u_i = u_i^e + u_i^0$, where $u_i^0 = -\Delta_i^{-1} f \in H_0^1(\Omega_i)$ and u_i^e is the harmonic extension of g into Ω_i and denoted by $\mathcal{H}_i g$.

For any $v \in H^1(\Omega_i)$ vanishing on $\partial\Omega_i \cap \partial\Omega$, the following relation can be identified:

$$\int_\Gamma \frac{\partial \mathcal{H}_i g}{\partial \nu_i} v = \int_{\Omega_i} \nabla \mathcal{H}_i g \cdot \nabla v.$$

The equation (5.4) is now equivalent to the equation $Sg = G$ on Γ, where

$$Sg := \frac{\partial \mathcal{H}_1 g}{\partial \nu_1} + \frac{\partial \mathcal{H}_2 g}{\partial \nu_2}, \quad G := \frac{\partial \Delta_1^{-1} f}{\partial \nu_1} + \frac{\partial \Delta_2^{-1} f}{\partial \nu_2}. \tag{5.5}$$

This operator, $S : H_{00}^{1/2}(\Gamma) \to H^{-1/2}(\Gamma)$ is known as the Steklov-Poincaré operator. The Hilbert space

$$H_{00}^{1/2}(\Gamma) = \left\{ v|_\Gamma, v \in H_0^1(\Omega) \right\},$$

is equipped with the inner product

$$\langle g, p \rangle_{H_{00}^{1/2}(\Gamma)} = \sum_{i=1}^{2} \int_{\Omega_i} \nabla \mathcal{H}_i g \cdot \nabla \mathcal{H}_i p, \quad g, p \in H_{00}^{1/2}(\Gamma).$$

Here, $H^{-1/2}(\Gamma)$ is the dual space of $H_{00}^{1/2}(\Gamma)$. Let $S = S_1 + S_2$, where

$$S_i g = \frac{\partial \mathcal{H}_i g}{\partial \nu_i}, \quad g \in H_{00}^{1/2}(\Gamma).$$

Therefore, S_i can be identified as the operator which takes the harmonic extension of g (to Ω_i) onto the normal derivative along Γ.

5.2.2.2 Poincaré-Steklov Operator for the Laplace Opeartor

This section will discuss the spectral version of the discrete Steklov–Poincaré operator for the Poisson problem [13].

Poincaré –Steklov operator was named after Henri Poincaré and Vladimir Steklov. This operator takes the value of the solution along Γ and maps it to the normal derivative along Γ. After solving the Steklov–Poincaré operator for the interface, those interface values can be used to reduce the global problem to independent boundary value problems for the subdomains. These new subdomain problems can be solved in parallel.

When a partial differential equation is discretized by a finite element or finite difference scheme, the discretized Poincaré–Steklov operator is equal to the Schur complement obtained by eliminating all degrees of freedom inside the domain. First of all, let us briefly examine the Poincaré–Steklov operator in a finite element context for the Poisson problem. Let the unknowns be partitioned as $[u_1, u_2, u_3]^T$, where u_1 and u_2 are the unknowns on Ω_1 and Ω_2, respectively, and u_3 are the unknowns along Γ. Take f to have also been partitioned similarly as $[f_1, f_2, f_3]^T$. Then the set

of discrete equations can be written as

$$\begin{bmatrix} A_{11} & 0 & A_{13} \\ 0 & A_{22} & A_{23} \\ A_{13}^T & A_{23}^T & A_{33} \end{bmatrix} \begin{bmatrix} u_1 \\ u_2 \\ u_3 \end{bmatrix} = \begin{bmatrix} f_1 \\ f_2 \\ f_3 \end{bmatrix}, \tag{5.6}$$

where A_{11} and A_{22} are discrete approximations for $-\Delta_i : H_0^1(\Omega_i) \to H^{-1}(\Omega_i), i = 1, 2$ respectively, and A_{33} is a discrete approximation to $-\Delta$ along Γ. Take all A_{ii} to be symmetric positive definite. By solving the first two equations, we obtain

$$u_1 = A_{11}^{-1}(f_1 - A_{13}u_3) \quad \textit{and} \quad u_2 = A_{22}^{-1}(f_2 - A_{23}u_3).$$

Substitution of u_1 and u_2 into the third equation gives

$$S_h u_3 = \widetilde{f}_3, \tag{5.7}$$

where

$$S_h = A_{33} - A_{13}^T A_{11}^{-1} A_{13} - A_{23}^T A_{22}^{-1} A_{23} \quad \textit{and} \quad \widetilde{f}_3 = f_3 - A_{13}^T A_{11}^{-1} f_1 - A_{23}^T A_{22}^{-1} f_2.$$

This matrix S_h is symmetric positive definite and named as the Schur complement of the block matrix in (5.6). In a finite element context, it can be shown that S_h, in fact, is a discrete approximation of the Steklov–Poincaré operator. Further,

$$S_{1,h} = A_{33}^{(1)} - A_{13}^T A_{11}^{-1} A_{13}, \tag{5.8}$$

where $A_{33}^{(1)}$ denotes the contribution to the stiffness matrix for nodes along Γ rising from integration in Ω_1. Similarly $S_{2,h} = A_{33}^{(2)} - A_{23}^T A_{22}^{-1} A_{23}$ and we can see that $S_h = S_{1,h} + S_{2,h}$. Here $S_{1,h}$ and $S_{2,h}$ are the matrix representations of S_1 and S_2,

respectively.

It can be shown that the action of $S_{1,h}$ or its inverse on a vector can be found by solving the Poisson equation with a Dirichlet or Neumann boundary condition on a subdomain. Therefore, there is no need to form $S_{1,h}$ or $S_{1,h}^{-1}$ explicitly and this allows for a more efficient computation of the action of $S_{1,h}$ and $S_{1,h}^{-1}$ on an arbitrary vector. Now let us consider the calculation of $S_{1,h}g$ when g is given. From (5.8),

$$S_{1,h}g = (A_{33}^{(1)} - A_{13}^T A_{11}^{-1} A_{13})g = G.$$

Therefore, calculating the action of $S_{1,h}$ on a given vector g requires solving the Dirichlet problem $-\Delta v_1 = 0$ on the subdomain Ω_1 with the boundary conditions $v_1 = g$ on Γ and $v_1 = 0$ on $\partial\Omega\backslash\Gamma$. Hence, the discrete problem can be written as,

$$\begin{bmatrix} A_{11} & A_{13} \\ A_{13}^T & A_{33}^{(1)} \end{bmatrix} \begin{bmatrix} v_1 \\ g \end{bmatrix} = \begin{bmatrix} 0 \\ G \end{bmatrix}. \tag{5.9}$$

It is evident that evaluating G is a two step calculation. First, calculate v_1 from the Dirichlet boundary value problem. Then compute $G = A_{13}^T v_1 + A_{33}^{(1)} g$. This shows that there is no need to form $S_{1,h}$ explicitly. A similar calculation can be carried out to find the action of $S_{1,h}^{-1}$ on a vector G. In this case, (5.9) is solved for v_1 and g and it is a discrete Neumann problem.

Now, let us consider the spectral version of the discrete Steklov–Poincaré operator for the Poisson problem. It is known that finite-difference or finite element operators are local and there is no communication between adjacent subdomains. However, in spectral methods, all operators are global and calculation of the derivative at any point requires all the nodes in the domain. Therefore, the spectral version (although having the same definitions as in finite-difference/finite element methods) is implemented differently because zero blocks do not exist anymore as in the system

(5.6). For ease of explanation, let us consider the 1D Poisson problem with the boundary conditions $v = g$ on Γ and $v = 0$ on $\partial\Omega\backslash\Gamma$.

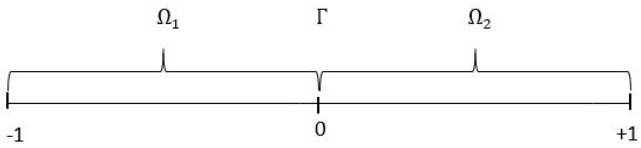

Figure 5.3: 1D Non-Overlapping subdomains.

For spectral methods, Legendre pseudospectral derivative matrix D is used and is defined using Gauss-Lobatto nodes from -1 to $+1$. To use D for subdomains, a re-scaling is needed. Further, to implement a non-homogeneous Neumann boundary condition at the interface, the spectral Tau method is adopted. Now, consider the first subdomain Ω_1. The discrete equations for the Ω_1 can be formulated as below.

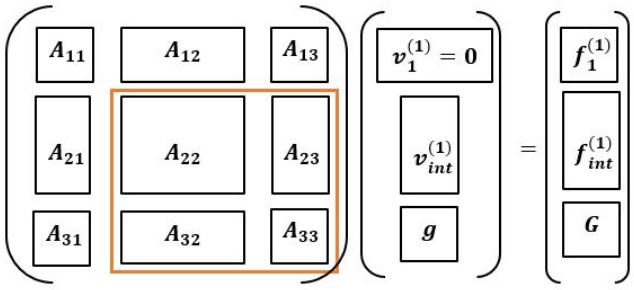

Figure 5.4: Subdomain 1.

Here, $G = \frac{\partial v}{\partial \nu_1}$, $v_1^{(1)}$ represents the first subdomain left boundary value and $v_{int}^{(1)}$ represents the interior values of the first subdomain. Now we have

$$A_{22}v_{int}^{(1)} + A_{23}g = f_{int}^{(1)},$$
$$A_{32}v_{int}^{(1)} + A_{33}g = G.$$

From the first equation we obtain

$$v_{int}^{(1)} = A_{22}^{-1}(f_{int}^{(1)} - A_{23}g). \tag{5.10}$$

Sustituting into the second equation yields

$$S_{1,h}g = G - A_{32}A_{22}^{-1}f_{int}^{(1)}, \tag{5.11}$$

where $S_{1,h} = A_{33} - A_{32}A_{22}^{-1}A_{23}$.

Now, consider the second subdomain Ω_2. The discrete equations for the Ω_2 can be formulated as below.

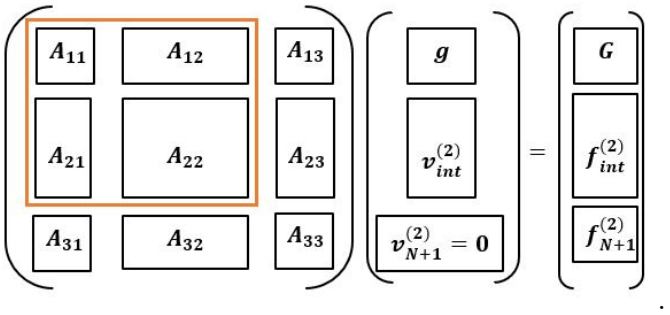

Figure 5.5: Subdomain 2.

Here, $G = -\frac{\partial v}{\partial \nu_1}$, $v_{N+1}^{(2)}$ represents the right boundary value of the second subdomain and $v_{int}^{(2)}$ represents the interior values of the second subdomain. Now we have

$$A_{11}g + A_{12}v_{int}^{(2)} = G,$$
$$A_{21}g + A_{22}v_{int}^{(2)} = f_{int}^{(2)}.$$

From the second equation we obtain

$$v_{int}^{(2)} = A_{22}^{-1}(f_{int}^{(2)} - A_{21}g). \tag{5.12}$$

Substituting into the first equation yields

$$S_{2,h}g = G - A_{12}A_{22}^{-1}f_{int}^{(2)}, \tag{5.13}$$

where $S_{2,h} = A_{11} - A_{12}A_{22}^{-1}A_{21}$. Similarly, the calculation thereof can be extended to the 2D case by using Kronecker products.

5.2.2.3 Dirichlet-Neumann Preconditioner

This section will focus on an optimal preconditioner to solve the transmission problem $S_h g = \widetilde{G}$ on Γ, the artificial interface. Here we consider Dirichlet-Neumann method, which is a domain decomposition preconditioner. It involves solving a Dirichlet boundary value problem on one subdomain and a Neumann boundary value problem on an adjacent subdomain. Once all unknowns are calculated for one subdomain, that data can be used to find the Neumann boundary condition (that is, the derivative) on the interface for the adjacent subdomain.

Recall that $S_h = S_{1,h} + S_{2,h}$, where $S_{i,h}$ is the term in S_h related to subdomain Ω_i, that is, the discrete form of S_i. Then, $S_{i,h}$, (where i is either 1 or 2) is a preconditioner for the system $S_h g = \widetilde{G}$. For clarity, we will take $i = 1$. Then the preconditioned system is

$$(I + S_{1,h}^{-1}S_{2,h})u_3 = S_{1,h}^{-1}\widetilde{G}. \tag{5.14}$$

Here, applying $S_{2,h}$ to u_3 involves solving a PDE with Dirichlet boundary condition along the interface Γ. Further, applying of $S_{1,h}^{-1}$ to some vector involves solving a PDE with Neumann boundary condition along the interface Γ. Therefore, this is called a Dirichlet–Neumann preconditioner. The ratio of the largest eigenvalue to the smallest eigenvalue, known as the condition number, can be proven to be bounded above by a constant independent of h for finite difference/element discretization.

5.2.2.4 Poincaré - Steklov Operator for the Biharmonic Opeartor

Let Ω be a domain with a smooth boundary which is bounded in $\mathbf{R}^N$. Suppose Ω is divided in to two non-overlapping subdomains, that is, $\overline{\Omega} = \overline{\Omega}_1 \cup \overline{\Omega}_2$ with $\Omega_1 \cap \Omega_2 = \varphi$. Assume that the artificial boundary $\Gamma = \overline{\Omega}_1 \cap \overline{\Omega}_2$ is nontrivial.

Now consider the biharmonic equation with homogeneous Dirichlet boundary conditions:

$$\Delta^2 u = f \ \ on \ \ \Omega, \quad u = 0 = \frac{\partial u}{\partial \nu} \ \ on \ \ \partial\Omega.$$

Here, $f \in H^{-2}(\Omega)$ and $u \in H_0^2(\Omega)$ and Δ denotes the Laplacian.

While Laplace equation requires only one boundary condition, in contrast, biharmonic equation requires two boundary conditions. Define the trace spaces

$$H_{00}^{1/2}(\Gamma) = \left\{ v|_\Gamma, v \in H_0^1(\Omega) \right\}, \quad H_{00}^{3/2}(\Gamma) = \left\{ v|_\Gamma, v \in H_0^2(\Omega) \right\},$$

with duals $H^{-1/2}(\Gamma)$ and $H^{-3/2}(\Gamma)$, respectively.

Now we shall derive the Poincaré - Steklov operator for the biharmonic operator [17], [25].

Let $p \in H_{00}^{3/2}(\Gamma)$ and $q \in H_{00}^{1/2}(\Gamma)$. For $i = 1, 2$, define $v_i \in H^2(\Omega_i)$ as the solution of

$$\begin{aligned} \Delta^2 v_i &= 0 \ \ on \ \ \Omega_i, \\ v_i &= p \ \ on \ \ \Gamma, \\ \frac{\partial v_i}{\partial \nu_i} &= q \ \ on \ \ \Gamma, \\ v_i = \frac{\partial v_i}{\partial \nu_i} &= 0 \ \ on \ \ \partial\Omega_i \backslash \Gamma, \end{aligned}$$

where ν_i is the unit outward normal with respect to $\Omega_i, i = 1, 2$.

Similarly, for $r \in H_{00}^{3/2}(\Gamma)$ and $s \in H_{00}^{1/2}(\Gamma)$, define $w_i \in H^2(\Omega_i)$ as the solution of

$$\begin{aligned} \Delta^2 w_i &= 0 \ \ on \ \ \Omega_i, \\ w_i &= r \ \ on \ \ \Gamma, \\ \frac{\partial w_i}{\partial \nu_i} &= s \ \ on \ \ \Gamma, \\ w_i = \frac{\partial w_i}{\partial \nu_i} &= 0 \ \ on \ \ \partial\Omega_i \backslash \Gamma. \end{aligned}$$

Here, all functions are assumed to be smooth. Then the PDE for v_i is multiplied by w_i and then integrated by parts to obtain

$$\int_\Gamma \left(\Delta v_i s - \frac{\partial \Delta v_i}{\partial \nu_i} r \right) = \int_{\Omega_i} \Delta v_i \Delta w_i.$$

Thus, the biharmonic Poincaré - Steklov operator $S_i : H_{00}^{3/2}(\Gamma) \times H_{00}^{1/2}(\Gamma) \to H^{-3/2}(\Gamma) \times H^{-1/2}(\Gamma)$ is defined by

$$S_i \begin{bmatrix} p \\ q \end{bmatrix} = \begin{bmatrix} -\frac{\partial \Delta v_i}{\partial \nu_i} \\ \Delta v_i \end{bmatrix}_\Gamma .$$

More generally, with $\langle \cdot, \cdot \rangle$ a duality pairing,

$$\left\langle \begin{bmatrix} r \\ s \end{bmatrix}, S_i \begin{bmatrix} p \\ q \end{bmatrix} \right\rangle = \int_{\Omega_i} \Delta v_i \Delta w_i.$$

5.3 Nonlinear Preconditioning

5.3.1 An Overview of Nonlinear Solvers

Many real-world situations are governed by nonlinear partial differential equations. Discretization techniques such as finite difference, finite element and spectral methods are used to solve nonlinear PDEs and require the formulation of large-scale algebraic systems. Such PDE solvers can be classified into several important categories.

- Newton-type methods: These methods always start with linearizing a global problem by using Newton's method or one of its inexact variants. A linear solver such as Krylov subspace methods can be used to solve the resulting nonlinear system. Matrix-free implementation techniques of these methods exist. Therefore, explicit formulation of the matrix of the linear system is not necessary. For instance, Jacobian-free Newton-Krylov methods can be used to formulate Jacobian-vector product. The inherent problem of Newton-type methods is, the convergence depends on the initial guess. If the initial guess is far from the exact solution, there is no guarantee that the method will converge. To overcome this problem, globalization techniques have to be introduced to the solver. Trust-region and line search methods are examples of such globalization techniques.

- Nonlinear Krylov methods: Namely, nonlinear conjugate gradients (NCG), nonlinear Richardson, nonlinear GMRES (NGMRES) and Anderson mixing methods are such nonlinear Krylov methods. The nonlinear Richardson is an extension of the linear Richardson iteration. Similarly, NCG is an extension of the linear conjugate gradient (CG) method. All nonlinear methods determine the step length using line search techniques. The Anderson mixing method and

NGMRES combine several former iterations and formulate a residual problem that is to be minimized.

- Decomposition methods: These methods regularly serve as nonlinear preconditioners or accelerators because there is no guarantee that the iterative method will converge. Here we consider the nonlinear additive Schwarz methods, which involve parallel solving of local subdomain problems and the summation of resulting corrections to determine a global search direction.

5.3.2 Background of Nonlinear Preconditioning

Discretization of PDEs often result in large algebraic systems and Newton methods are a popular choice for solving them. As an example, Newton-Krylov-Schwarz methods are successfully implemented in many PDEs. However, for systems with unbalanced nonlinearities, poor choice of an initial guess leads to frequent "nonlinear stiffness". This is the main problem of these methods. For such nonlinearly stiff problems, Newton's method could waste significant computational resources due to a high number of futile iterations, or the method may diverge. Globalization techniques such as line search and trust-region are employed to ensure convergence. However, convergence may be extremely slow for difficult problems.

Nonlinear elimination and nonlinear preconditioning are two well-known approaches used to handle strong nonlinearities. In the nonlinear elimination, before applying a global Newton iteration, local high nonlinearities are eliminated by removing the variables that cause the nonlinearities. In nonlinear preconditioning, nonlinearities are reduced by solving a preconditioned system instead of the original system. In this chapter, we focus on the nonlinear preconditioning techniques for overlapping domain decomposition.

Nonlinear Schwarz algorithms are very popular iterative methods that can be used to solve nonlinear systems. However, numerical results show that they are usually not very strong in handling nonlinearities, except for monotone systems. Fortunately, the nonlinear Schwarz works well as a nonlinear preconditioner. In order to overcome unbalanced nonlinearities and improve global convergence properties, two methods have been developed; namely, the Additive Schwarz Preconditioned Inexact Newton (ASPIN) algorithm and the Restricted Additive Schwarz Preconditioned Exact Newton (RASPEN) algorithm. The ASPIN algorithm was first introduced by Cai and Keyes [8] in 2002. The main idea of ASPIN is, instead of solving the original system, solve a corresponding nonlinearly preconditioned system which has the same solution as the original system. Here, an inexact Jacobian is used because directly calculating the exact Jacobian is computationally expensive and inconvenient. ASPIN algorithm has been implemented for some formidable problems successfully such as Navier-Stokes flows at high Reynolds numbers. The RASPEN method was introduced by five mathematicians in 2016 [14] and it is identified as a superior preconditioner for Newton's method. While RASPEN is quite similar to ASPIN, all components of RASPEN are directly defined by the iterative method. Therefore, RASPEN converges when used as an iterative solver whereas ASPIN may not. Further, various improvements have been proposed and analyzed for both methods, such as two-level ASPIN and two-level RASPEN, which employ a coarse grid for global communication, achieving a convergence rate independent of the number of subdomains.

5.3.3 Inexact Newton with Backtracking

This section describes the classical Inexact Newton method with Backtracking (INB), which plays an essential role in nonlinear preconditioning. INB method is a nonlinear solver that can be used to solve a transformed global system.

Suppose, there is a discrete nonlinear function $F : \mathbb{R}^n \to \mathbb{R}^n$. We want to find a vector $x^* \in \mathbb{R}^n$ such that

$$F(x^*) = 0,$$

where $F = [F_1, F_2, ..., F_n]^T$ and $x = [x_1, x_2, ..., x_n]^T$. Newton's method for solving $F(x) = 0$ with respect to the current approximation $x^{(k)}$, is given below in Algorithm I.

Algorithm I: Newton's method

$x^{(0)}$ is an initial guess which is given.

for $k = 0, 1, 2, \ldots$ until convergence **do**

Solve $F'(x^{(k)})d^{(k)} = F(x^{(k)})$.

Set $x^{(k+1)} = x^{(k)} - d^{(k)}$.

end

If the number of unknowns is large, it is generally very expensive to solve Newton equations at each step because we have two functions to evaluate with each iteration $F(x^{(k)})$ and $F'(x^{(k)})$. The latter is especially computationally expensive when n is large. Further, it is not guaranteed that Newton's method will converge if the exact solution x^* is too far from the given initial guess x^0. Hence, using iterative methods to solve Newton equations approximately for an inexact Newton direction is more practical. This is known as the Inexact Newton (IN) method and is described below in Algorithm II.

Algorithm II: IN (Inexact Newton method)

$x^{(0)}$ is an initial guess which is given.

for $k = 0, 1, 2, \ldots$ until convergence **do**

Choose $\eta_k \in [0, 1)$.

Find $d^{(k)}$ which satisfies

$$\left\| F(x^{(k)}) - F'(x^{(k)}) d^{(k)} \right\| \leq \eta_k \left\| F(x^{(k)}) \right\|.$$

Set $x^{(k+1)} = x^{(k)} - d^{(k)}$.

end

Here η_k is known as a "forcing term" and it is evident that Algorithm II reduces to the Newton's method when $\eta_k = 0$. GMRES is a well known Krylov subspace method that can be used to solve the Jacobian linear system and η_k is used to determine the accuracy.

Unfortunately, it is possible that the Inexact Newton method also may not converge given that x^0 is too far away from x^*. Hence, a globalization strategy such as line search, needs to be incorporated to the Inexact Newton method to ensure convergence.

The line search algorithm tries to find a $x^{(k+1)}$ using the function $f(x) = \frac{1}{2} \|F(x)\|^2$. This is done by reducing the step length by some factor in the descent direction $d^{(k)}$ until a "good enough" $x^{(k+1)}$ is found. First, the full Newton step is tried by taking $\lambda^{(k)} = 1$. If $x^{(k+1)} = x^{(k)} - d^{(k)}$ is not acceptable according to $f(x)$, then the step length $\lambda^{(k)}$ is reduced until a $\lambda^{(k)}$ is found such that $x^{(k+1)} = x^{(k)} - \lambda^{(k)} d^{(k)}$ is acceptable. Backtracking line search method is described below in Algorithm III.

Algorithm III: Backtracking line search

Input: $x^{(k)}$ and $d^{(k)}$.

Define$f(x) = \frac{1}{2} \|F(x)\|^2$. Take $\alpha \in (0, 1)$ and $0 < \theta_{min} < \theta_{max} < 1$.

Let $\lambda^{(k)} = 1$.

while $f(x^{(k)} - \lambda^{(k)} d^{(k)}) > f(x^{(k)} - \alpha \lambda^{(k)} \nabla f(x^{(k)})^T d^{(k)})$ **do**

choose some $\theta \in [\theta_{min}, \theta_{max}]$.

$\lambda^{(k)} = \theta \lambda^{(k)}$.

end

Recall that, Inexact Newton method can be combined with backtracking line search to ensure convergence. Therefore, a new method is formulated by combining Algorithms 2 and 3. This new method, named as Inexact Newton backtracking (INB), is described in Algorithm IV.

Algorithm IV: INB (Inexact Newton backtracking algorithm)

$x^{(0)}$ is an initial guess which is given.

for $k = 0, 1, 2, \ldots$ until convergence **do**

Choose $\eta_k \in [0, 1)$.

Find $d^{(k)}$ such that

$$\left\| F(x^{(k)}) - F'(x^{(k)}) d^{(k)} \right\| \leq \eta_k \left\| F(x^{(k)}) \right\|.$$

Determine $\lambda^{(k)}$ using Algorithm III.

Set $x^{(k+1)} = x^{(k)} - \lambda^{(k)} d^{(k)}$.

end

Unfortunately, Algorithm 4 may not be effective for difficult problems, for instance, Navier-Stokes and MHD equations at high Reynolds numbers. The next section will introduce nonlinear preconditioning which is a state-of-the-art technique that is able to handle such difficult problems.

5.3.4 Additive Schwarz Preconditioned Inexact Newton (ASPIN)

In the first part of this chapter (spectral domain decomposition), we discussed the concept of linear preconditioning. However, linear preconditioning is not suitable for nonlinear systems with strong nonlinearities such as Navier-Stokes and MHD equations. This section will discuss nonlinear preconditioning techniques for such nonlinear systems. Consider a given nonlinear function $F : \mathbb{R}^n \to \mathbb{R}^n$. Starting from an initial guess $u^{(0)} \in \mathbb{R}^n$, find a vector $u^* \in \mathbb{R}^n$ such that

$$F(u^*) = 0.$$

Here $F = (F_1, \ldots, F_n)^T, F_i = F_i(u_1, \ldots, u_n)$, and $u = (u_1, \ldots, u_n)^T$. The above nonlinear system can be solved using Inexact Newton algorithms. However, Inexact Newton algorithms often stagnate even with the application of global strategies such as linesearch. This is especially the case for problems with unbalanced nonlinearities. The reason for this stagnation is that Inexact Newton is not equipped to properly handle such nonlinearities. To find the same solution $u^* \in \mathbb{R}^n$, instead of trying to solve the system $F(u^*) = 0$, we can solve an equivalent nonlinearly preconditioned system $\mathcal{F}(u^*) = 0$ which has more balanced nonlinearities.

While $\mathcal{F}$ and F must have the same solution, it is very possible that they have different forms. In general, $\mathcal{F}$ is a function of both F and u. However, it is not necessary to explicitly know how $\mathcal{F}$ depends on F or u. For instance, the form of $\mathcal{F}$ could be a composite function

$$\mathcal{F}(u^*) \equiv G(F(u^*)) = 0.$$

Here, G is known as a nonlinear preconditioner. Listed below are some important properties of the preconditioner $G : \mathbb{R}^n \to \mathbb{R}^n$ thereof:

1. If $G(x) = 0$, then $x = 0$.
2. G is close to F^{-1} in some sense.
3. $G(F(w))$ is easily computable for given $w \in \mathbb{R}^n$.
4. If a Newton–Krylov-type method is used for solving $\mathcal{F}(x) = 0$, then the matrix-vector product $(G(F(w)))'v$ should also be easily computable for $w, v \in \mathbb{R}^n$.

It is not required to explicitly form the nonlinear preconditioner G - it is defined implicitly.

Next, we will describe a nonlinear preconditioner based on the additive Schwarz method; specifically, the Additive Schwarz Preconditioned Inexact Newton (ASPIN) method, which was proposed by Cai and Keyes [8]. While methods such as Inexact Newton do not converge for flows with high Reynolds numbers, numerical results show that the ASPIN method works well in such cases.

The formulation of the ASPIN algorithm will now be explained in detail. Let us consider a nonlinear system

$$F(u) = 0. \tag{5.15}$$

Take

$$\Omega = \bigcup_{i=1}^{N} \Omega_i, \tag{5.16}$$

to be a global domain which has been subdivided into N subdomains that overlap one another. The corresponding nonlinearly preconditioned system

$$\mathcal{F}(u) = 0 \tag{5.17}$$

can be formulated in the following manner. First of all, using the subdomains of Ω, the subspace of $\mathbb{R}^n$ is introduced as well as the corresponding restriction and prolongation (extension) matrices. Then an $n \times n$ restriction matrix R_i is defined as follows. If $k \in \Omega_i$, then the kth column of R_i is the kth column of the $n \times n$ identity matrix $I_{n\times n}$; and if $k \notin \Omega_i$, the kth column of R_i is zero. Subsequently, R_i^T is taken as the prolongation operator P_i and it is assumed that R_i and P_i satisfy the relation $R_iP_i = I_{\Omega_i}$, the identity on Ω_i.

The subdomain nonlinear function can be defined as

$$F_{\Omega_i} = R_iF,$$

by applying the restriction operator R_i to F. Next, let G_i denote nonlinear subdomain solution operator such that, $u_i^n = G_i(u^{n-1})$. Therefore, the local inverse $G_i : \Omega \to \Omega_i$ is defined as the solution of

$$R_iF(P_iG_i(u) + (I - P_iR_i)u) = 0. \tag{5.18}$$

Further, we define subdomain correction $C_i(u) \in \Omega_i$ such that

$$F_{\Omega_i}(u + P_iC_i(u)) = R_iF(u + P_iC_i(u)) = 0, \quad i = 1, \ldots, N. \tag{5.19}$$

Then, the preconditioned function is defined as

$$\mathcal{F}(u) = \sum_{i=1}^{N} P_i C_i(u). \tag{5.20}$$

This is known as the ASPIN. A Newton algorithm with an inexact Jacobian is used to solve the preconditioned system (5.17). Using the definition (5.19), we can write

$$F_{\Omega_i}(u + P_i C_i(u)) = F_{\Omega_i}(P_i(R_i u + C_i(u)) + u - P_i R_i u) = 0.$$

Assume that unique solutions to the local problems exist. Therefore, with comparison to (5.18), it can be deduced that

$$G_i(u) = R_i u + C_i(u). \tag{5.21}$$

Therefore, ASPIN can be written in the form

$$\mathcal{F}(u) = \sum_{i=1}^{N} P_i C_i(u) = \sum_{i=1}^{N} P_i G_i(u) - \sum_{i=1}^{N} P_i R_i u. \tag{5.22}$$

Now let us see how to compute the Jacobian matrix of ASPIN. For simplicity, take

$$u^{(i)} := P_i G_i(u) + (I - P_i R_i)u \quad and \quad J(u) = F^{'}(u). \tag{5.23}$$

By differentiation of (5.18), we obtain

$$G_i^{'}(u) = -(R_i J(u^{(i)}) P_i)^{-1} R_i J(u^{(i)}) + R_i. \tag{5.24}$$

Now, we can obtain the Jacobian of ASPIN in (5.22)

$$\mathcal{J}(u) = \mathcal{F}^{'}(u) = \sum_{i=1}^{N} P_i G_i^{'}(u) - \sum_{i=1}^{N} P_i R_i. \tag{5.25}$$

Using (5.24),

$$\mathcal{J}(u) = -\sum_{i=1}^{N} P_i (R_i J(u^{(i)}) P_i)^{-1} R_i J(u^{(i)}). \tag{5.26}$$

Direct calculation of this exact Jacobian is both expensive and inconvenient. Hence, the inexact Jacobian $\widehat{\mathcal{J}}$ is introduced to replace the exact Jacobian.

$$\widehat{\mathcal{J}}(u) = -\sum_{i=1}^{N} J_{\Omega_i}^{-1}(u) J(u), \tag{5.27}$$

where $J_{\Omega_i}^{-1}(u) = P_i (R_i J(u) P_i)^{-1} R_i$. When F is affine, $\widehat{\mathcal{J}}$ turns out to be the additive Schwarz preconditioned matrix.

The ASPIN algorithm can be summarized as below [8].

Algorithm : ASPIN

Recall algorithms 3 and 4 in section 5.3.3.

Let $\alpha \in (0, 1)$ and $0 < \theta_{min} < \theta_{max} < 1$ be given.

Suppose $u^{(0)}$ is a given initial guess. Let k be the current iteration and $u^{(k)}$ be the current approximate solution. Then, a new approximate solution $u^{(k+1)}$ at iteration $k + 1$ can be computed as follows.

1. Follow the steps below to compute the nonlinear residual $g^k = \mathcal{F}(u^{(k)})$.

   (a) Starting from $g_i^{(k)} = 0$, find $g_i^{(k)} = P_i C_i(u^{(k)}),\ i = 1, \ldots, N$, by solving the subdomain nonlinear systems

   $$F_{\Omega_i}(u^{(k)} - g_i^{(k)}) = 0.$$

(b) Form the global residual

$$g^k = \mathcal{F}(u^{(k)}) = \sum_{i=1}^{N} g_i^{(k)}.$$

(c) Check the stopping conditions on $g^{(k)}$.

2. Find the inexact Newton direction $d^{(k)}$ by approximately solving the Jacobian system,

$$\sum_{i=1}^{N} J_{\Omega_i}^{-1} J d^{(k)} = g^{(k)},$$

such that

$$\left\| g^{(k)} - \sum_{i=1}^{N} J_{\Omega_i}^{-1} J d^{(k)} \right\| \leq \eta_k \left\| g^{(k)} \right\|,$$

where $\eta_k \in [0, 1)$ is a forcing term.

3. Compute the approximate solution

$$u^{(k+1)} = u^{(k)} - \lambda^{(k)} d^{(k)},$$

where the step length $\lambda^{(k)}$ is determined by the backtracking line search algorithm.

5.3.5 Restricted Additive Schwarz Preconditioned Exact Newton (RASPEN)

In this section, we shall discuss a significantly better preconditioner for Newton's method, specifically, the RASPEN (Restricted Additive Schwarz Preconditioned Exact Newton) method. While it is similar to ASPIN, all components of RASPEN are directly defined by the iterative method. It is known that ASPIN, when used as iterative solver, does not converge in the overlap without relaxation. However, in contrast, RASPEN can be effectively be used as an iterative solver.

Consider a 1D nonlinear function $\mathcal{L}u$ (for example, $-\partial_x((1+u^2)\partial_x u)$) as described in [14].

$$\begin{aligned} \mathcal{L}u &= f \quad in \;\; \Omega := [0, L], \\ u(0) &= 0, \\ u(L) &= 0, \end{aligned} \tag{5.28}$$

The classical parallel Schwarz method for the two overlapping subdomains $\Omega_1 := [0, \beta]$ and $\Omega_2 := [\alpha, L]$, $\alpha < \beta$ is

$$\begin{aligned} \mathcal{L}(u_1^n) &= f \qquad\qquad in \;\; \Omega_1 := [0, \beta], \\ u_1^n(0) &= 0, \\ u_1^n(\beta) &= u_2^{n-1}(\beta), \\ \mathcal{L}(u_2^n) &= f \qquad\qquad in \;\; \Omega_2 := [\alpha, L], \\ u_2^n(\alpha) &= u_1^{n-1}(\alpha), \\ u_2^n(L) &= 0. \end{aligned} \tag{5.29}$$

A sequence of approximate solutions relating to each subdomain can be calculated using the method thereof. Those subdomain solutions can be combined together to form a global approximate solution which is more convenient to use. The simplest

way to form this global solution is to imagine a non-overlapping partition and select data from each subdomain as shown below.

$$u^n(x) = \begin{cases} u_1^n(x), & \text{if } 0 \le x < \frac{\alpha+\beta}{2}, \\ u_2^n(x), & \text{if } \frac{\alpha+\beta}{2} \le x \le L. \end{cases} \tag{5.30}$$

Therefore, extension operators $\widetilde{P}_i$ need to be used to form a global solution,

$$u^n = \widetilde{P}_1 u_1^n + \widetilde{P}_2 u_2^n.$$

As opposed to ASPIN, we take $\widetilde{P}_i$ as the "restricted" prolongation operator and assume that R_i and $\widetilde{P}_i$ satisfy $\sum_{i=1}^{N} \widetilde{P}_i R_i = I_\Omega$, the identity on Ω. For ease of understanding, we depict the difference between prolongation operator P_i and restricted prolongation operator $\widetilde{P}_i$ for the 1D case. Condiser the global domain $\Omega = [-1, 1]$ and two overlapping subdomains $\Omega_1 = [-1, a]$ and $\Omega_2 = [b, 1]$ where $b < a$.

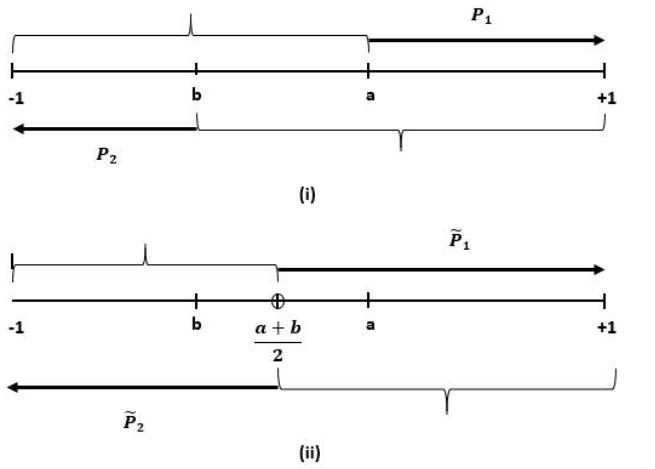

Figure 5.6: Prolongation operators.

The prolongation operator P_1 in (i) of Figure 5.6 extends a function defined on first subdomain $[-1, a]$ to global domain Ω by zero. Similarly, one can define prolongation

operator for the second subdomain. In the restricted prolongation operators in (ii) of Figure 5.6, instead of extending the function from Ω_i to Ω, we select data from $[-1, \frac{a+b}{2})$ for the first subdomain and $[\frac{a+b}{2}, 1]$ for the second subdomain and choose $\widetilde{P}_1$, $\widetilde{P}_2$ such that $\widetilde{P}_1 R_1 + \widetilde{P}_2 R_2 = I_\Omega$.

Now, Newton's method can be used to accelerate the nonlinear fixed point iteration (5.29). Let the local solutions in the nonlinear subdomains be

$$u_1^n = G_1(u^{n-1}), \qquad u_2^n = G_2(u^{n-1}), \tag{5.31}$$

where G_1 and G_2 are solution operators. Therefore, the classical parallel Schwarz method (5.29) can be written for N subdomains as,

$$u^n = \sum_{i=1}^{N} \widetilde{P}_i G_i(u^{n-1}) =: \mathcal{G}(u^{n-1}), \quad i = 1, \ldots, N. \tag{5.32}$$

Consider the nonlinear equation

$$\mathcal{F}(u) := \mathcal{G}(u) - u = \sum_{i=1}^{N} \widetilde{P}_i G_i(u) - u = 0. \tag{5.33}$$

The fixed point iteration (5.32) can be used as a preconditioner when solving (5.33) using Newton's method. This method is named as RASPEN.

Similar to the ASPIN, RASPEN method can be formulated in correction form. Recall that $G_i : \Omega \to \Omega_i$ are solutions of

$$R_i F(P_i G_i(u) + (I - P_i R_i)u) = 0. \tag{5.34}$$

Then, using Newton's method, RASPEN solves the nonlinear problem

$$\mathcal{F}(u) = \sum_{i=1}^{N} \widetilde{P}_i G_i(u) - u = 0. \tag{5.35}$$

The corresponding fixed point iteration to the preconditioned nonlinear function (5.35) is

$$u^n = \sum_{i=1}^{N} \widetilde{P}_i G_i(u^{n-1}). \tag{5.36}$$

Further, the correction form of RASPEN for equation (5.35) can be written as

$$\mathcal{F}(u) = \sum_{i=1}^{N} \widetilde{P}_i (G_i(u) - R_i u) =: \sum_{i=1}^{N} \widetilde{P}_i C_i(u), \tag{5.37}$$

where $C_i(u) := G_i(u) - R_i u$ is the correction. Now, equation (5.34) can be written in terms of $C_i(u)$ as $R_i F(u + P_i C_i(u)) = 0$.

Further, the Jacobian of RASPEN can be deduced from (5.35).

$$\mathcal{J}(u) = \mathcal{F}'(u) = \sum_{i=1}^{N} \widetilde{P}_i G_i'(u) - I = -\sum_{i=1}^{N} \widetilde{P}_i (R_i J(u^{(i)}) P_i)^{-1} R_i J(u^{(i)}), \tag{5.38}$$

since the identity cancels.

In the next chapter, we will present some numerical experiments for the stream function formulation of the unsteady Navier-Stokes and MHD equations using both ASPIN and RASPEN methods.

6

Numerical Experiments

We implemented, using MATLAB, space-time Legendre and Chebyshev collocation methods for all PDEs discussed in this thesis. Results pertaining to Legendre collocation are presented in this section. We observed almost identical results for the Chebyshev case but they are not given.

6.1 Space-time Legendre collocation method for the 1D and 2D unsteady Stokes equations.

Consider the stream function formulation of the 1D unsteady Stokes equation

$$(\psi_t)_{xx} = \psi_{xxxx} + f,$$

with homogeneous Dirichlet boundary conditions and initial condition $\psi(x,-1) = \psi_0(x)$. Take f when the exact solution is $\psi(x,t) = e^{x+t}\sin(\pi t/2)\sin^2(\pi x)$. Spectral convergence is clearly illustrated in the left figure of Figure 1. The error is the largest error of the numerical solution at the Legendre nodes at the final time $t = 1$. Note that the error is $O(10^{-11})$ at N = 20.

Now consider Legendre collocation method for the stream function formulation of

the 2D unsteady Stokes equation

$$(\psi_t)_{xx} + (\psi_t)_{yy} = \psi_{xxxx} + \psi_{yyyy} + 2\psi_{xxyy} + f,$$

with homogeneous Dirichlet boundary conditions and initial condition $\psi(x, y, -1) = \psi_0(x, y)$. Take f when the exact solution is $\psi(x, y, t) = \pi e^{(x+2y+t)} \sin^2(\pi x) \sin^2(\pi y)$. Spectral convergence is clearly illustrated in the right figure of Figure 6.1. Both 1D and 2D unsteady Stokes equations are solved by the Hessenberg-Schur algorithm.

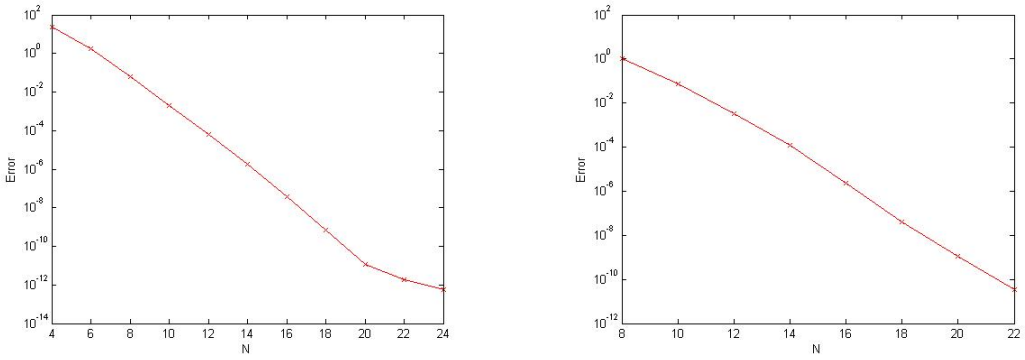

Figure 6.1: Convergence of Legendre Collocation method for the 1D (left) and 2D (right) unsteady Stokes equations.

The spectrum of the 1D and 2D spectral Legendre operators and plots of the spectral condition numbers as functions of N are shown in Figures 6.2 and 6.3. Also, Figure 6.4 shows the streamline patterns at $t = 1$ for the 2D unsteady Stokes equations.

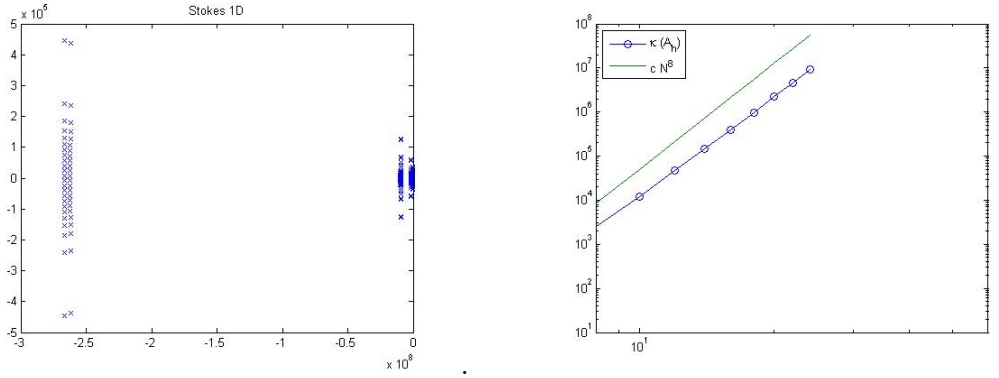

Figure 6.2: Spectrum (left) and spectral condition number (right) for the 1D unsteady Stokes equation.

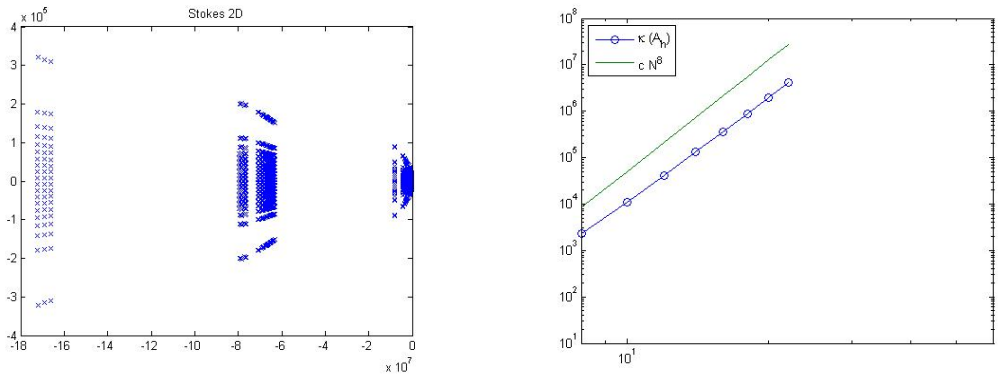

Figure 6.3: Spectrum (left) and spectral condition number (right) for the 2D unsteady Stokes equation.

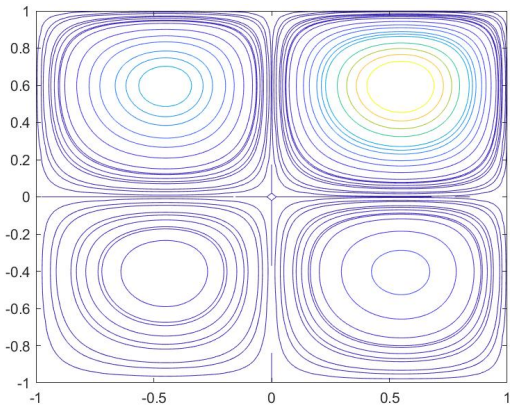

Figure 6.4: Streamline patterns for the 2D unsteady Stokes equations at $t = 1$.

Further, if there are non-homogeneous boundary conditions for 1D Stokes equation $\psi_{xxxx} = f$ such that, $\psi(-1) = 0 = \psi^{'}(-1)$ and $\psi(1) = a, \psi^{'}(1) = b$, spectral Tau method is used to implement this non-homogeneous Neumann boundary condition. As a result, Neumann boundary condition adds an extra equation to the system which becomes rectangular. While both pseudoinverse and QR factorization can be used to solve this rectangular system, QR factorization is more accurate and also cheaper than using pseudoinverse. Therefore, in this thesis we used QR factorization to solve all non-homogeneous boundary value problems.

Next, we present numerical results for nonlinear PDEs. For all nonlinear PDEs, we take zero function as the initial guess and use the iteration defined for each nonlinear PDE. The iteration procedure is terminated whenever the infinity norm of the difference of two consecutive iterates is less than $\epsilon = 10^{-13}$.

6.2 Space-time Legendre collocation method for the unsteady Navier-Stokes equation.

Consider first the stream function formulation of the unsteady Navier-Stokes equation

$$-\Delta\psi_t + \frac{1}{Re}\Delta^2\psi - \psi_y\psi_{xxx} + \psi_x\psi_{yyy} + \psi_x\psi_{yxx} - \psi_y\psi_{xyy} = f,$$

with homogeneous Dirichlet boundary conditions and initial condition $\psi(x, y, -1) = \psi_0(x, y)$. Take f when the exact solution is $\psi(x, y, t) = \frac{1}{2}e^t x \sin^2(\pi x)\sin^2(\pi y)$. See the Figure 6.5 for the spectral convergence.

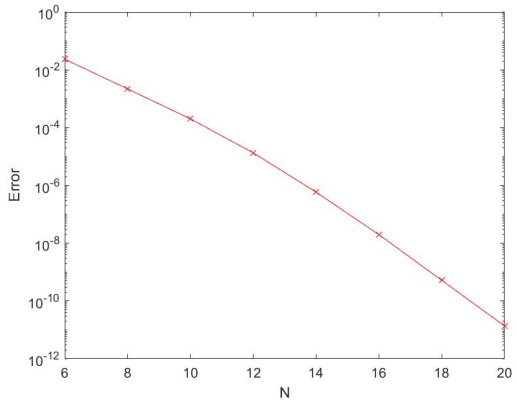

Figure 6.5: Convergence of Legendre Collocation method for the unsteady Navier-Stokes equation for $Re = 100$.

In Table 6.1 we consider the case when $N = 20$ is fixed and Re is varying. It can be seen that the number of fixed-point iterations is increasing as Re increases.

Re	No of fixed-point iterations
0.01	4
1	10
10	20
100	37
500	85

Table 6.1: No of fixed-point iterations for the unsteady Navier-Stokes equation for different Reynolds numbers when $N = 20$.

Additionally, the Navier-Stokes equations were implemented for the well-known regularized driven cavity flow where the upper wall is moving to the right at speed of $(x^2-1)^2$ while the other three boundaries are kept stationary. In the classical driven cavity flow, the upper wall moves at a constant speed of one. However, this yields a singularity at both upper corners. The regularized driven cavity removes these singularities. The streamline patterns of ψ for the unsteady regularized driven cavity flow for $Re = 100$ and $Re = 500$ are shown in Figure 6.6. When we compare our results with the literature results of Jie Shen [33], we can see that secondary vortices appeared when $Re \geq 2000$ in his study. Also, his calculations were based on a 65×65 uniform grid, while our results are based on a 20×20 grid. In Jie Shen's method, he used a second-order projection scheme proposed by Kim and Moin for the temporal discretization in conjunction with a Chebyshev-Tau space discretization. However, our solver is unable to compute the solution when Re exceeds much above 500.

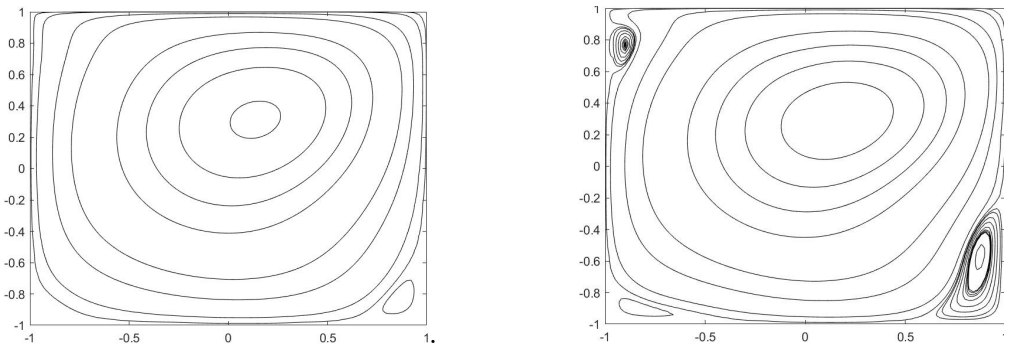

Figure 6.6: Streamline patterns for ψ for $Re = 100$ (left) and $Re = 500$ (right) for the unsteady regularized driven cavity Navier-Stokes equation.

Further, we have implemented Navier-Stokes for the two-sided regularized driven cavity flow. Here, we consider two cases, namely, parallel and anti-parallel wall motions. In the parallel motion, both the upper and lower walls move from left to right in the x-direction with the same velocity $(x^2-1)^2$. In the anti-parallel wall motion, the upper and lower walls move in opposite directions along the x-axis with the same velocity $(x^2-1)^2$. Figure 6.7 shows the streamline patterns for ψ when $Re = 500$ for the parallel wall motions. For the parallel wall motion, the streamlines are found to be symmetrical with respect to the horizontal centerline.

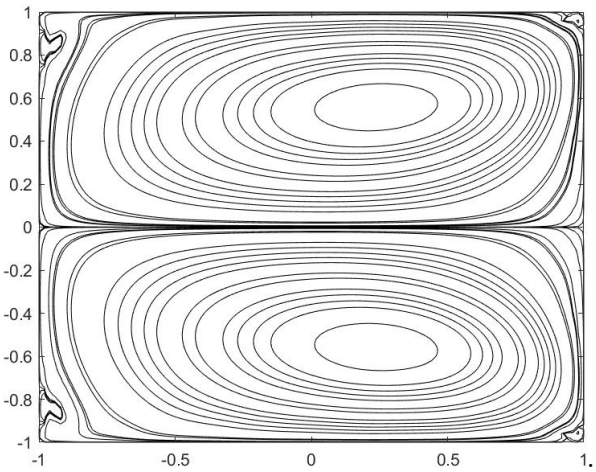

Figure 6.7: Streamline patterns for ψ for $Re = 500$ for parallel wall motions for the two-sided regularized driven cavity flow.

Figure 6.8 shows streamline patterns of ψ for the unsteady, two-sided, regularized driven cavity flow when $Re = 100$ and $Re = 500$ for the anti-parallel wall motions on a 20×20 grid. It can be observed that, two secondary vortices appear near the top left and the bottom right corners of the cavity for $Re = 500$. When comparing our results with the literature results of [30], secondary vortices appear when $Re \geq 1000$. Also, their results were based on the Lattice Boltzmann Method (LBM) and a 513×513 lattice structure was used.

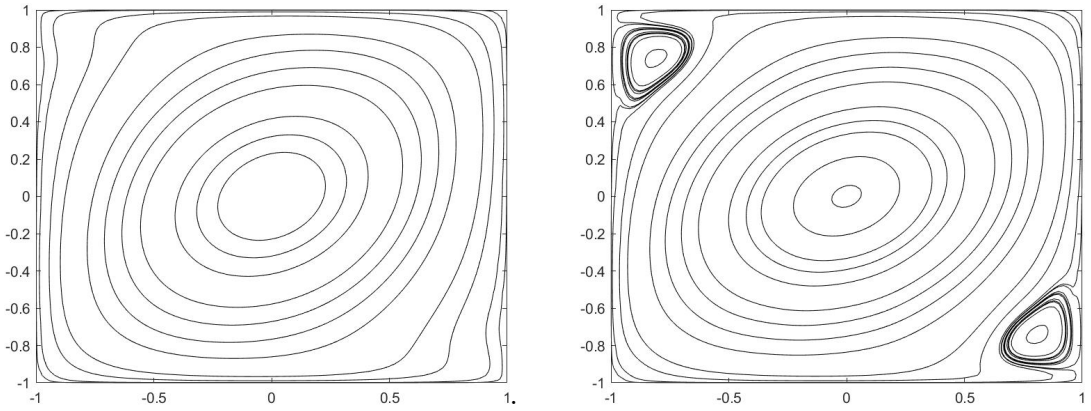

Figure 6.8: Streamline patterns for ψ for $Re = 100$ (left) and $Re = 500$ (right) for anti-parallel wall motions for the two-sided regularized driven cavity flow.

Fewer number of iterations are required for regularized driven cavity flow with compared to two-sided regularized driven cavity flows to achieve the convergence.

6.3 Space-time Legendre collocation method for the unsteady MHD equations.

Consider the stream function formulation of the unsteady MHD equations with the set of boundary conditions (4.14), (4.17) and initial conditions $\psi(x, y, -1) = \psi_0(x, y)$ and $\phi(x, y, -1) = \phi_0(x, y)$.

$$-\Delta\psi_t + \frac{1}{Re}\Delta^2\psi - \psi_y\psi_{xxx} + \psi_x\psi_{yyy} + \psi_x\psi_{yxx} - \psi_y\psi_{xyy} = \phi_{yxx}\phi_x + \phi_{yyy}\phi_x$$
$$-\phi_{xxx}\phi_y - \phi_{xyy}\phi_y + f,$$
$$-\Delta\phi_t + \frac{1}{Re_m}\Delta^2\phi = \psi_{xxy}\phi_x - \psi_x\phi_{xxy} + \psi_y\phi_{yyx} - \psi_{yyx}\phi_y + \psi_y\phi_{xxx} - \psi_x\phi_{yyy} + \psi_{yyy}\phi_x$$
$$-\psi_{xxx}\phi_y + 2\psi_{xy}\phi_{xx} - 2\psi_{xx}\phi_{xy} + 2\psi_{yy}\phi_{yx} - 2\psi_{yx}\phi_{yy} + g.$$

Take f and g when the exact solutions are $\psi(x, y, t) = \frac{1}{4}e^t x \sin^2(\pi x)\sin^2(\pi y)$ and $\phi(x, y, t) = \frac{1}{4}e^t(3x - x^3)(5y^3 - 3y^5)\sin(\pi x)\sin(\pi y)$ respectively. See the Figure 6.9 for the spectral convergence of ψ and ϕ.

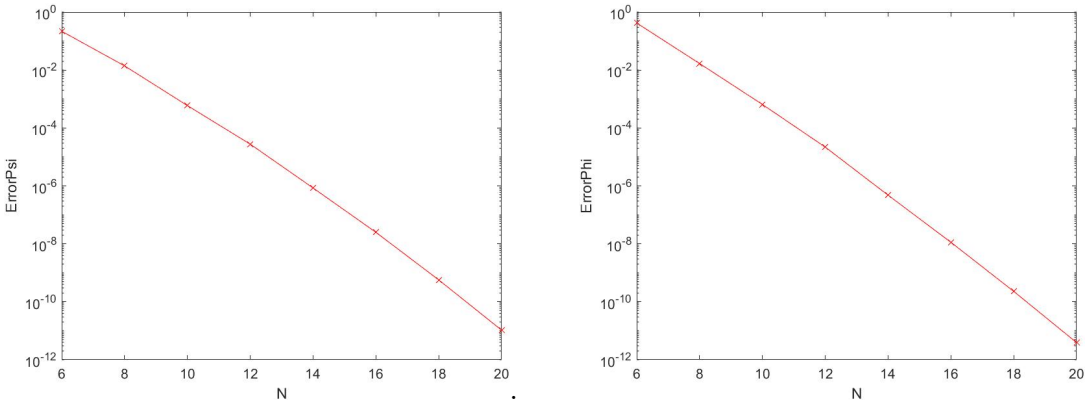

Figure 6.9: Convergence of Legendre collocation method for the unsteady MHD equations for $Re = Re_m = 10$.

In Table 6.2 we consider the case when $N = 20$ is fixed and Re, Re_m are varying. It can be seen that the number of fixed-point iterations is increasing as Re, Re_m increase.

Re	Re_m	No of fixed-point iterations
0.01	0.01	4
1	1	11
10	10	24
100	10	64
500	10	105

Table 6.2: No of fixed-point iterations for the unsteady MHD equations for different Reynolds numbers when $N = 20$.

Further, we implemented unsteady MHD equations for the regularized driven cavity flow where the upper wall is moving to the right at speed of $(x^2 - 1)^2$. Figures 6.10, 6.11 show streamlines patterns for both ψ and ϕ at $t = 1$ for the regularized driven cavity flow when Reynolds numbers are varying.

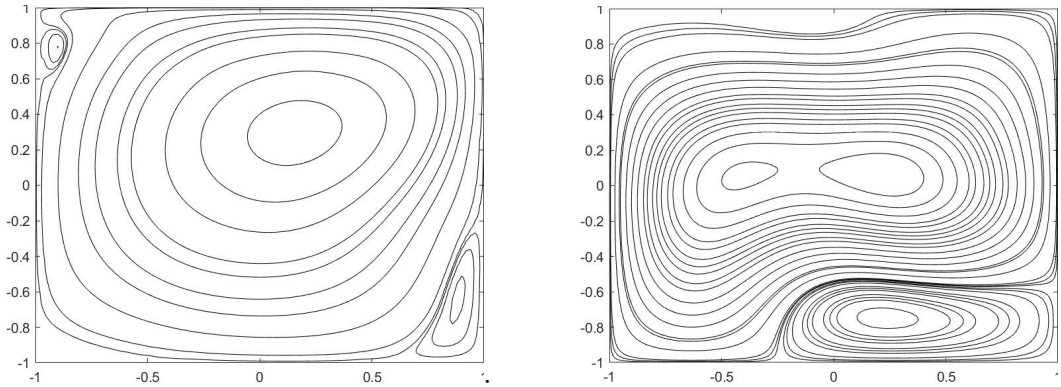

Figure 6.10: Streamline patterns of ψ (left) and ϕ (right) when $Re = 500$ and $Re_m = 10$ for the unsteady regularized driven cavity MHD equations.

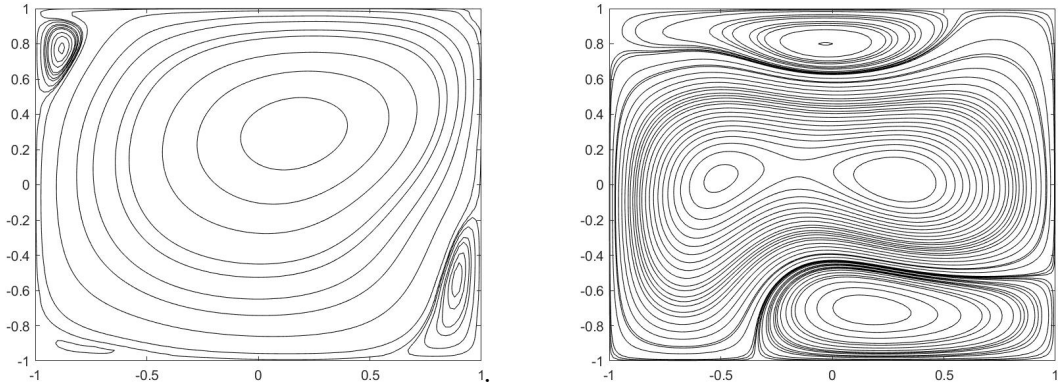

Figure 6.11: Streamline patterns of ψ (left) and ϕ (right) when $Re = 1000$ and $Re_m = 15$ for the unsteady regularized driven cavity MHD equations.

Also, we implemented unsteady MHD equations using spectral methods for periodic boundary conditions. Here we used Fourier spectral methods for space variables and the Legendre collocation method for time variable. We considered the simplest case where the spatial domain is $(0, 2\pi)$ and the temporal domain is $(-1, 1)$.
Let x_j be evenly spaced points in $[0, 2\pi)$, $j = 0, \ldots, N-1$, where N is odd and D_h be the $N \times N$ matrix, called the Fourier pseudospectral derivative matrix, which is given by

$$(D_h)_{kk} = 0, \qquad (D_h)_{kj} = \frac{(-1)^{k-j}}{2\sin((k-j)\pi/n)}, \quad j \neq k.$$

Consider the well-known Orszag-Tang vortex problem for MHD equations. The

computational domain is a periodic, two-dimensional square $\Omega = (0, 2\pi)^2$. The initial conditions at $t = 0$ are given by

$$u = (-\sin(y), \sin(x)), \qquad B = (-\sin(y), \sin(2x)),$$

where periodic boundary conditions exist for ψ, ϕ and their normal derivatives. The streamlines of ψ and ϕ at $t = 1$ for the two-dimensional MHD flow is illustrated in the Figure 6.12.

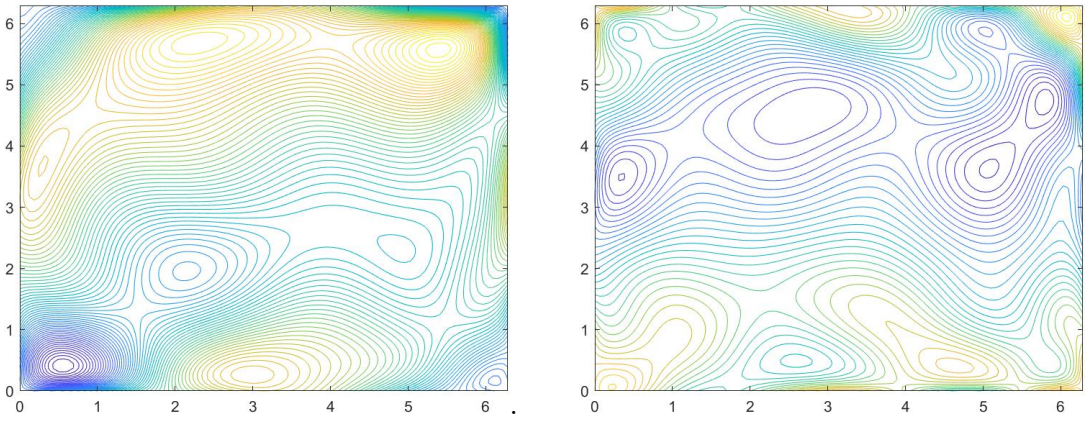

Figure 6.12: Streamlines of ψ and ϕ at $t = 1$ for the two-dimensional MHD flow for $Re = 10$ and $Re_m = 10$.

Next we present numerical results corresponding to the spectral domain decomposition.

6.4 Non-overlapping spectral domain decomposition.

Now we consider the non-overlapping domain decomposition. All of the non-overlapping domain decomposition results are based on the global domain $\Omega = (-1,1) \times (-1,1)$ and two non overlapping subdomains $\Omega_1 = (-1,0) \times (-1,1)$ and $\Omega_2 = (0,1) \times (-1,1)$. Here we used the Poincaré-Steklov operator defined for the Biharmonic operator as explained in the section 5.2.2.4.

6.4.1 Dirichlet-Neumann method for the 2D unsteady Stokes equation.

Consider the stream function formulation of the 2D unsteady Stokes equation

$$(\psi_t)_{xx} + (\psi_t)_{yy} = \frac{1}{Re}(\psi_{xxxx} + \psi_{yyyy} + 2\psi_{xxyy}) + f, \tag{6.1}$$

with homogeneous Dirichlet boundary conditions for the global domain Ω and initial condition $\psi(x,y,-1) = \psi_0(x,y)$. Take f when the exact solution is $\psi(x,y,t) = \frac{1}{4}e^{(1+t)}(1-x^2)^2(1-y^2)^2(x-e^{(1-x)})(x+e^{(1+x)})$. Note that $\epsilon = 10^{-10}$ is the tolerance of the GMRES method. Spectral convergence is shown in the Figure 6.13. Further, some numerical results of non-overlapping spectral domain decomposition method for the 2D Stokes equation are presented in Table 6.3. In Table 6.3, we present number of GMRES iterations for Dirichlet-Neumann method and condition number for the Dirichlet-Neumann preconditioner ($\kappa(S_1^{-1}S_2)$) for the 2D Stokes equation for varying Reynolds numbers and N. It can be seen that the number of GMRES iterations is insensitive to variations in Re, and increase linearly with N. On the other hand, $\kappa(S_1^{-1}S_2)$ appears to be bounded above by a constant independent of N.

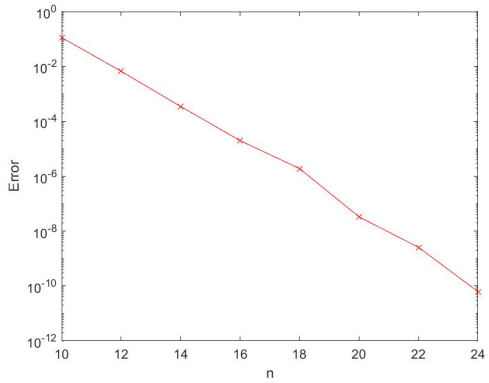

Figure 6.13: Convergence of non-overlapping spectral domain decomposition method for the 2D unsteady Stokes equation for $Re = 1000$.

	Re = 100		Re = 1000		Re = 10000	
N	No of GMRES iterations	$\kappa(S_1^{-1}S_2)$	No of GMRES iterations	$\kappa(S_1^{-1}S_2)$	No of GMRES iterations	$\kappa(S_1^{-1}S_2)$
10	13	61.175	14	56.266	14	56.065
12	14	57.974	14	49.145	14	49.102
14	18	69.079	16	55.974	17	55.313
16	20	56.235	20	45.268	20	45.064
18	22	52.94	21	40.159	22	39.411
20	25	53.792	23	42.656	23	42.442

Table 6.3: Number of GMRES iterations and condition number of the Dirichlet-Neumann preconditioner for the 2D Stokes equation for varying Re and N.

6.5 Overlapping spectral domain decomposition.

Now we present numerical results corresponding to overlapping domain decomposition. All of the overlapping domain decomposition results are based on the global domain $\Omega = (-1, 1) \times (-1, 1)$ and two overlapping subdomains $\Omega_1 = (-1, a) \times (-1, 1)$ and $\Omega_2 = (b, 1) \times (-1, 1)$ where $b < a$. All of the error convergence results are shown below based on a small overlap where $a = 0.1$ and $b = -0.1$. We divided overlapping domain decomoposition results into two parts, linear and nonlinear problems. For the linear problems, we implemented our programs using Additive Schwarz method and for the nonlinear equations we used nonlinear preconditioning methods, ASPIN and RASPEN. First of all we present the error convergence results for the linear case.

6.5.1 Additive Schwarz method for the 2D unsteady Stokes equation.

Consider the stream function formulation of the 2D unsteady Stokes equation (6.1) with homogeneous Dirichlet boundary conditions for the global domain Ω and initial condition $\psi(x, y, -1) = \psi_0(x, y)$. Take f when the exact solution is $\psi(x, y, t) = \frac{1}{4}e^{(x+t)}x(1-x^2)^2\sin^2(\pi y)$. See the Figure 6.14 for the spectral convergence.

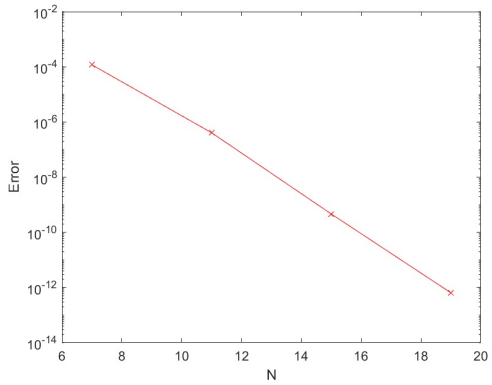

Figure 6.14: Convergence of Additive Schwarz method for the 2D unsteady Stokes equations for $Re = 1000$.

Some numerical results of Additive Schwarz method for the 2D unsteady Stokes equations are presented in Table 6.4, Figure 6.15 and Table 6.5. In Table 6.5, we show the number of GMRES iterations, error and condition number of the Additive Schwarz preconditioned operator for fixed overlap ($a = 0.1$ and $b = -0.1$), varying Re and N. It can be seen that the number of GMRES iterations is insensitive to variations in Re. Also, number of GMRES iterations are independent of N as shown in Table 6.5. That is, it remains constant when N is varying. Further, according to table 6.4 and Figure 6.15, we can conclude that the number of GMRES iterations decrease as overlap widens.

	Re = 1000		Re = 10000	
Overlap region	No of iterations	Error	No of iterations	Error
a=0.1, b= -0.1	10	2.1777×10^{-13}	10	2.4976×10^{-13}
a=0.25, b= -0.25	9	6.1299×10^{-14}	9	6.195×10^{-14}
a=0.4, b= -0.4	8	5.7905×10^{-14}	8	4.9176×10^{-14}

Table 6.4: No of GMRES iterations and error for the unsteady 2D Stokes equation for fixed $N = 20$ and varying Re and overlap.

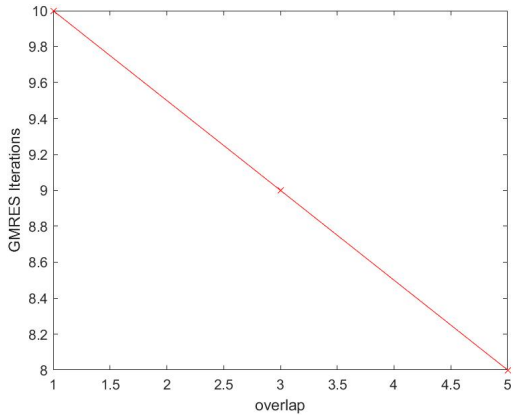

Figure 6.15: Number of GMRES iterations vs overlap for fixed $N = 20$ and $Re = 1000$.

	Re = 1000			Re = 10000		
N	No of iterations	Error	Condition Number	No of iterations	Error	Condition Number
8	9	3.2046×10^{-5}	2.1951	9	3.0345×10^{-5}	2.1956
12	9	5.6732×10^{-8}	2.4876	9	5.0193×10^{-8}	2.4888
16	10	4.0982×10^{-11}	2.8229	9	3.4573×10^{-11}	2.8256
20	10	2.177×10^{-13}	3.1788	10	2.4976×10^{-13}	3.1834

Table 6.5: Number of GMRES iterations, error and condition number of the Additive Schwarz preconditioner for fixed overlap, varying Re and N.

Moreover, using graphs, we present some time comparisons of Additive Schwarz method for the 2D unsteady Stokes equation. In the left figure of Figure 6.14, we show how execution time changes with N for fixed overlap ($a = 0.1$ and $b = -0.1$) and $Re = 1000$. Also, the execution times for different overlaps when $N = 20$ and $Re = 1000$ are illustrated on the right of Figure 6.16. It can be seen that execution time increases as overlap widens. Further, it increases like N^s, where $s = 5.5169$ is

the slope of the loglog plot .

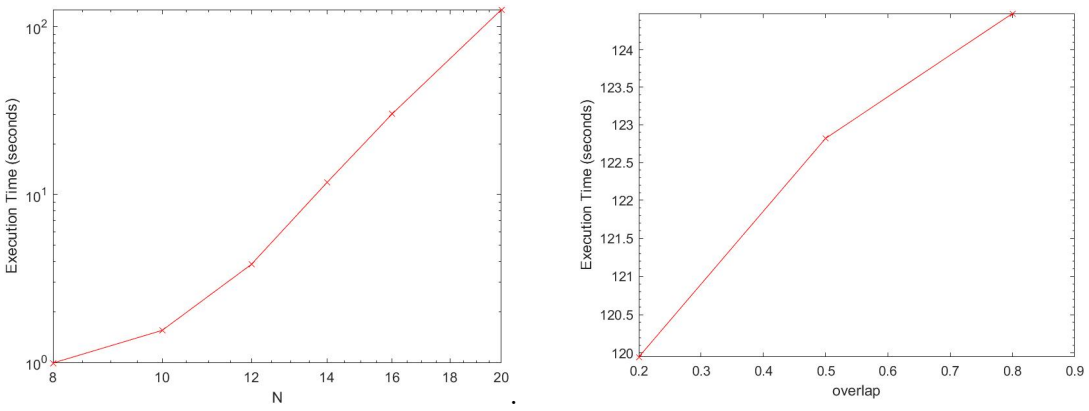

Figure 6.16: Time comparisons of Additive Schwarz method for the 2D unsteady Stokes equation.

The run times (seconds) for different Reynolds numbers when there is a fixed overlap ($a = 0.1$ and $b = -0.1$) and $N = 20$ are shown in Figure 6.17. It is seen that the execution time is essentially independent of Re.

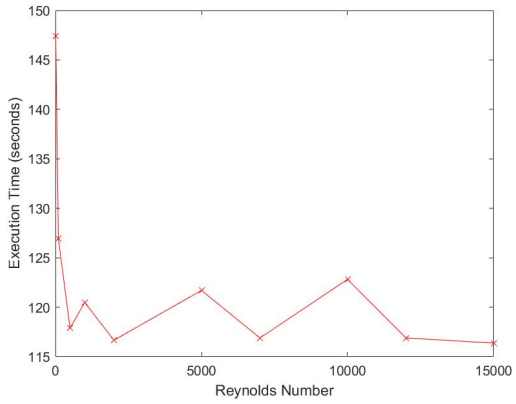

Figure 6.17: Execution times for different Reynolds numbers when overlap is fixed and $N = 20$.

6.5.2 Nonlinear preconditioning methods.

Let us now move onto nonlinear PDEs. For all nonlinear PDEs, we take the initial guess as zero function and use both ASPIN and RASPEN methods to solve each nonlinear PDE. These one-level nonlinear preconditioners are based on the solution of the nonlinear equations defined on the overlapping subdomains with proper boundary conditions. We only present the error convergence results using the RASPEN method because it converges faster than ASPIN. Finally, a comparison between these two methods will be given. The stopping criteria for global preconditioned nonlinear iteration is

$$||\mathcal{F}(u^k)|| \leq \epsilon_{global-nonlinear}||\mathcal{F}(u^{(0)})||.$$

Also, take $\epsilon_{global-nonlinear} = 10^{-11}$. Find the Newton direction by solving the Jacobian system using GMRES. The stopping criteria for global linear iteration is

$$||\mathcal{F}(u^k) - \sum_{i=1}^{N} J_{\Omega_i}^{-1} J d^{(k)}|| \leq \epsilon_{global-linear}||\mathcal{F}(u^{(k)})||,$$

We select $\eta_k = \epsilon_{global-linear} = 10^{-4}$ for all the tests. The stopping criteria for local nonlinear iteration on each subdomain is

$$||\mathcal{F}_{\Omega_i}(g_{i,l}^k)|| \leq \epsilon_{local-nonlinear}||\mathcal{F}_{\Omega_i}(g_{i,0}^k)||,$$

We select $\epsilon_{local-linear} = 10^{-11}$ for all the tests.

6.5.2.1 RASPEN method for the unsteady Navier-Stokes equation.

Consider the stream function formulation of the unsteady Navier-Stokes equation

$$-\Delta\psi_t + \frac{1}{Re}\Delta^2\psi - \psi_y\psi_{xxx} + \psi_x\psi_{yyy} + \psi_x\psi_{yxx} - \psi_y\psi_{xyy} = f,$$

with homogeneous Dirichlet boundary conditions for the global domain Ω and initial condition $\psi(x, y, -1) = \psi_0(x, y)$. Take f when the exact solution is $\psi(x, y, t) = \frac{1}{4}e^{(x+t)}x(1-x^2)^2\sin^2(\pi y)$. See the Figure 6.18 for the spectral convergence.

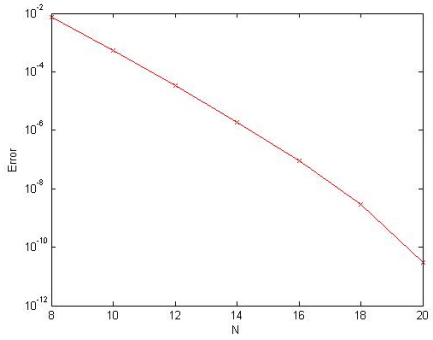

Figure 6.18: Convergence of RASPEN method for the unsteady Navier-Stokes equation for $Re = 10000$.

As the Reynolds number increases, the nonlinear system becomes increasingly difficult to solve. In Figure 6.4, we showed the error convergence of the Legendre collocation method for the unsteady Navier-Stokes equation for $Re = 100$ without domain decomposition. In that case, it fails to converge once the Reynolds number passes $Re = 500$. However, both ASPIN and RASPEN methods converge for a much larger range of Reynolds numbers, plus it takes only a small number of iterations compared to the former method. Some numerical results of RASPEN method are presented in Table 6.6, for fixed $N = 20$ and varying overlap. It can be seen that the number of outer iterations is insensitive to variations in Re. Also, number of outer iterations and error decrease as overlap widens.

	Re = 1000		Re = 10000	
Overlap region	No of iterations	Error	No of iterations	Error
a=0.1, b= -0.1	10	3.518923×10^{-11}	10	1.031628×10^{-11}
a=0.25, b= -0.25	9	1.63248×10^{-11}	9	9.984157×10^{-12}
a=0.4, b= -0.4	7	9.65492×10^{-12}	7	3.169521×10^{-12}

Table 6.6: No of global iterations and error for the unsteady Navier-Stokes equation for different Reynolds numbers and overlapping sizes when $N = 20$.

Table 6.7 shows a numerical comparison between ASPIN and RASPEN methods for the unsteady Navier-Stokes equation for fixed overlap ($a = 0.1$ and $b = -0.1$), varying Re and N. According to table 6.7 and Figure 6.19, we can see that number of outer iterations is independent of N for both ASPIN and RASPEN. That is, it remains constant when N is varying.

		Re = 1000		Re = 10000	
		No of iteartions	Error	No of iterations	Error
N = 8	ASPIN	15	6.340079×10^{-4}	15	5.4853×10^{-4}
	RASPEN	10	6.340079×10^{-4}	10	5.4853×10^{-4}
N = 16	ASPIN	13	5.166221×10^{-8}	13	3.134856×10^{-8}
	RASPEN	10	5.166169×10^{-8}	10	3.133932×10^{-8}
N = 20	ASPIN	13	3.52916×10^{-11}	13	1.08512×10^{-11}
	RASPEN	10	3.518923×10^{-11}	10	1.031628×10^{-11}

Table 6.7: Comparison of ASPIN and RASPEN for the unsteady Navier-Stokes equation for fixed overlap and Re, N are varying.

In Figure 6.19, we show a numerical comparison of number of outer iterations between ASPIN and RASPEN methods for the unsteady Navier-Stokes equation for fixed overlap ($a = 0.1$ and $b = -0.1$), $Re = 1000$ and varying N.

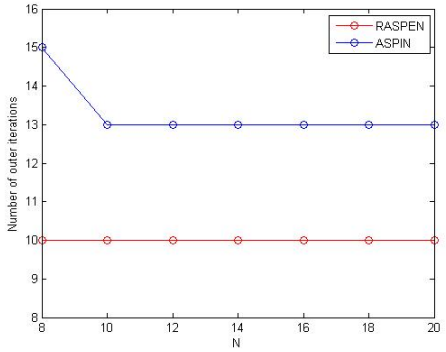

Figure 6.19: Number of outer iterations for ASPIN and RASPEN for the unsteady Navier-Stokes equation for fixed overlap, $Re = 1000$ and varying N.

Moreover, using graphs, we present some time comparisons of RASPEN method

for the unsteady Navier-Stokes equation. In the left figure of Figure 6.20, we show how execution time changes with N for fixed overlap ($a = 0.4$ and $b = -0.4$) and $Re = 1000$. Also, the execution times for different overlaps when $N = 20$ and $Re = 1000$ are illustrated in the right figure of Figure 6.20. It can be seen that execution time increases as overlap widens. Further, it increases like N^s, where $s = 8.6734$ is the slope of the loglog plot .

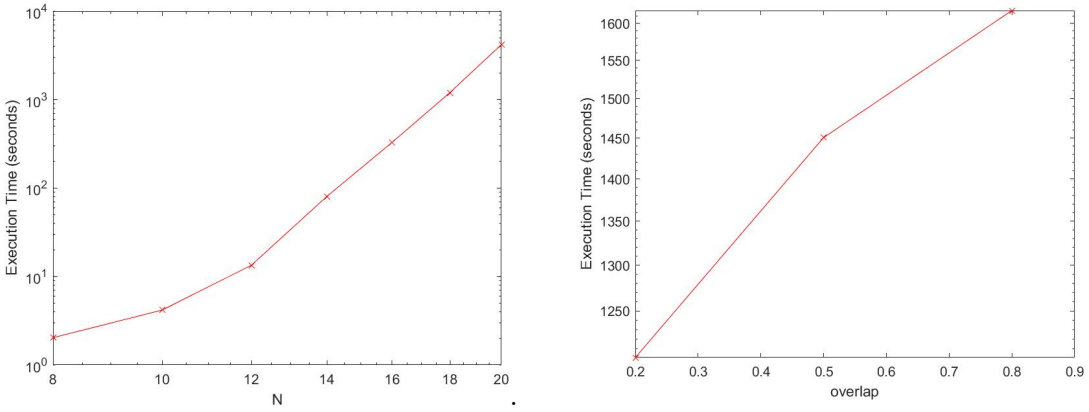

Figure 6.20: Time comparisons of RASPEN method for the unsteady Navier-Stokes equation.

Additionally, Navier-Stokes equation was implemented for the well-known regularized driven cavity flow using RASPEN method for high Reynolds numbers. The streamline patterns of ψ for the unsteady regularized driven cavity flow for high Reynolds numbers at $t = 1$ are shown in Figure 6.21.

Figure 6.22 shows streamline patterns of ψ for the unsteady, two-sided, regularized driven cavity flow for $Re = 15000$ for the parallel (left) and anti-parallel (right) wall motions using RASPEN method.

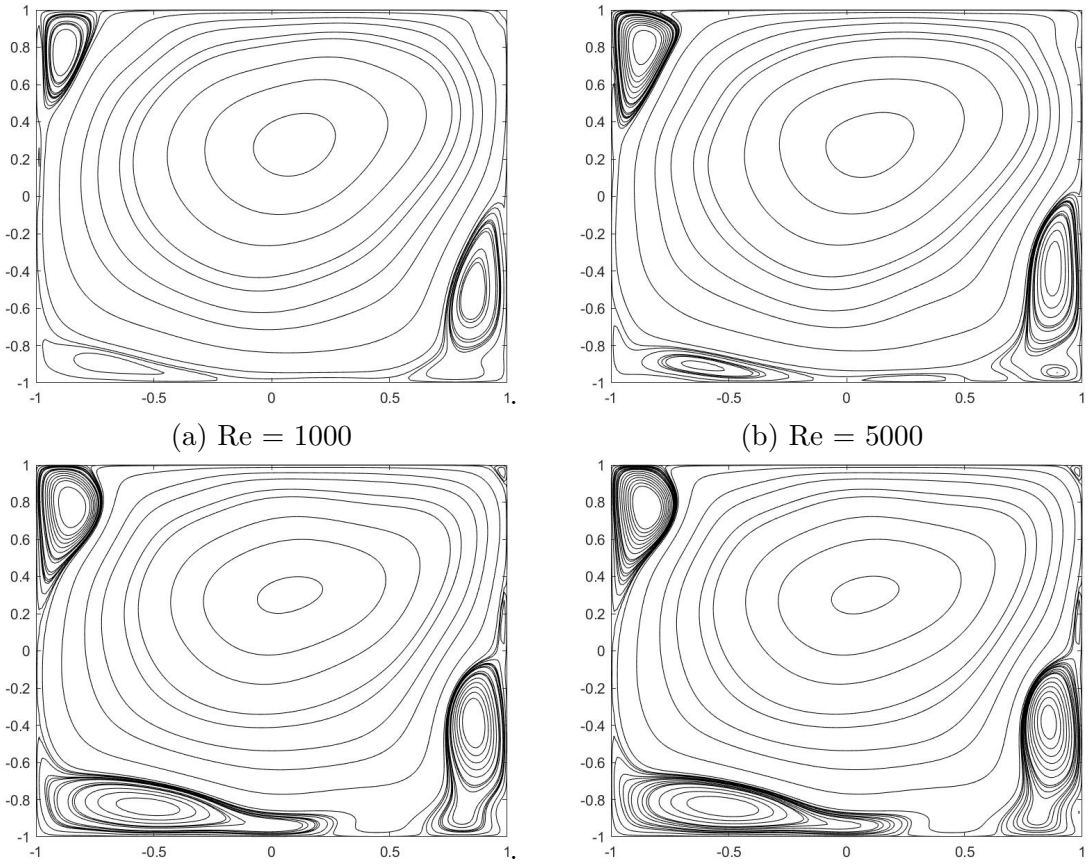

(a) Re = 1000 (b) Re = 5000

(c) Re = 15000 (d) Re = 25000

Figure 6.21: Streamline patterns for ψ for high Reynolds numbers for the unsteady regularized driven cavity Navier-Stokes equation using RASPEN.

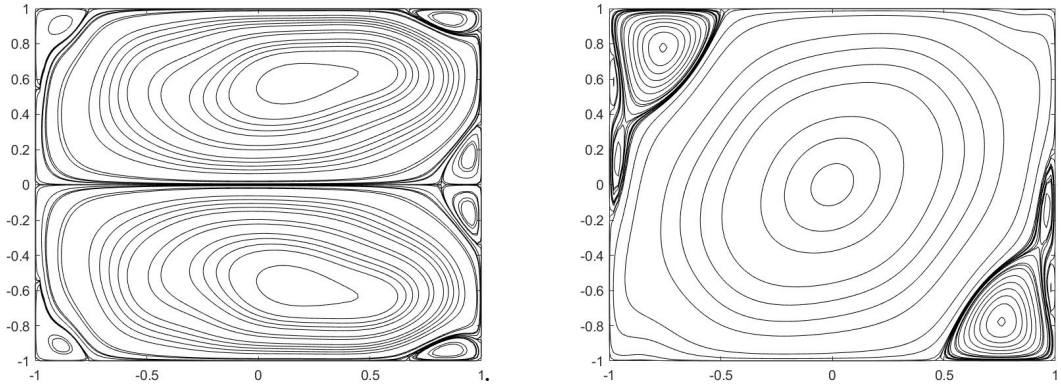

Figure 6.22: Streamline patterns of ψ for $Re = 15000$ for parallel (left) and anti-parallel (right) wall motions for the unsteady two-sided regularized driven cavity Navier-Stokes equation using RASPEN.

6.5.2.2 RASPEN method for the unsteady MHD equations.

Now, consider the stream function formulation of the unsteady MHD equations with the set of boundary conditions (4.14), (4.17) and initial conditions $\psi(x, y, -1) = \psi_0(x, y)$ and $\phi(x, y, -1) = \phi_0(x, y)$.

$$-\Delta\psi_t + \frac{1}{Re}\Delta^2\psi - \psi_y\psi_{xxx} + \psi_x\psi_{yyy} + \psi_x\psi_{yxx} - \psi_y\psi_{xyy} = \phi_{yxx}\phi_x + \phi_{yyy}\phi_x$$
$$-\phi_{xxx}\phi_y - \phi_{xyy}\phi_y + f,$$
$$-\Delta\phi_t + \frac{1}{Re_m}\Delta^2\phi = \psi_{xxy}\phi_x - \psi_x\phi_{xxy} + \psi_y\phi_{yyx} - \psi_{yyx}\phi_y + \psi_y\phi_{xxx} - \psi_x\phi_{yyy} + \psi_{yyy}\phi_x$$
$$-\psi_{xxx}\phi_y + 2\psi_{xy}\phi_{xx} - 2\psi_{xx}\phi_{xy} + 2\psi_{yy}\phi_{yx} - 2\psi_{yx}\phi_{yy} + g.$$

Take f and g when the exact solutions are $\psi(x, y, t) = \frac{1}{4}e^{(x+t)}(1-x^2)^2 x \sin^2(\pi y)$ and $\phi(x, y, t) = \frac{1}{4}e^t(3x - x^3)(5y^3 - 3y^5)\sin(\pi x)\sin(\pi y)$ respectively. See the Figure 6.23 for the spectral convergence of ψ and ϕ.

In the previous case, in Figure 6.9, we showed the error convergence of the Legendre collocation method for the unsteady MHD equations for $Re = Re_m = 10$ without using domain decomposition. In that case, it fails to converge once the Reynolds numbers exceed $Re = Re_m = 10$ due to substantial nonlinearities of the MHD equations. However, unsteady MHD equations converge for a much larger range of Reynolds numbers when implemented using ASPIN or RASPEN methods.

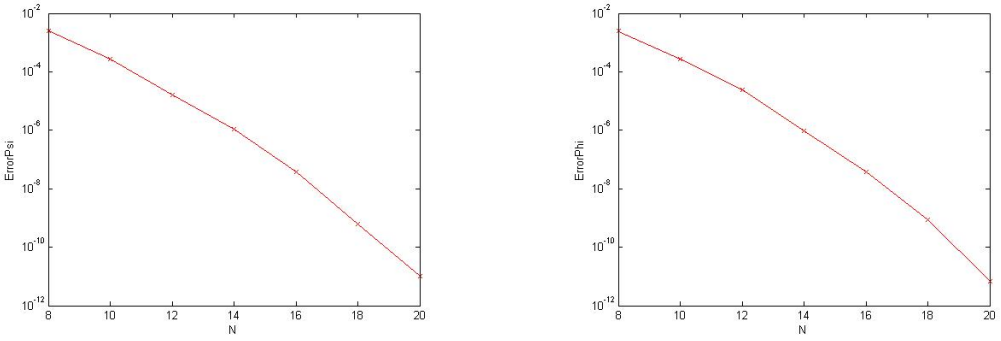

Figure 6.23: Convergence of RASPEN method for the unsteady MHD equation for $Re = Re_m = 10000$.

Below presented are some numerical results of the RASPEN method for the unsteady MHD equations. In Table 6.8 we consider the case when $N = 20$ is fixed and overlap is varying. It can be seen that the number of outer iterations is insensitive to variations in Re. Also, number of outer iterations and error decrease as overlap widens.

	$Re = Re_m = 1000$		
Overlap region	No of iterations	Error	
		ψ	ϕ
a=0.1, b= -0.1	11	1.25138×10^{-11}	9.89162×10^{-12}
a=0.25, b=-0.25	11	9.34865×10^{-12}	8.51243×10^{-12}
a=0.4, b= -0.4	10	8.32489×10^{-12}	7.38526×10^{-12}

	$Re = Re_m = 10000$		
Overlap region	No of iterations	Error	
		ψ	ϕ
a=0.1, b= -0.1	11	9.65718×10^{-12}	8.81729×10^{-12}
a=0.25, b=-0.25	11	8.79265×10^{-12}	7.43851×10^{-12}
a=0.4, b= -0.4	10	6.28345×10^{-12}	4.98632×10^{-12}

Table 6.8: Number of global iterations for the unsteady MHD equations for fixed $N = 20$, varying Reynolds numbers and overlapping sizes.

Now, in Table 6.9, we consider a fixed overlap ($a = 0.1$ and $b = -0.1$) but N and Reynolds numbers are varying. According to table 6.9 and Figure 6.24, we can see that number of outer iterations is independent of N for both ASPIN and RASPEN. That is, it remains constant when N is varying.

	$Re = Re_m = 1000$		
N	No of iterations	Error	
		ψ	ϕ
8	11	3.47953×10^{-4}	2.75312×10^{-4}
16	11	1.19805×10^{-8}	1.14013×10^{-8}
20	11	1.25138×10^{-11}	9.89162×10^{-12}

	$Re = Re_m = 10000$		
N	No of iterations	Error	
		ψ	ϕ
8	11	3.39227×10^{-4}	1.54028×10^{-4}
16	11	1.03562×10^{-8}	9.86451×10^{-9}
20	11	9.65718×10^{-12}	8.81729×10^{-12}

Table 6.9: Number of global iterations and error of RASPEN method for the unsteady MHD equations for fixed overlap but different Reynolds numbers and N.

Moreover, Figure 6.24 shows a numerical comparison of number of outer iterations between ASPIN and RASPEN methods for the unsteady MHD equations for fixed overlap ($a = 0.1$ and $b = -0.1$), $Re = Re_m = 1000$ and varying N.

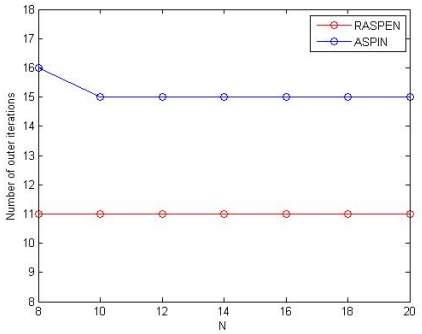

Figure 6.24: Number of outer iterations for ASPIN and RASPEN for the MHD equations for fixed overlap, $Re = Re_m = 1000$ and varying N.

Therefore, we can conclude that RASPEN needs substantially fewer iterations than ASPIN to obtain convergence for both Navier-Stokes and MHD equations.

7

Conclusions

The primary goal of this work is to solve two well-known nonlinear PDEs, namely, Navier-Stokes and Magnetohydrodynamic equations using space-time spectral methods. The stream function formulation of the two equations were used to implement space-time spectral collocation. The main distinction of this work is that spectral methods are used for both space and time. We have shown that when the solution is analytic, the rate of convergence of the numerical solution is exponential; that is, the error decays exponentially.

Further, we implemented Bartels-Stewart and Hessenberg-Schur algorithms to solve the linearized version of Navier-Stokes equation; the Stokes problem. To solve Stokes equation using above algorithms, we proved that the matrix B_2 defined in (3.16) is invertible for both Chebyshev and Legendre cases. Also, we implemented the biharmonic equation using overlapping and non-overlapping linear preconditioning; Additive Schwarz and Dirichlet-Neumann methods respectively. For Dirichlet-Neumann method, we introduced the spectral version of discrete Steklov–Poincaré operators for Laplace and Biharmonic operators [25]. All of the above methods resulted in spectral convergence.

As Reynolds numbers increased, using space-time collocation methods to solve the

above two nonlinear PDEs became increasingly difficult. Due to the strong nonlinearities of Navier-Stokes and MHD equations, we implemented them for high Reynolds numbers using two nonlinear preconditioning methods, ASPIN and RASPEN. Both ASPIN and RASPEN methods resulted in spectral convergence of Navier-Stokes and MHD even for high Reynolds numbers. According to numerical results, we can conclude that RASPEN is a substantially better preconditioner than ASPIN.

Eventually, we implemented Navier-Stokes equation for the well known regularized driven cavity flow using space-time spectral collocation methods. Secondary vortices were observed for both regularized driven cavity flow and two-sided regularized driven cavity flow with anti-parallel wall motions for $Re = 500$. Further, we implemented regularized driven cavity flow using RASPEN method for high Reynolds numbers and secondary vortices were observed for all three driven cavity flows.

For our future works, we hope to observe secondary vortices for the MHD equations for high Reynolds numbers using RASPEN method and also Hopf-bifurcation for both Navier-Stokes and MHD at high Reynolds numbers. Further, we will extend all of our domain decomposition results to more subdomains and we will implement both Navier-Stokes and MHD equations using two-level RASPEN methods to obtain convergence rate independent of the number of subdomains. We would also like to compare a non-overlapping nonlinear preconditioner with the RASPEN method.

Bibliography

[1] M. Adams, A. Brandt, and R. Samtaney, *Toward textbook multigrid efficiency for fully implicit resistive magnetohydrodynamics*, J. Comput. Phys., 229 (2010), pp. 6208–6219.

[2] J. Aurentza, R. Slevinsky, *On symmetrizing the ultraspherical spectral method for self-adjoint problems*, J. Comput. Phys., 410 (2020).

[3] R. Bartels, G. Stewart, *Solution of the matrix equation $AX + XB = C$*, Commun. ACM 15 (1972), no. 9, pp. 820–826.

[4] C. Bernardi, Y. Maday, *Spectral Methods, Techniques of Scientific (Computing (Part 2), Handbook of Numerical Analysis*, Elsevier, 1997.

[5] J. Boyd, *Chebyshev and Fourier Spectral Methods*, 2nd ed., Dover, Mineola, New York, 2001.

[6] P. Brune, M. Knepley, B. Smith, and X. Tu, *Composing Scalable Nonlinear Algebraic Solvers*, SIAM (2015), vol. 57, no. 4, pp. 535–565

[7] X. Cai, F. Dobrian, D.Keyes, and S. Ovtchinnikov, *Additive Schwarz-based fully coupled implicit methods for resistive Hall magnetohydrodynamic problems*, J. Comput. Phys., 225 (2007), pp. 1919–1936.

[8] X. Cai, D. Keyes, *Nonlinearly Preconditioned Inexact Newton Algorithms*, SIAM J. SCI. COMPUT (2002), vol. 24, no. 1, pp. 183–200.

[9] L. Chacon, E. Cyr, R. Pawlowski, J. Shadid, and R. Tuminaro, *New Approximate Block Factorization Preconditioner for Two-Dimensional Incompressible (Reduced) Resisitive MHD*, SIAM J. SCI. COMPUT (2013), vol. 35, No. 3, pp. B701–B730.

[10] L. Chacon, J. Finn, and D. Knoll, *An Implicit, Nonlinear Reduced Resistive MHD Solver*, J. Comput. Phys., 178 (2002), pp. 15–36 .

[11] X. Dai, Y. Maday, *Stable Parareal in time method for first- and second-order hyperbolic systems*, SIAM Journal on Scientific Computing 35 (2013), no. 1, pp. 52–78.

[12] P. Davidson, *Introduction to Magnetohydrodynamics*, Cambridge Texts in Applied Mathematics, 2001.

[13] M. Deville, P. Fischer, and E. Mund, *High-order methods for incompressible fluid flow*, Cambridge University Press, 2002.

[14] V. Dolean, M. Gander, W. Kheriji, F. Kwok, and R. Masson, *Nonlinear Preconditioning: How to use a Nonlinear Schwarz Method to Precondition Newton's Method*, SIAM J. SCI. COMPUT (2016), vol. 38, No. 6, pp. A3357-A3380.

[15] F. Fambri, *A novel structure preserving semi-implicit finite volume method for viscous and resistive magnetohydrodynamics*, Max Planck Institute for Plasma Physics, 2020.

[16] M. Gander, *50 years of time parallel time integration, multiple shooting and time domain decomposition methods*, Contrib. Math. Comput. Sci. 9 (2015), pp. 69–113.

[17] M. Gander, Y. Liu, *On the Definition of Dirichlet and Neumann Conditions for the Biharmonic Equation and Its Impact on Associated Schwarz Methods*, Springer International Publishing, 2017.

[18] M. Gander, S. Vandewalle, *Analysis of the parareal time–parallel time–integration method*, SIAM Journal on Scientific Computing 29 (2007), no. 2, pp. 556–578.

[19] J. Gerbeau, C. LeBris, T.Lelievre, *Mathematical Methods for the Magnetohydrodynamics of Liquid Metals*, Oxford Science Publications, 2006.

[20] D. Gottlieb and S. Orszag, *Numerical Analysis of Spectral Methods: Theory and Applications*, Society for Industrial and Applied Mathematics, Philadelphia, Pa., 1977.

[21] B. Guo, *Spectral Methods and Their Applications*, World Scientific Publishing Co., Singapore, 1998.

[22] G. Horton, S. Vandewalle, *A space-time multigrid method for parabolic partial differential equations*, SIAM J. Sci. Comput. 16 (1995), no. 4, pp. 848–864.

[23] W. Liu, J. Sun, and B. Wu, *Space-time spectral collocation method for the one-dimensional Sine- Gordon equation*, Numerical Methods for Partial Differential Equations 31 (2015), no. 3, pp. 670–690.

[24] S. Lui, *Legendre spectral collocation in space and time for PDEs*, Numer. Math., 136 (2017), pp. 75-99.

[25] S. Lui, *Optimized Schwarz Methods for the Biharmonic Equation*, (Preprint).

[26] S. Lui, *Numerical Analysis of Partial Differential Equations*, John Wiley & Sons, Inc., Hoboken, NJ, USA, 2011.

[27] S. Lui, S. Nataj, *Spectral collocation in space and time for linear PDEs*, J. Comput. Phys., 424 (2021) 109843.

[28] S. Lui, S. Nataj, *Chebyshev spectral collocation in space and time for the heat equation*, Elect. Trans. Numer. Anal., 52 (2020), pp. 295-319.

[29] L. Pavarino, A. Toselli, *Recent Developments in Domain Decomposition Methods*, 2002.

[30] D. Perumal, A. Dass, *Simulation of Incompressible Flows in Two-Sided Lid-Driven Square Cavities. Part II - LBM*, ISSR Journals (2010), vol. 2(1), pp. 25-38.

[31] S. Orszag, C. Tang, *Small-scale structure of two-dimensional magnetohydrodynamic turbulence*, J. Fluid Mech (1979), vol. 90, pp. 129-143.

[32] D. Reynolds, R. Samtaney, and C. Woodward, *A fully implicit numerical method for single-fluid resistive magnetohydrodynamics*, Journal of Computational Physics 219 (2006), pp. 144–162.

[33] J. Shen, *Hopf Bifurcation of the Unsteady Regularized Driven Cavity Flow*, J. Comput. Phys., 95 (1991), pp. 228-245.

[34] J. Shen, *Numerical Simulation of the Regularized Driven Cavity Flows at High Reynolds Numbers*, Computer Methods in Applied Mechanics and Engineering 80 (1990), pp. 273-280.

[35] J. Shen, T. Tang, and L.Wang, *Spectral Methods*, Springer-Verlag, Berlin, Heidelberg, 2011.

[36] H. Tal-Ezer, *Spectral methods in time for parabolic problems*, SIAM Journal on Numerical Analysis 26 (1989), no. 1, pp. 1–11.

[37] H. Tal-Ezer, *Spectral methods in time for hyperbolic equations*, SIAM Journal on Numerical Analysis 23 (1986), no. 1, pp. 11–26.

[38] T. Tang, X. Xu, *Accuracy enhancement using spectral postprocessing for differential equations and integral equations*, Commun. Comput. Phys. 5 (2009), no. 2, pp. 779–792.

[39] A. Toselli, O. Widlund, *Domain Decomposition Methods - Algorithms and Theory*, 2005.

[40] L. Trefethen, *Spectral Methods in Matlab*, SIAM, Philadelphia, 2000.

[41] L. Trefethen, J. Weideman, *The eigenvalues of second-order spectral differentiation matrices*, SIAM J. Numer. Anal. 25 (6) (1988), pp. 1279–1298.

[42] ____, *Legendre spectral collocation method for second-order nonlinear ordinary partial differential equations*, Discrete Continuous Dynamical Systems 19 (2014), pp. 299–322.

[43] ____, *A Legendre spectral method in time for first-order hyperbolic equations*, Applied Numerical Mathematics 57 (2007), no. 1, pp. 1 –11.